Representation of Human Body Stimuli within the Human Visual System

A DISSERTATION
SUBMITTED TO THE FACULTY OF THE
UNIVERSITY OF MINNESOTA
BY

Alexander Joseph Bratch

IN PARTIAL FULFILLMENT OF THE REQUIREMENTS
FOR THE DEGREE OF
DOCTOR OF PHILOSOPHY

Advisor: Dr. Daniel Kersten
Co-advisor: Dr. Stephen Engel

March 2021

Acknowledgements

I would first like to thank each of my committee members. My primary advisor, Dr. Daniel Kersten - I'm honored to have had the chance to work with you. Your mentorship, support, and guidance over the course of my degree has been exemplary. I will miss our conversations, both about science but also on the many unrelated topics we so often ended up discussing. My co-advisor, Dr. Stephen Engel – your input on this work and all of your advice along the way has been so incredibly valuable. My minor program advisor, Dr. Essa Yacoub – I cannot thank you enough for taking the time to mentor me on high field fMRI methods, your support is greatly appreciated. Finally, my committee chair, Dr. Sheng He – I sincerely appreciate all of the valuable feedback and suggestions you have provided.

I would like to thank the many members of the Computational Vision Lab and the Engel Vision and Imaging Lab – it has been a wonderful environment for collaboration, discussion, and professional development. I would like to thank Doug Addleman and Mari Gades – I'm not quite sure how I would have gotten through this degree without our many tea times, especially our early PhD years. I'd like to thank APC lab members Juraj Mesik, Emily Allen, and Danny Guest, both for all of the research advice and for all of the fun times when we managed to take a break and get out of the lab. I'd like Phil Burton, who trained me early on in both fMRI acquisition and data analysis. Finally, I would like to thank Luca Vizioli for the incredibly valuable help you provided.

To all of my family and friends outside of the university, your help and support throughout my PhD has been wonderful and will never be forgotten. Specifically, I'd like to thank my amazing mother, who was always there to take a phone call even on the hardest of days. Most importantly, I must thank my incredible wife Erika – I can say with utmost confidence that this work would not have been possible without you. Even on the longest of days and latest of nights spent working, you have always been there to lift my spirits.

This work was support in part by the following funding sources: R01 EY029700, NIH T32 EB008389, NIH T32 EY025187, High Performance Connectome Upgrade for 3T MR Scanner (1S10OD017974-01), P41 EB015894S10, RR026783 "Multichannel Transmit Frontend for 7 Tesla" WM KECK Foundation, and by the University of Minnesota, College of Liberal Arts Brain Imaging Grant.

Abstract

The human body is a unique and complex visual stimulus, the accurate representation of which is critical for social interaction/communication, acquisition of complex skills, and even basic survival. In a series of studies, using behavioral and neuroimaging techniques, the visual representation of some of the basic features of body perception (e.g., individual parts and their relationships) were explored. First, using a behavioral adaptation paradigm, sensitivity to the relative proportions between limbs was explored. We found that human observers were highly sensitive to relative limb proportion and further demonstrated that this effect appears to depend on body and limb specific mechanisms. Second, an fMRI experiment was used to assess the sensitivity of body-selective cortical areas to the spatial configuration of pairs of limb parts. We found that activity in body-selective areas systematically varies with the typicality of their spatial configuration. Finally, advanced sub-millimeter fMRI techniques were used investigate whether body-selective cortex contained subordinate representations of body stimuli (e.g., their individual parts). We found that the body-selective area of the right extrastriate cortex yields the highest responses to hands above all other stimuli. Furthermore, advanced spatial mapping techniques revealed that this cortical area contains spatially consistent clusters of voxels which preferentially respond to hands. Taken together, these results help to clarify how individual body parts and the relationships between them are represented within the human visual system.

Table of Contents

List of Tables

List of Figures

1. Background

Our visual world is filled with a chaotic, dynamic assortment of information. As such, our visual system is faced with an immense computational challenge: turning this mass of information into a usable set of data in order to drive behavior. In short, our visual system must be able to take often ambiguous, noisy information across a wide dynamic range of color, luminance, and scale, and rapidly process and apply a usable subset of this information within a given set of task constraints. While we are faced with an enormous number of complex stimuli and tasks which exemplify these challenges, perhaps one of the most unique and prevalent examples is the perception of the human body in the natural world.

Much like the face, the human body is a stimulus that occurs quite frequently in our daily life and carries with it a great deal of information. The ability to quickly detect and analyze a human figure in the natural world has implications not just for general purpose social interactions, but for safety and survival even in today's modern world. However, detecting and extrapolating data from a potential human figure is no easy feat. There is inherently a high degree of stimulus variance, given the wide range of body types and clothing. Because of their agency and mobility (regardless of whether they are currently in motion), human bodies additionally have a vast range of poses in which they can move and rest, making them prone to self-occlusion. This mobility also means they are quite likely to be occluded by other objects in their environment, further diminishing the available information. Finally, humans are a very curious, explorative creature, meaning there is an imaginative range of settings and contexts in which you may or may not expect to find a person. As such, the visual system must be equipped with mechanisms able to handle this wide range of potential variation.

In the past 50 years, the fields of neuroscience and psychophysics have unveiled mechanisms and linking principles of the visual system; it is now widely held that the object recognition processing stream consists of a hierarchy of areas, each of which is tuned to features of incrementally higher complexity. Furthermore, face selective areas have been found throughout the visual system of humans and non-human primates, demonstrating the same type of hierarchical structure. Consistent with these principles and findings are studies which have found patches of neurons in mid and high level visual areas that appear

to be selective for individual body parts (Bracci et al., 2015; Downing et al., 2001; Orlov et al., 2010; Peelen & Downing, 2005; Taylor et al., 2007). Such findings have been displayed in both humans and non-human primates (Desimone et al., 1984).

While these areas do exist, the precise nature of their computational role remains elusive. Specifically, it is important to consider and identify features we as observers appear to be sensitive to within a behavioral context. From there, one can then begin to consider what computations/featural processing these brain areas may be responsible for. What individual features are these areas responsible for processing? How do these areas ultimately yield a representation of human bodies, and do we see parallels between similar high-level categories (e.g., faces) in both basic single level and hierarchical processing? Finally, what have we learned from comparative studies in other species (e.g., non-human primates) and do these results agree with those found in humans?

1.1 Human Behavior/Psychophysics

The psychophysics of static human bodies is an area which is relatively understudied when compared to other visual categories, such as faces and "biological motion" (i.e. body movements). Given the similar role of face and body perception in both social and survival situations, as well as their inherent linkage, one may be able to draw parallels between the vast literature of face and biological motion perception, to that of body perception. For instance, do we see evidence of sensitivity (or lack thereof) to stimulus attributes such as orientation/viewpoint and gender? Do we expect to see evidence of a parametrically organized feature space of bodies and body parts, similar to the 'face space' described by Leopold and colleagues (Leopold et al., 2001)? And finally, do we see the type of configuration-based effects for bodies which are characteristic of faces (Maurer et al., 2002)?

Given that adaptation to gender has been demonstrated for both faces (Webster et al., 2004) and point light walkers (Troje et al., 2006), it would be plausible to assume the same would be true for static bodies. Using an adaptation paradigm in which subjects viewed morphed silhouettes which varied on a gender continuum, Palumbo and colleagues (Palumbo et al., 2013) revealed that there do appear to be adaptation effects for gender. Subjects experienced strong shifts in their point of subjective equality (PSE) when adapting

to extreme ends of the continuum (e.g., adapting to female shifted percepts of gender in the direction of male). However, such a phenomenon has been demonstrated using cross category adaptation, showing that adapting to faces and testing on bodies (or vice versa) yields similar effects (Ghuman et al., 2010; Kessler et al., 2013; Palumbo et al., 2015; Weigelt et al., 2010). Thus, it may be the case that this is a high level, cognitive after-effect which feeds back to visual areas rather than a sensitivity and adaptation to the explicit visual features of genders. Nonetheless, it is possible that the effect is due to an interaction of both cognitive and visual features, a hypothesis which has been supported by failing to achieve gendered biological motion adaptation when adapting to faces (Hiris et al., 2016). As such, further investigation is needed to disentangle the precise root of this effect, particularly in the context of static human body stimuli.

Another likely feature of interest, which has been frequently studied across a wide range of visual categories, is that of viewpoint. For instance, do we expect sensitivity to the viewing angle of a body stimulus? Does exposure to a given viewpoint bias further perceptions of differing viewpoints? And how does viewpoint interact with other stimulus attributes? Adaptation paradigms, in which observers are exposed to a given viewpoint (i.e. rotations in depth about a vertical axis) for long durations, has be use to probe this question in the case of faces (Fang & He, 2005; Ryu & Chaudhuri, 2006) as well as general object categories (Fang & He, 2005). In both cases, it has been shown that there is indeed a degree of sensitivity to viewpoint, in that observers experienced shifts in perceived viewpoint (i.e., after-effects) after adapting to a given viewpoint. Given these findings, what do we expect from static bodies? Lawson and colleagues (2009) used a similar adaptation paradigm to that of Fang & He (2005) to address this question. They found large after-effects as a result of viewpoint adaptation, suggesting that we do indeed see similar effects of viewpoint tuning with bodies as we do with faces and other objects, thereby suggesting sensitivity to viewpoint in terms of rotation in depth of the target. Intriguingly, it has also been shown, using concurrent adaptation paradigms, that effects of adaptation to gender, body size, and full body pose persist through various changes in viewpoint (Kessler et al., 2013; Sekunova et al., 2013). Such effects have also been demonstrated, although to a lesser extent, in the context of biological motion using identity and viewpoint (Jokisch et al., 2006). However, robustness to viewpoint in body perception demonstrated by these concurrent paradigms

isn't necessarily surprising. Given the degree of articulation and wide range potential presentation locations and viewpoints, it seems plausible to maintain sensitivity to features irrespective of changes in viewpoint and orientation.

Perhaps one of the obvious features to explore would be that of configuration. In essence, are we sensitive to canonical representations of the configuration of body parts which form a wholly configured pose? In the field of face perception, configural effects have long been noted, specifically in the context of face inversion. The classical finding is that inversion disproportionately affects face perception relative to other object categories, in terms of performance in identification, emotional discrimination, amongst others. Initial theories surrounding this phenomenon attributed the impact of inversion to the disruption of configural processing (Valentine, 1988; Yin, 1969). Similar effects have additionally been noted for biological motion using point light walkers. For instance, it has been revealed that inversion of point light walkers impairs the ability of observers to discriminate the walker's direction of motion (Hirai et al., 2011; Troje, 2003; Troje & Westhoff, 2006).

Do we see evidence of similar inversion effects in body perception? Two studies by Reed and colleagues used classic face inversion paradigms to reveal that we do indeed see negative impacts, both in RT and accuracy, when whole bodies are inverted. Specifically, Reed and colleagues (2003) used a change detection paradigm with either upright or inverted faces, bodies, and houses. It was found that, just as with faces, inverted bodies led to an increase in RT and a decreases in accuracy, whereas inverting houses yielded no change in performance when detecting changes in the small changes in category-dependent features. To examine body inversion effects in further detail, Reed and colleagues (2006) had subjects discriminate changes between individual body parts or scrambled collections of body parts. In this case, inversion had no impact on performance. Collectively, these results suggest that inversion may be disrupting feature discrimination in the case of whole, configured bodies rather than the individual components, which is consistent with the classical notions surrounding inversion effects in faces (Valentine, 1988; Yin, 1969).

More recent studies have sought to further disentangle potential interactions with body inversion effects. For instance, Kessler and colleagues (2013) have shown that there

is a persistence of gender adaptation when fully inverting bodies, suggesting that we may not have as great of sensitivity to dramatic inversion effects for bodies as we do for faces. Furthermore, it has been demonstrated that the removal of the head or blocking of the facial features dramatically decreases the body inversion effect (Brandman & Yovel, 2010; Minnebusch et al., 2009; Yovel et al., 2010), suggesting that body inversion effects may be simply due to engagement of the face processing network. Taken together, these results leave a somewhat muddled impression. However, the somewhat conflicting results may again be explained by the necessary robustness to dramatic variation in appearance and presentation mandated for the perception of bodies. Thus, while there may be configural mechanisms at play for bodies, perhaps probing these mechanisms using inversion is not the optimal approach.

While the features such as gender, viewpoint, and configuration are important and necessary to consider, it is worth asking whether there has been any investigation into low to mid-level elements of body perception. What are the attributes that behaviorally define body parts, such as color, length/proportion/ratio of parts, etc.? Are these features represented orthogonally or on an inter-related plane of representation? Similar questions have been addressed in the domain of face perception. In face perception, for instance, Leopold and colleagues (2001) have demonstrated the sensitivity to aspect ratios and various face shape profiles and the continuum of these features. While no such studies have been directly conducted for body perception, the sensitivity to body size (e.g., the fatness and thinness) of whole bodies and parts has been demonstrated with adaptation (Glauert et al., 2009; Winkler & Rhodes, 2005). Nonetheless, major gaps remain in the behavioral domain as a whole, and in order to begin building a full picture of the intermediate features responsible for achieving a complete human body percept, these questions must be addressed.

1.2 Comparative Neurophysiology

Some of the first evidence for neural selectivity for human bodies comes from single unit studies of non-human primates. Individual neurons have been found in the inferior temporal cortex (IT) of Rhesus Macaques which are exclusively sensitive to biological stimuli such as hands and faces (Desimone et al., 1984; Gross et al., 1972). The

neurons in question typically showed robustness to variations in stimulus properties such as size, viewpoint, and orientation. Furthermore, while neurons were found which showed tuning to more mid-level object classes (e.g., squares, circles), sharpest tuning was found in neurons selective for faces and body parts. In the wake of these initial single unit recording studies, large scale, multi-electrode recording methods have been used to confirm these findings, revealing that a large proportion of neurons in IT show strong, exclusive tuning to face and body features (Kiani et al., 2007; Pinsk et al., 2009) as well as other complex objects, with dissociations made between animate and inanimate stimulus classes (Kriegeskorte et al., 2008).

Further studies have now revealed between 6 and 8 large face-selective patches of neurons, located in relatively consistent locations within the macaque IT, parietal, and occipital cortex. This set of patches is now commonly referred to as the 'face patch network' and is hypothesized to represent a unified network for processing face stimuli (Grimaldi et al., 2016; Meyers et al., 2015; Sebastin Moeller et al., 2008; Doris Y. Tsao et al., 2006; Vanduffel et al., 2014). Likewise, two to three large, consistently localized body-selective patches have been identified in the macaque using fMRI. They are typically located within the middle of the superior temporal sulcus (mSTS) and the anterior superior temporal sulcus (aSTS) (Bell et al., 2008; Pinsk et al., 2005, 2009; Popivanov et al., 2012; Doris Y. Tsao et al., 2003) and suggest that a similar, 'body patch network' may also exist as a separate processing network in the macaque visual cortex.

Given the existence of localized areas selective for bodies in the macaque, the precise nature of their response properties, and ultimately their potential role in an integrated body processing network must be considered. The initial single unit findings of Desimone and colleagues (1984) and Gross and colleagues (1972) suggest that the response properties of neurons within these patches are invariant to low level features, such as orientation of local stimulus elements, viewpoint (in terms of rotation of the viewing angle), and image scaling. This is consistent with both a wide range of studies demonstrating that object-selective IT neurons typically show invariance to low level features and image transformations as well as the prevailing view that high level vision is robust to such features (Booth & Rolls, 1998; DiCarlo et al., 2012; DiCarlo & Cox, 2007; Vogels & Orban, 1996; Wallis & Rolls, 1997). In order to elucidate the precise low-level

features and transformations to which body-selective areas display robustness, Popivanov and colleagues (2015) conducted a rigorous single-unit based investigation of the mSTS body patch. They found that neurons in this patch were highly invariant to both image size and translation. However, they did find modulation of firing rates as a function of orientation, with strong reductions in firing rate occurring when bodies were rotated 45 degrees or greater from their 'typical' orientation on the Y axis (where 180 degrees would be full inversion of the body). Furthermore, they found that these neurons had a strong lower visual field bias. Taken together, these results show robustness to the type of variation we would expect to encounter with human bodies; bodies often translate across the visual field and vary widely in scale. These results also suggest sensitivity to the typicality by which bodies are viewed and the potential consequences of different views. Specifically, we tend to foveate the face during social interactions, consequently placing the body in the lower visual field. We also rarely see misoriented or inverted bodies. Thus, receptive fields for human bodies have likely developed as a result of this typicality.

Evidence showing invariance to low level features, as well as the relatively high position in the visual hierarchy, would suggest that perhaps shape characteristics of bodies and body parts themselves may be the feature to which mSTS body patch neurons are tuned. Such a theory is consistent with previous findings of shape dimension coding in macaque IT (Bao & Tsao, 2018; Caspari et al., 2014; Kayaert et al., 2003, 2005; Op De Beeck et al., 2001). However, one could also argue that the representation might exist on the dimensions of nearest neighbor representation (e.g., arm is similar to hand given its spatial proximity in either 2D image or 3D global space). The latter theory would be consistent with the apparent experiential/typicality based tuning noted above (Popivanov et al., 2015) for features such as orientation and visual field bias. In line with the former hypothesis, Popivanov and colleagues (2015) found that mSTS body patch neurons typically showed similar firing rates to silhouettes of bodies. Furthermore, they found elevated firing for object categories that were visually similar to bodies, such as animals with particularly pronounced limbs, suggesting representation based on the similarity of body-like components. Consistent with this notion are findings from multimodal studies in macaques. Using fMRI, single and multi-unit electrodes, and LFP recordings, several groups have found that the mSTS body patch seems to code bodies based on gross

similarity of the whole body (e.g., similarity both within and across species) as well as between individual body parts, in that, for example, hands and feet seem to be represented similarly, based on their visual similarity (Kalfas et al., 2017; Popivanov et al., 2014, 2016). Together, current evidence suggests that mSTS seems to be sensitive to high level shape-based features which are consistent with bodily features.

While evidence above suggests a shape-based representation for bodies in the mSTS patch, is there evidence for selectivity of higher-level visual features (e.g., identity, posture, etc.)? And what do we observe from aSTS? Finally, is there evidence suggesting an integration of these two body selective areas? These questions have only recently been undertaken; however, the limited evidence is nonetheless compelling. Kumar, Popivanov, and Vogels (2017) explored responses of the mSTS and aSTS body patches to identity, posture, and viewpoint/orientation using single unit and LFP recording. They found that responses in the aSTS patch are far more robust to viewpoint and orientation than those of the mSTS patch. Furthermore, they observed that while both changes in posture and categorical identity could be readily decoded in both mSTS and aSTS, decoding performance was significantly higher in the aSTS. These results illustrate a shift from mid to higher level features as information flows to higher level body areas, a finding which is consistent with observations in the face patch network (e.g., Meyers et al., 2015).

Given the apparent transformation of information coding when moving up the hierarchy, and the consistency with face patch findings, it seems sensible to assume these body patches represent an inherently linked processing network. Premereur and colleagues (2016) explored this question using a combined fMRI-microstimulation paradigm in which BOLD activity across both face and body patches was observed during direct stimulation of various face and body patches. They found that the mSTS and aSTS body patches do indeed appear to communicate, more so in a feedforward than in a feedback fashion. The same was found to be true for the face patch network. Intriguingly, they also found that these two networks appear fairly independent; activation of either the face or body patch network elicits very little activity in the opposing network. Thus, it appears as though the mSTS and aSTS do in fact represent a distinct and independent processing network for body stimuli.

Taken together, it is clear that in non-human primates, body stimuli represent a special stimulus class, the perception of which is underpinned by dedicated neural circuitry. The representation of bodies appears to be split across at least two cortical areas, a patch of neurons in the middle STS and in the anterior STS. Current evidence suggests a shape and viewpoint-based representation in the middle STS patch, while representation in the anterior STS is geared more towards higher level features, such as identity and pose. Finally, causal evidence from direct stimulation suggests that these two patches do indeed communicate with one another, representing a relatively distinct and independent processing network for body stimuli. While further work is needed to elucidate the precise stimulus features being coded by these patches, as well as their relative contribution to the perceptual representation, evidence for a body processing network in non-human primates is unequivocal.

1.3 Human Neuroscience

When considering the results above in 1.2, it seems likely that we would expect to see neural signatures in humans for the perception of human bodies. Indeed, a wealth of research has been conducted on this subject using a wide range of techniques, from non-invasive electrophysiology (EEG, MEG) to fMRI. Several groups have additionally been able to tackle this question with intracranial recordings. Furthermore, causal implications have been explored as the result of lesions and disease states as well as using methods of temporary inactivation (e.g., TMS). Collectively these results have begun to shed light on the features and associated mechanisms underpinning human neural processing of the human body.

1.3.1 Electrophysiology

Several studies have used non-invasive electrophysiology (namely EEG) to reveal fast detection mechanisms for human body stimuli and animate stimuli as a whole (H. Liu et al., 2009; Thorpe et al., 1996; VanRullen & Thorpe, 2001). Furthermore, in conjunction with the well-known finding of the N170 ERP component for face perception (Bentin et

al., 1996; Bötzel et al., 1995), there has been found to be a similar ERP component for human bodies. Thierry and colleagues (2006) first noted the presence of a component elicited exclusively by human body stimuli, finding a negative signal approximately 190 ms post stimulus onset. As such, this component has been since referred to as the N190. Thierry and colleagues (2006) further explored the response properties of this component, discovering generalization to both stick figures and silhouette depictions of bodies. Using source localization methods, they found the origin of the signal to be around the right posterior extrastriate cortex. More recent investigations of the N190 component have supported this source localization and have additionally shown sensitivity to body parts presented in isolation as well as sensitivity to inversion effects (Mohamed et al., 2011; Moreau et al., 2018; Taylor, Roberts, et al., 2010).

Further work has explored electrophysiological signatures of body perception using intracranial LFP recordings secondary to seizure monitoring in epilepsy patients. The first study to examine body perception found electrodes sensitive to human bodies in both the posterior STS as well as the ventral temporal lobe, around the fusiform gyrus. However, arrays were not placed in the lateral occipital/extrastriate cortex and thus no data was available for this region (McCarthy et al., 1999). Pourtois and colleagues (2007) examined responses in a patient with an electrode array placed across the extrastriate cortex. An electrode was found near the middle temporal gyrus/inferior temporal sulcus boundary that responded significantly stronger to bodies than all tested categories. Consistent with EEG findings, these responses were found to peak approximately 190 ms from onset, with a peak at 250 ms. Finally, Kadipasaoglu and colleagues (2016) examined intracranial responses to a wide variety of different visual categories across 26 patients. They found electrodes around the STS, the lateral extrastriate cortex, and the ventral temporal cortex showing strong responses for human bodies.

Recently, studies have employed MEG to explore body representation in humans. Several investigations of general object perception, which made use of vast, comprehensive stimulus sets, have noted the decodability of animate vs inanimate stimuli, as well as subordinate classes (e.g., bodies versus animals) (Carlson et al., 2013; Cichy et al., 2014; Contini et al., 2017). Furthermore, these studies have shown that this decodability arises relatively early post stimulus onset versus other object categories. In specific investigations

of body processing, Ishizu and colleagues (2010) examined differential effects for bodies and faces. They observed results consistent with EEG findings in that the typical time series peak for bodies occurred approximately 190 ms post stimulus onset. Moreover, source localization suggested the lateral extrastriate cortex (with right hemispheric dominance) was the source of the signal. Meeren and colleagues (Meeren et al., 2013) also investigated differential effects for bodies and faces, finding similar time series data to Ishizu and colleagues (2010). Furthermore, source localization suggested that, in addition to lateral extrastriate areas, major signal contributions came from the fusiform gyrus within the same response time frame, with large activation in orbitofrontal regions following shortly thereafter.

Collectively, these results demonstrate a reasonable degree of consistency with findings in non-human primates, in that there seem to be specific areas of the ventral visual stream which are associated with selective processing for human stimuli. Moreover, the precise stimulus features necessary for eliciting these responses (e.g., inversion, abstract depiction) parallel the results in non-human primates, suggesting relatively high-level representation for body stimuli. As such, these results lay a strong foundation for more in-depth evaluations of the featural coding as well as the cortical source of these signals.

1.3.2 fMRI

Some of the most compelling evidence suggesting the importance, specialization for, and sensitivity to human bodies, as well as their subordinate features, comes from exploration with functional MRI (fMRI). The advent of fMRI has yielded an explosion of findings in human visual neuroscience as a whole, revealing that the perception of phenomenologically important of visual categories, such as faces and biological motion, appears to be underpinned by dedicated brain regions (e.g., the Occipital Face Area (Dubois et al., 1999; Halgren et al., 1999) and Fusiform Face Area for faces (Kanwisher et al., 1997); the posterior Superior Temporal Sulcus for biological motion (Grossman & Blake, 2002; Puce & Perrett, 2003)). Within this body of work, it has been shown that there appear to be two areas of the human visual cortex which are selective for static human body stimuli: the Extrastriate Body Area, or EBA (Downing et al., 2001) and the Fusiform Body Area, or FBA (Peelen & Downing, 2005).

Downing and colleagues (Downing et al., 2001) were the first to reveal an area of the visual cortex selective for human bodies. Using a basic block design paradigm, they presented numerous visual categories to human subjects (e.g., faces, bodies, body parts, tools, and various other inanimate objects). They found a bilateral (though right-dominant) area in the lateral extrastriate visual cortex that responded significantly higher when whole bodies and/or individual body parts were contrasted with other combinations of visual categories (including faces). The area in question was found consistently within the middle temporal gyrus and superior temporal sulcus, and partially overlapped with motion selective area MT. Further experiments by Downing and colleagues (Downing et al., 2001) showed robustness of the responses to variation in low level features of the bodies; stick figures, silhouettes, and line drawings of bodies and individual body parts elicited a similar activity profile, demonstrating robustness to abstract forms/variation in low level features. Finally, Downing and colleagues (Downing et al., 2001) were able to show that, while this area showed larger responses to animals than to control objects, the response to human bodies was still higher than both, solidifying that this appears to be an area with tuning to primarily human body stimuli. Given its location and selectivity profile, Downing and colleagues (Downing et al., 2001) coined the term Extrastriate Body Area, or EBA, to describe this cortical area.

Shortly after the discovery of the EBA, Peelen & Downing (Peelen & Downing, 2005) replicated the results of Downing and colleagues (Downing et al., 2001) using nearly identical stimuli and procedures. However, they additionally found an area which appeared to show comparable selectivity to human bodies as the EBA. This area was found to be within the right fusiform gyrus (again, consistent with source localization studies in 1.3.1), neighboring and partially overlapping with face-selective FFA. Additional experiments showed that not only was this area indeed exclusive in its selectivity to human bodies, but also demonstrated the same robustness to low level features (e.g., similar responses to stick figures, silhouettes) as the EBA. Furthermore, this area appeared to show slightly higher sensitivity than the EBA to the scrambling of image components. In light if its selectivity profile and anatomical location, this region was denoted as the Fusiform Body Area, or FBA.

When considering these findings, one major question must be addressed before further dissecting the functionality and subordinate response properties of these cortical areas: given their overlap with neighboring, non-body selective cortical areas, are the EBA and FBA truly distinct cortical areas? In the context of EBA and its proximity to/overlap with motion selective area MT, it has been shown, using both univariate (Taylor et al., 2007) and multivariate (Downing et al., 2007) analysis techniques, that there are indeed dissociable responses to bodies and motion from EBA and MT, respectively, and that the non-overlapped portions of EBA respond at chance level to motion. It has been argued that much of the overlap observed in initial studies of EBA was due to low resolution imaging and spatial smoothing during preprocessing. Using high resolution, non-smoothed data, it has been revealed that not only is this overlap quite minimal, but that EBA actually consists of three distinct patches surrounding area MT (Ferri et al., 2013; Weiner & Grill-Spector, 2011).

Regarding the FBA and its proximity and overlap with face selective FFA, findings have mirrored that of the EBA. It has been shown that, while these areas neighbor and potentially overlap (depending on resolution and preprocessing), both individual voxels within the FFA and FBA tend to show exclusive selectivity to either faces or bodies, respectively, without showing selectivity to the converse (Schwarzlose et al., 2005; Taylor et al., 2007; Weiner & Grill-Spector, 2013). Thus, it appears that not only do we have cortical areas selective for human bodies, but these areas do show a relatively distinct response profile to this stimulus category.

Since their respective discoveries, many groups have sought to further understand the underlying mechanisms and overall roles the EBA and FBA play in the perception of human bodies. The initial findings of Downing and colleagues (Downing et al., 2001) and Peelen & Downing (Peelen & Downing, 2005) already demonstrate the robustness to low level features, in that stick figures and silhouettes yield comparable BOLD responses from these areas. Such a finding is consistent with similar results illustrated in non-human primates and in humans using EEG (see 2.2 and 2.3.1 for details). In line with these findings is a result from Op de Beeck and colleagues (2010), who showed that color versus black and white images of bodies (as well as faces and various other objects) had little impact on the response magnitude in cortical areas tuned to each category. Taken together, these

results suggest that, so long as the visual features are consistent with the abstract form of bodies, then they will be coded as such. This has an intuitive appeal, given our phenomenological ability to decipher various abstract forms of human representation in mediums such as surrealist and impressionist art. However, if low level features are discounted, to what features are the EBA and FBA sensitive?

Given the importance and behavioral sensitivity to viewpoint and reference framed, noted above in 1.1.1, it has been proposed that the EBA and FBA are sensitive to these phenomena. Taylor, Wiggett, and Downing (2010) directly investigated the phenomenon of viewpoint using an fMRI adaptation paradigm in which subjects were shown human bodies across a wide range of viewpoints. They found that, in both EBA and FBA, there was a degree of viewpoint tuning (e.g., increasing rebound in adaptation with increasing angular viewpoint differences). However, it was further shown that these effects could be abolished with post stimulus masking. The interpretation of this result was that the viewpoint dependent tuning in EBA and FBA was driven by later waves of neural activity. Thus, while evidence exists which favors viewpoint tuning in these areas, the precise nature of the mechanism remains unclear.

The question of viewpoint tuning has been further addressed, albeit in somewhat more abstract terms, by looking at phenomena such as reference frames and view typicality. Chan, Peelen, and Downing (2004) as well as Saxe, Jamal, and Powell (2006) probed whether the EBA showed a variable BOLD response pattern to egocentric versus allocentric viewpoints. Both groups found higher responses in the right EBA (but not left EBA) for allocentric versus egocentric viewpoints. This was taken to suggest that the right EBA is perhaps more sensitive to representation of other animate agents in the visual environment, as opposed to self-representation. Chan and colleagues (2010) investigated whether view typicality impacted BOLD responses to human bodies (both whole and individual parts) as well as faces. They presented subjects with vertically split stimuli (e.g., a left or right side of a body) on either left or right of fixation. They found that when stimuli where in their typically experienced viewpoints (e.g., left side of the body in the right visual field), a higher BOLD response was elicited, contributing further evidence toward the viewpoint sensitivity of the EBA.

These findings suggesting viewpoint tuning in the EBA are indeed consistent with viewpoint dependency found in the mSTS body patch in non-human primates (see 2.2), in nearby face selective areas (Ewbank et al., 2011; Ewbank & Andrews, 2008; Fang et al., 2007), and in general object selective areas such as the Lateral Occipital Complex (LOC) (Kourtzi et al., 2003). However, it is also worth considering that biological motion sensitive posterior superior temporal sulcus (pSTS) appears to have a viewpoint invariant representation of biological motion (Grossman, 2010). One argument for this incongruency could be made on the grounds that former mentioned face, object, and static body selective areas all exist within the ventral visual hierarchy, while pSTS exists within the dorsal hierarchy. Given the inherent motion-based variability in biological motion as well as the action-based processing of the dorsal hierarchy (Goodale & Milner, 1992; Rizzolatti & Matelli, 2003), invariance to viewpoint may ultimately lead to action-based representation, whereas viewpoint tuning may help contribute to more precise object templates in ventral areas. Nonetheless, further work is needed to solidify this theory, and to explore these representational questions in greater depth.

Given that both the EBA and particularly the FBA are located at a relatively high position in the ventral visual hierarchy, as well as evidence of shape-based tuning in the macaque body patches (see 1.2), one may find robustness to low level features not surprising and that higher level features such as shape may be a likely candidate for selectivity. Furthermore, evidence from face literature suggests that neighboring face selective cortical areas show significant tuning to face shape, feature distribution, and aspect ratio of these features (Gilaie-Dotan & Malach, 2007; Jiang et al., 2006; Yovel & Kanwisher, 2004). Bracci and colleagues (2015) recently investigated the representation of individual body parts using representation similarity analysis (RSA). Data were compared to models based on attributes such as stimulus shape (based on ratings of perceived similarity), physical proximity (in image space), and semantic relationship (in regards to a semantic/functional word model). They found that patterns of activity in both the EBA and FBA were most consistent with shape-based models, while frontal and parietal regions were more consistent with semantic models. This result is consistent with the findings of Orlov, Makin, and Zohary (2010), who had analyzed responses to body parts throughout the entirety of the occipital-temporal cortex. They found that ROIs in both lateral occipital

and ventral temporal cortex showed specificity to arms typically showed high responses to legs, and vice versa. The same was true of hand and foot ROIs, again suggesting a shape-based representation relative to physical distance. Moreover, these results are consistent with findings in the mSTS body patch in macaques (Kalfas et al., 2017; Popivanov et al., 2014, 2016).

However, a recent study has demonstrated that, while shape does appear to be a feature for which body selective areas are strongly tuned, interactions appear to exist between shape and other lower level features. Proklova, Kaiser, and Peelen (2016) that neither shape or textures are necessarily predictive of the patterns of activity in occipital temporal cortex for animate versus inanimate stimuli. This is specifically noted in boundary cases where shape can be very similar (e.g., snake vs. rope, bird vs. plane, etc.). They conclude that there is a necessary interaction between these features that defines the response profiles, particularly in the case of ill-defined category boundaries.

Additionally, investigations into tuning for higher level features (e.g., gender, body weight) have ultimately contributed evidence in favor of shape-based tuning. Hummel and colleagues (2013) demonstrated, in the context of an fMRI adaptation paradigm, that the FBA, but not the EBA, shows strong adaptation effects when presenting bodies of variable fatness and thinness. Aleong and Paus (Aleong & Paus, 2009) also showed fMRI adaptation effects related to body size exclusively in the FBA, and further found similar effects for gender in both EBA and FBA. While both of these stimulus features may be regarded as high level, the result is the same: modulation of shape-based features of the standard human body template.

As we move from lower to higher level features, we begin to see a surge in literature as well as an apparent differentiation in the roles of the EBA and FBA. Taylor, Wiggett, and Downing (Taylor et al., 2007) developed an experiment in which subjects were presented with body parts in increasing size and superordinate relationship (e.g., finger → hand → arm → full body). They found that the EBA (in both hemispheres) appears to show increasing activation with increasing body part size/superordinate relationship. Conversely, the FBA showed something like a step function, in that there was generally low, undifferentiable activity for any given individual body part, but a large response for whole, configured bodies. This finding has been further demonstrated using scrambled

versus whole images of bodies, finding that the FBA typically shows greater sensitivity to scrambling, in terms of reduced activation, than the EBA (Bauser & Suchan, 2015). The interpretation of these findings has been that the EBA is responsible for the representation of individual parts, irrespective of configuration, while the perhaps integrates the information of the individual parts, and ultimately represents information pertaining to wholly configured bodies.

Consistent with this interpretation are findings that features which may be attributed more to the whole body (rather than individual parts) modulate responses in the FBA, but not EBA. Examples include global body size (Aleong & Paus, 2009; Hummel et al., 2013), pose and posture (Cross et al., 2010), identity (Hodzic et al., 2009), and integration of face and body information (Bernstein et al., 2014). Furthermore, it has long been proposed that neighboring FFA plays a role in holistic, configural representations of faces, while OFA is more selective for face parts (Henriksson et al., 2015; Loffler et al., 2005; Schiltz & Rossion, 2006; Yovel & Kanwisher, 2004, 2005). Given the relatively similar positions of EBA to OFA and FFA to FBA, a similar relationship for body processing would seem rational. While current results are consistent with this interpretation, further work is needed to solidify these organizational principles. Nonetheless, considering the EBA to be 'part sensitive' and FBA to be 'whole sensitive' seems to be a useful manner by which to both categorize these cortical areas and begin building a further framework for their role in representation.

1.3.3 Disorders, Lesions, and TMS

In an effort to establish causal roles of various cortical regions selective for human bodies it is important to consider cases of lesions and disorders which may either disrupt or abolish the areas of interest. Additionally, the recent advent of Transcranial Magnetic Stimulation (TMS) has enabled experimenters to temporarily inactivate regions of cortex, thereby experimentally simulating the impact of a lesion. Moreover, such studies not only afford the opportunity to draw causal inferences but can reveal double dissociations, underscoring the processing specificity of cortical regions.

In the context of lesions, a small number of case reports have noted specific processing deficits for human bodies, in the absence of deficits for other visual categories

(Sacchett & Humphreys, 1992; Suzuki et al., 1997). However, as these investigations occurred before knowledge of cortical areas selective to body stimuli, these investigations did not speculate as to the roles of such areas, nor did they give precise descriptions of the areas involved. More recently, Grewe and colleagues (2015) described the case of an epileptic patient with widespread damage to the right fusiform gyrus. This patient showed greatly reduced performance on mental rotation and viewpoint tasks for bodies, but not for faces. As such, a causal role for the fusiform gyrus (presumably the FBA) in body perception is thereby implied. In order to draw more targeted conclusions, which are difficult given single cases, Moro and colleagues (Valentina Moro et al., 2008) conducted a large, multicase study in which they investigated "body agnosia" in 28 patients. Using a two-choice match-to-sample task, featuring bodies, body parts, faces, and objects, they showed that damage to areas surrounding the middle temporal gyrus and inferior temporal sulcus (i.e., the location of the EBA) typically resulted in the highest reduction of performance. Further, they found a slight right hemisphere bias for this effect. Additionally, damage to the areas surrounding the fusiform gyrus (i.e., the locations of the FBA), again with a right hemisphere bias. Those with damage to these areas occasionally, but not necessarily, showed deficits in face processing. Moreover, these patients with occipital-temporal damage only showed agnosia to body form, and not body action. The converse was found to be true for damage to frontal-parietal areas, implying a double dissociation for static body perception in the EBA and FBA.

Disease-state evidence for processing deficits for human body stimuli has additionally come from the prosopagnosia literature. Prosopagnosia, colloquially referred to as face blindness, is a rare condition in which patients suffer from deficits in facial processing, such as identification. Often this occurs at the result of trauma to or lesions of the occipital-temporal cortex (Landis et al., 1986; Levine & Calvanio, 1989; Meadows, 1974), such as in some of the cases noted by Moro and colleagues (Valentina Moro et al., 2008). As a result, these findings have implied a causal role for the FFA in face perception (Barton et al., 2002; Uttner et al., 2002). Given the inherent relation between face and body stimuli as well as the neighboring of the FFA and the FBA on the fusiform gyrus, it is plausible to assume that lesion-related face processing deficits may also yield similar deficits for bodies. However, the evidence is currently limited and somewhat contradictory.

Susilo and colleagues (Susilo et al., 2015) described a patient who had a large portion of their right ventral temporal lobe removed as the result of a arteriovenous malformation. Difficulty recognizing faces was one of the first symptoms this patient experienced before diagnosis and following excision. However, after excision of the right temporal lobe (and with it, the FFA and FBA), the patient was found to experience no deficits in body detection or sex, posture, identity, and expression discrimination. Somewhat conversely, Moro and colleagues (2012) examined a patient with bilateral damage to the ventral temporal lobes (including both fusiform gyri) as the result of a post-operative stroke. This patient showed reduced discrimination performance as well as reduced identification performance for both face and body stimuli, indicating a co-occurrence of prosopagnosia and body agnosia.

In rare cases, prosopagnosia does not result from any discernable cause. Such cases are often referred to as congenital or developmental prosopagnosia (Behrmann & Avidan, 2005; Le Grand et al., 2006; McConachie, 1976). In the majority of these cases, the patients do not show deficits to any other visual categories, including bodies (B. C. Duchaine & Nakayama, 2006; B. Duchaine & Nakayama, 2005; Susilo & Duchaine, 2013), although there have been reports of general object recognition deficits in developmental prosopagnosia (De Gelder et al., 1998; Farah, 1996). Recently, two recent studies have noted the presence of body agnosia in conjunction with developmental prosopagnosia. Righart and De Gelder (2007) examined four developmental prosopagnosia patients with normal object recognition in the context of an ERP study. They found that latencies for both faces and bodies were significantly more variable for prosopagnosia patients and that the magnitude of these ERPs was greatly reduced. Furthermore, they showed an absence of the typical inversion effect commonly seen in face ERP studies; whereas controls showed reduced amplitudes for inverted faces and bodies, inversion resulted in no significant variation in amplitude in three of the four patients tested. Biotti, Gray, and Cook (2017) examined a group of twenty patients with developmental prosopagnosia in a delayed match-to-sample paradigm using faces, bodies, body parts, and cars. On a group analysis level, patients with developmental prosopagnosia showed a generally reduced performance for bodies and body parts, with significant effects additionally being found for several individual cases. There additionally appeared to be a reduction in performance

for cars, though the magnitude of this effect was significantly smaller than bodies and was found in less individual cases.

Finally, recent studies have made use of TMS in an attempt to causally implicated apparent body selective regions in the processing of body stimuli. As the fusiform gyrus, and thus the FBA, does not sit adjacent to the skull, it is regarded as 'out of range' for typical TMS systems. As such, these studies have focused solely on the EBA. Urgesi, Berlucchi, & Aglioti (2004) employed a delayed match-to-sample task with body parts, face parts, and motorcycle parts while subjects underwent TMS of the right EBA. They found a performance reduction only in the body part condition when stimulation was applied to the right EBA. Pitcher and colleagues (2009) used a similar paradigm, but additionally examined stimulation of the right OFA and right LO complex. They found a triple dissociation for stimulation; OFA stimulation only reduced face performance, EBA stimulation only reduced body performance, and LO stimulation only reduced object performance. Urgesi and colleagues (2007) had subjects perform a delayed match-to-sample task for the poses of upright or inverted bodies while TMS was applied to the right EBA 150 ms post stimulus onset. They found that EBA stimulation reduced performance during the inverted but not the upright task, which was interpreted to show that the EBA was necessary for the processing of local but not global features of bodies. Finally, van Koningsbruggen, Peelen, and Downing (2013) had subjects detect people or cars in briefly presented scenes. When TMS was applied to the right EBA, they saw a reduction in d prime as well as an increased reaction time for people but not for cars, revealing the specificity of the EBA for body stimuli. Furthermore, the effects were noted when stimuli were presented in both left or right visual hemifields, indicating that while there is lateralization of the EBA, this doesn't correspond hemifield biases.

Taken together, there exists a fairly large body of evidence in line with the notion that both the FBA and the EBA play a causal role in the perception of human bodies. TMS evidence provides a fairly consistent line of evidence, specifically when considering the triple dissociation revealed by Pitcher and colleagues (2009). However, there is a degree of inconsistency in the lesion literature, both in the presence and absence of prosopagnosia. One potential explanation for this inconsistency the variable damage to white matter across lesion patients. It has been shown that there exist disturbances in both the functional

(Avidan & Behrmann, 2009; Lohse et al., 2016) and structural (Gomez et al., 2015; Thomas et al., 2009) connectivity of developmental prosopagnosia patients. Thus, one theory would be that the variation in both lesion and developmental prosopagnosia patients could be due to the preservation of essential white matter tracts that allow still-intact nodes of the face or body network to function.

1.4 Conclusions

This chapter has served to detail an extensive assortment of literature pertaining to the features and representational elements which underpin the perception of human bodies. Human behavior, as well as neural recording in humans and non-human primates, have yielded multiple lines of converging evidence, revealing robustness to low level features, tuning for high level components such as gender and identity, and strong evidence in favor of shape-based coding of body information. Furthermore, at least two cortical areas of both human and non-human primate have been implicated in body perception, each of which show a distinct feature tuning and potentially hierarchical organization. Moreover, lesion and TMS studies have served to establish a causal link between these areas and perceptual ability surrounding human body stimuli.

While a great deal of progress has been made on this subject, many open questions still remain. In the context of the following chapters, two fundamentally important areas will be explored which have been thus far underexplored. Firstly, more basic aspects of how independent body parts are represented and related to one another (e.g., via simple spatial relationships) will be investigated using both psychophysics and fMRI. Secondly, the representation of individual body parts within body-selective cortical regions will be explored using cutting edge, sub-millimeter fMRI methodology.

2. Visual adaptation selective for individual limbs reveals hierarchical human body representation

The spatial relationships between body parts are a rich source of information for person perception, with even simple pairs of parts providing highly valuable information. Computation of these relationships would benefit from a hierarchical representation, where body parts are represented individually. We hypothesized that the human visual system makes use of such representations. To test this hypothesis, we used adaptation to determine whether observers were sensitive to changes in the length of one body part relative to another. Observers viewed forearm/upper arm pairs where the forearm had been either lengthened or shortened, judging the perceived length of the forearm. Observers then adapted to a variety of different stimuli (e.g., arms objects, etc.) in different orientations and visual field locations. We found that following adaptation to distorted limbs, but not non-limb objects, observers experience a shift in perceived forearm length. Furthermore, this effect partially transferred across different orientations and visual field locations. Taken together, these results suggest the effect arises in high level mechanisms specialized for specific body parts, providing evidence for a representation of bodies based on parts and their relationships. Portions of this work were presented at the 2017 Vision Science Society (VSS) annual meeting (Bratch, Engel, et al., 2017), and this work has been accepted for publication in the Journal of Vision.

2.1 Introduction

The perception of human bodies is critical for social behavior (cf. Hu et al., 2020). The determination of the spatial relationships between body parts, referred to here as pose estimation, is a particularly important source of information for a range of visual functions, including the recognition and interpretation of the actions of others. Because of its practical importance, the computational problem of pose estimation has recently received considerable attention (cf .Cao et al., 2019; Chen & Yuille, 2014). A key question has been how to represent body structure for efficient and robust pose computation. One approach is to represent body structure in terms of parts (e.g. hands, elbow, shoulder, etc.) constrained by their plausible spatial relationships (distance and angle). Visual computation then proceeds hierarchically first integrating low-level features into parts, then to part relationships, and finally to whole bodies (Chen & Yuille, 2014; Park et al., 2018).

Human neuroimaging studies have provided evidence consistent with this hierarchical computation, specifically identifying distinct representations for body parts vs. whole bodies. Studies of body selective cortical areas have demonstrated a cortical region sensitive to individual parts, but insensitive to their configuration/spatial relationships (the extrastriate body area or EBA, (Downing et al., 2001)). Conversely, research has found a region which is sensitive to the configuration of body parts as a whole, but not necessarily the individual parts themselves (the fusiform body areas or FBA, (Peelen & Downing, 2005)). Such findings are consistent with the idea of an underlying neural mechanism for pose estimation based on a hierarchical organization of parts and relationships.

Recently, a number of investigations have used adaptation to explore perceptual representations of bodies. Adaptation, the process by which the visual system routinely updates its sensitivity to visual features, has been shown to operate at many levels of visual processing, from low-level features such as orientation, spatial frequency and color, to higher level properties including viewpoint and shape, and class-specific attributes such as inter-eye distance, identity, and gender of faces (cf. Blakemore & Campbell, 1969; Kaliukhovich & Vogels, 2016; Webster, 2015 for a review). Adaptation studies have also revealed interactions between lower and higher-level representations, possibly involving unidirectional and bidirectional signaling within the visual hierarchy (He et al., 2012; X.

Liu & Engel, 2020; H. Xu et al., 2008). While previous adaptation studies on body representation have revealed effects along high level dimensions including gender (Ghuman et al., 2010; Kessler et al., 2013; Palumbo et al., 2013, 2015; Weigelt et al., 2010) as well as viewpoint (Lawson et al., 2009) size and weight (Ambroziak et al., 2019; Brooks et al., 2018; Glauert et al., 2009; Winkler & Rhodes, 2005), the hierarchical nature of body perception remains underexplored using adaptation.

Here, we investigated the hierarchical nature of body perception using adaptation. Specifically, we tested for the existence of distinct adaptable, high-level representations of individual body parts. We generated a set of forearm/upper arm limb pairs where the forearm had been lengthened or shortened. Observers viewed these arms and judged whether their forearms appeared too long or too short before and after adapting to arms, and other similar but semantically distinct objects, across different stimulus orientations and visual field locations. If adaptation arises from high level body-part specific mechanisms, then it should transfer across visual field orientations and locations but not transfer to visually similar images of other body parts and non-body objects.

2.2 Experiment 1

Neurons that represent high-level visual features have receptive fields whose responses are relatively invariant to low-level manipulations such as retinal position and orientation (Gross et al., 1969). If visual adaptation causes changes in the response properties of such neurons, then effects of adaptation should transfer to different orientations. If, on the other hand, adaptation arises from neurons in early visual areas, where receptive fields are sharply tuned for orientation, then its effects should be relatively orientation-specific. The goal of Experiment 1 was to distinguish between these alternatives by measuring the extent to which adaptation to body parts transfers to other orientations in the visual field. Observers judged forearm length across two different orientations and subsequently adapted to a shortened forearm in one orientation. The shift in perceived forearm length was then assessed across the adapted and non-adapted orientations.

2.2.1 Materials & Methods

2.2.1.1 Observers

Ten observers (7 male; 3 female) participated in Experiment 1. All observers had normal or corrected to normal vision, were naive to the purpose of the experiment, and provided written informed consent. The experiment was approved by the Institutional Review Board of the University of Minnesota and procedures conformed to the Declaration of Helsinki.

2.2.1.2 Apparatus

Stimuli were presented on a 24" NEC LCD display (resolution: 1920 x 1080 pixels; size: 52.7 x 29.6 cm; 55.6 x 33.0 degrees of visual angle from a viewing distance of 50 cm). A chin rest was used to maintain a constant viewing distance and head position. Stimuli were generated using MakeHuman 1.1.1 and Blender 2.79 and were presented within the Matlab programming environment (Version R2016a) using in-house software and the Psychophysics Toolbox (Brainard, 1997).

2.2.1.3 Stimuli

The images used for Experiment 1 were synthesized from an upper arm and forearm extracted from an average proportioned MakeHuman avatar with a skeletal rig. A custom rigging environment in Blender was used to generate individual images from this limb set. For all stimuli, the elbow joint of this limb set was positioned at approximately 90 degrees (see Figure 2.1).

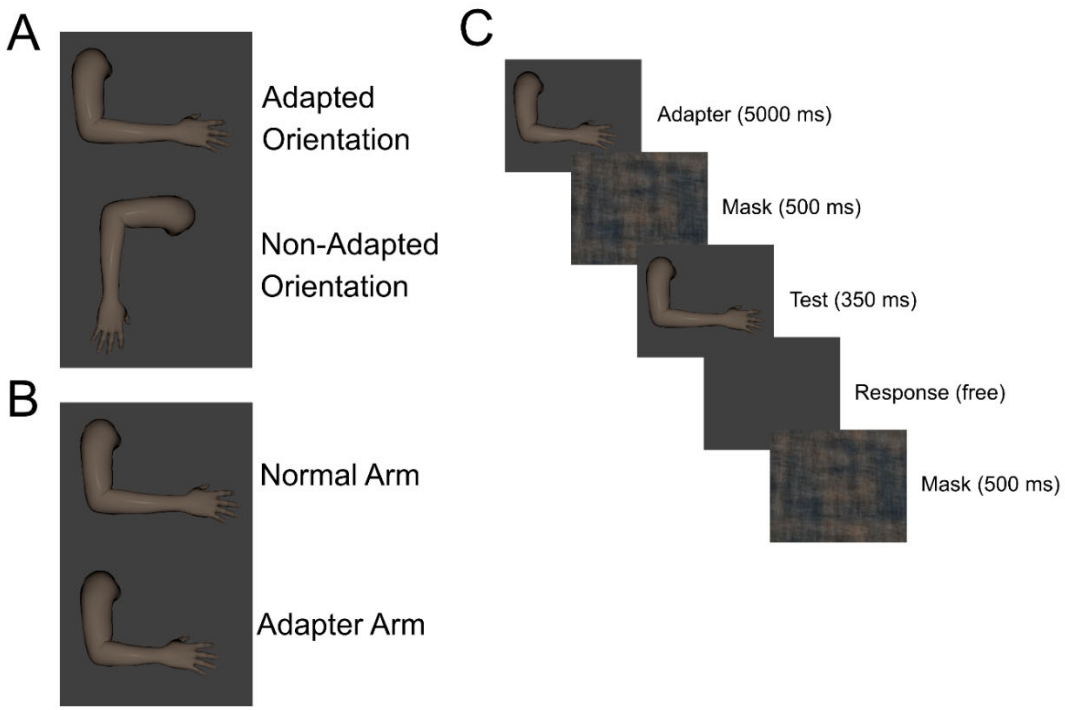

Figure 2.1. Overview of the stimuli and procedure used in Experiment 1. A. The two orientations of the test stimuli. B. Examples of the normal length forearm and 75% length forearm used as the adapter. C. Procedure used for assessing adaptation in Experiment 1. Following an initial adaptation period, observers saw a "top-up" adapter image (5000 ms) prior to each test image (350 ms) and response period (free). The test image was flanked by a phase scrambled mask image (500 ms).

To manipulate the relative proportions of the upper arm to the forearm ("physical arm length"), renderings were created by scaling the bone comprising the forearm (yielding a percent change of physical length). Seven total images were generated by setting the scale factor from 85% to 115% of veridical at 5% increments (7 total bins, shortest forearm: 9.4 degrees of visual angle; longest forearm: 12.0 degrees of visual angle). In Experiment 1, observers viewed these stimuli at two orientations: with the hand pointing to the right of the display (rightward, Figure 2.1a) or with the hand pointing to the bottom of the display (downward, Figure 2.1a). During adaptation, observers viewed an arm with a shortened forearm, where the bone had been scaled to 75% (forearm: 8.5 degrees of visual angle, Figure 2.1b). This adapter was only presented in the rightward orientation. All images were presented in color on a low luminance gray background.

2.2.1.4 Procedure

Observers were tested individually in a dedicated testing room. Prior to the start of the experiment, observers were informed that an image of an arm would appear in the center of the display on each trial and that, on a given trial, the forearm would appear either lengthened or shortened. They were instructed to respond, using a computer keyboard, whether the presented arm on a given trial appeared to be "too long" or "too short". Observers were allowed to move their eyes freely during the experiment.

A first block of trials measured perceived arm length in neutral, "baseline" conditions. An overview of the procedure can be seen in Figure 2.1c. On a given baseline trial, an arm image appeared in the center of the display for 350 ms, followed by a blank gray screen, during which observers indicated their response. After a response was collected, a mask consisting of a phase scrambled arm stimulus was presented for 500 ms prior to the start of the next trial. Baseline performance was assessed for both arm orientations in an intermixed block. Twenty five trials were presented for each of the seven physical arm lengths at each orientation for a total of 350 trials.

A second block of trials measured perceived arm length following adaptation. Observers adapted by viewing the image of the arm with a shortened forearm, presented in the center of the display, for 5 minutes. As in baseline assessment, observers were allowed to move their eyes freely – they were not instructed to fixate. Perceived arm length was then measured while using a "top-up" paradigm to maintain adaptation. The trial structure was identical to baseline assessment, with the addition of a 5 second adapting image presentation followed by a 500 ms phase scrambled mask preceding the test stimulus presentation on each trial. As in the baseline block, 25 trials were presented for each physical arm length at each orientation, in a mixed block of 350 trials.

2.2.1.5 Data Analysis

For each observer, we first calculated the proportion of "too long" responses for each of the seven physical arm lengths. This was done independently for each orientation in both the baseline and post adaptation conditions. The resulting data was then fitted with

a logistic function, enabling us to determine the point of subjective equality (PSE), defined as the physical forearm length estimated to produce "too long" responses on 50% of trials.

The average response rate across observers and associated fits are shown in Figure 2.2. A leftward shift in the PSE on the physical arm length axis indicates an elevation in the number of “too long” responses, and thus indicates that the previously "normal" arm appeared too long following adaptation to the shortened forearm. Finally, we computed the shift in PSE as PSE at Baseline minus PSE at Post-test.

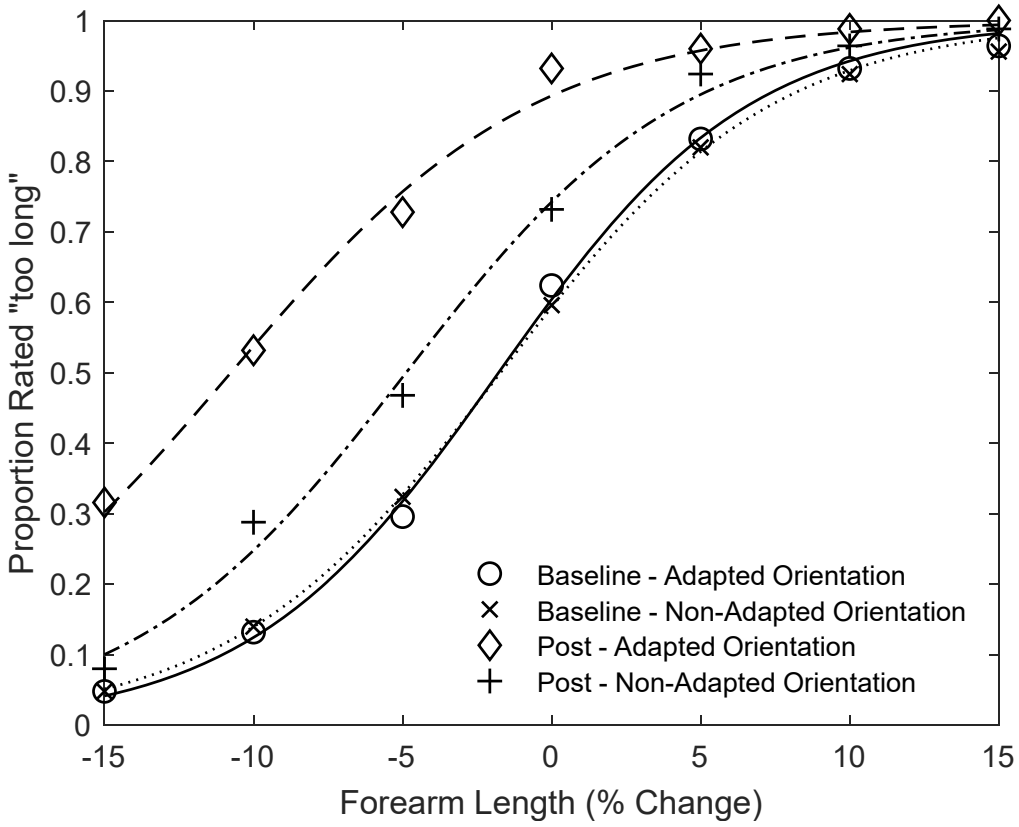

Figure 2.2. The average response rate and psychometric fits across observers (N = 10) in the baseline and post adaptation conditions in each orientation. The proportion of trials rated as “too long” is displayed as a function of forearm length.

A linear mixed effects model, constructed within the R programming environment using the LMER package (Bates et al., 2015), was used to assess the results of Experiment

1. The model was constructed using the PSE values derived from the psychometric fits described in the previous paragraph. Fixed effects included adaptation (baseline vs. post), orientation (adapted vs. non adapted), and the interaction between adaptation and orientation. Random effects included random slopes and intercepts for each individual observer. The fixed effects of the model were then analyzed using F-tests in the context of a Type III analysis of variance (ANOVA) using the car package (Fox & Weisberg, 2019). Additionally, specific linear contrasts were analyzed with F-tests using the phia package (De Rosario-Martinez, 2015) and p-value correction via the Holm-Bonferroni method.

2.2.2 Results

To examine the impact of adaptation on perceived arm length, we measured the points of subjective equality (PSEs; forearm lengths that appeared "normal") before and after exposure to the shortened forearm (see Figure 2.2 and Methods).

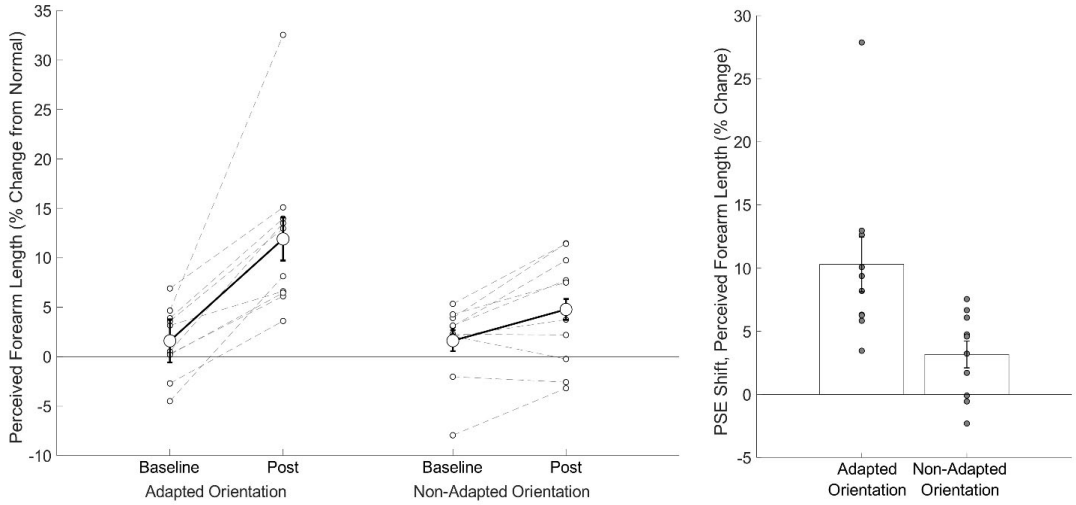

Figure 2.3. Results for Experiment 1. Left. Average (large, open circles connected by dark solid lines) and individual (small, open circles connected by dashed lines) PSEs in each orientation before and after adaptation. Right. PSE shifts (PSE at Baseline minus PSE at Post test) for each orientation, with individual data shown for each observer (small, gray circles). Error bars represent standard error of the mean (SEM).

Following adaptation to a shortened forearm, observers perceived test arms as being longer, and there was a trend for this effect to transfer across orientations. Figure 2.3 (left) displays PSEs for each individual observer (small gray circles connected by dashed lines) as well as the mean across observers (large open circle connected by solid lines). Figure 2.3 (right) summarizes these results in terms of the mean PSE shift from baseline for each orientation. For the adapted orientation, the perceived forearm length shifted by approximately 10%, while for the non-adapted orientation perceived forearm length shifted by approximately 3%. An ANOVA revealed significant main effects of adaptation [$F(1, 9.43) = 21.07$, $p < 0.01$)] and orientation [$F(1, 9.26) = 5.57$, $p < 0.05$)], as well as a significant interaction effect between adaptation and orientation [$F(1, 18) = 19.88$, $p < .001$)]. Planned contrasts confirmed a significant shift from baseline for the adapted orientation [$F(1, 13.93) = 38.01$, $p < 0.001$)] and a trend in the non-adapted orientation [$F(1, 13.93) = 3.58$, $p < 0.1$)], as well as a significant difference between the adapted and non-adapted PSE shifts [$F(1, 9) = 19.88$, $p < 0.01$)].

2.3 Experiment 2

The goal of Experiment 2 was to provide stronger evidence that adaptation to arm length could be attributed to higher level representations. Observers once again made judgments about forearm length but did so before and after adapting to three different adapter types, which varied between high and low level: an arm, a leg, and a pipe segment. To provide a more robust test for high-level representations, stimuli were presented mirrored about either side of a central fixation cross. If adaptation is based on relatively high-level mechanisms, as opposed to retinotopic-level mechanisms, then the effects should be at least partially invariant to change in arm orientation as a function of mirroring and to the overall change in retinotopic position. Furthermore, if the effect is in fact based on high-level mechanisms, the various adapter classes would enable us to determine if the effects arose from general object/shape mechanisms (in the case of transfer from the pipe adapter), general body processing mechanisms (in the case of transfer from the leg adapter), or limb specific mechanisms (in the case of transfer only from the arm adapter).

2.3.1 Materials & Methods

2.3.1.1 Observers

Twenty-four observers (9 male; 15 female) participated in Experiment 2. All observers had normal or corrected to normal vision, were naive to the purpose of the experiment, and provided written consent. The experiment was approved by the Institutional Review Board of the University of Minnesota and procedures conformed to the Declaration of Helsinki.

2.3.1.2 Apparatus

Stimuli were presented on the same monitor used in Experiment 1, but with the viewing distance changed to 60 cm (size: 52.7 x 29.6 cm; 47.4 x 27.7 degrees of visual angle). A chin rest was used to maintain a constant viewing distance. Stimulus generation and presentation was performed using the same methods in Experiment 1.

2.3.1.3 Stimuli

Experiment 2 used the same arm images as Experiment 1 (shortest: 7.8 degrees of visual angle; longest: 10 degrees of visual angle). However, while a free-viewing paradigm was used in Experiment 1, stimuli in Experiment 2 were presented on either side of a central fixation cross (Figure 2.4b).

In addition to the shortened arm adapter used in Experiment 1, we used two additional adapters: a shortened leg and a copper pipe (Figure 2.4a). The shortened leg adapter was generated using the same procedure as the arm adapter; the lower leg bone was scaled to 75% of its original length. Additionally, the rendering camera distance was adjusted such that the leg subtended approximately the same visual angle as the shortened arm adapter. The copper pipe adapter was created such that it had similar mid-level geometric properties (same angular size and part length ratios) to the arm and leg adapters, but with small shape differences (e.g. pipe joints) consistent with a very different high-level semantic category. All adapters subtended approximately 7.1 degrees of visual angle in length.

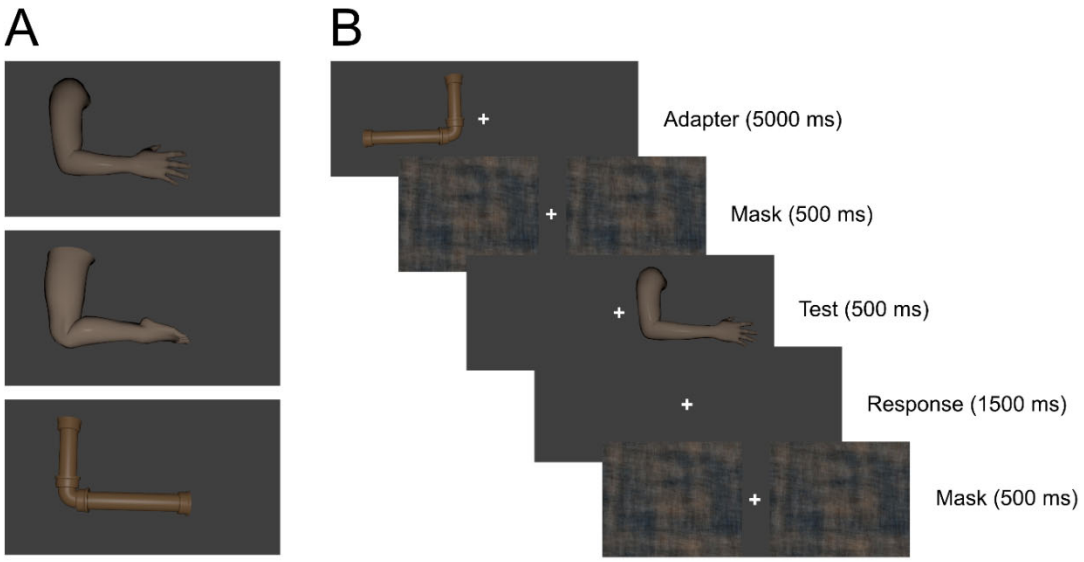

Figure 2.4. Overview of the stimuli and procedure used in Experiment 2. A. The three adapter types (arm, leg, and pipe) used in Experiment 2. B. Procedure used for assessing adaptation in Experiment 2. Adapter images were presented in one hemifield (5000 ms) prior to each test trial (500 ms) and response period (1500 ms). The test image was flanked by a phase scrambled mask image (500 ms).

2.3.1.4 Procedure

Each observer participated in 3 sessions. Each session was similar to those in Experiment 1, but used a different adapter (arm, leg, or pipe). Order of the adapter was counterbalanced across observers. The adapter in this experiment was presented either to the left or right of fixation, and this factor was also counterbalanced across observers.

Task and response instructions were the same as in Experiment 1, with four main differences: 1) observers were instructed to maintain fixation on the central cross throughout the duration of the experiment. 2) Observers were given a fixed duration 1500 ms interval in which to respond before the mask image was presented at the beginning of the next trial. 3) Test images and adapters were shifted away from the central cross, either to the left or right, such that the edge of the stimulus was approximately 0.5 degrees away from the cross center. 4) There was no initial adaptation period. Adapting images were presented only in the 5 sec "top-up" intervals at the start of each trial. Additionally, prior to beginning the baseline portion of the experiment on the first session, observers were

familiarized with the stimulus set and the presentation paradigm. Observers also completed 50 practice trials at the start of their first session.

Baseline perception of arm length was measured at the start of each session, in a block of 210 trials containing 15 trials at each of the 7 physical arm lengths presented in each hemifield. Trial order within this 210 trial block was randomized. A second 210 trial block in each session then measured perceived arm length in the presence of an adaptor.

2.3.1.5 Data Analysis

Quality metrics were used in Experiment 2 to assess the viability of data for each observer. Specifically, an observer who responded to less than 90% of trials or who's psychometric function fits produced a slope less than or equal to 0 were excluded from the final analysis. Of the 24 observers who participated in Experiment 2, 22 observers met the predefined data quality criteria and were entered into the analysis.

The analysis of Experiment 2 used the same methods and software packages as Experiment 1. In short, the 50% PSEs were derived from logistic fits (see Figure 2.5), entered into a linear mixed effects model, and analyzed using an ANOVA and F-test linear contrasts. Fixed effects included adaptation (baseline vs. post), hemifield (adapted vs. non adapted), and adapter (arm vs. leg vs. pipe) and random effects included random slopes and intercepts for each individual observer.

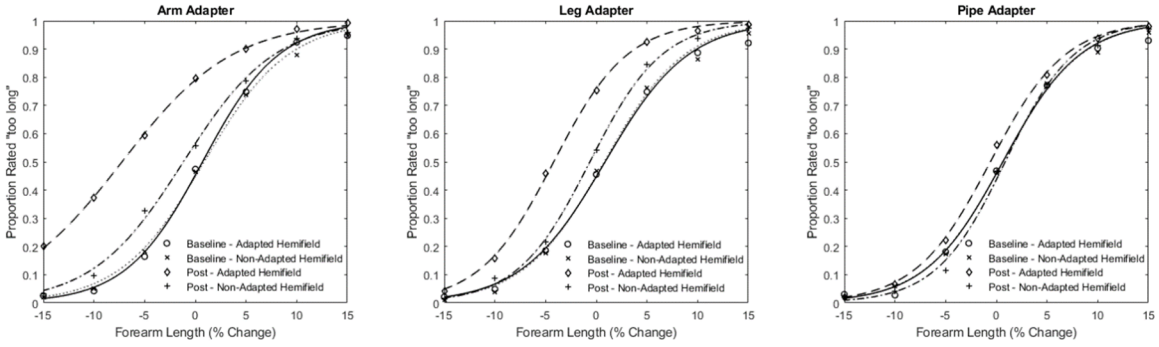

Figure 2.5. The average response rate and psychometric fits across observers in the baseline and post adaptation conditions in each hemifield for each adapter type. The proportion of trials rated as "too long" is displayed as a function of forearm length.

2.3.2 Results

As in Experiment 1, we assessed adaptation by comparing the PSEs when perceiving arm length before and after adaptation. This was assessed across the three adapter types (shortened arm, shortened leg, and pipe) and both hemifields (adapted and non-adapted). Figure 2.6 summarizes these results in terms of the mean PSE shift from baseline for each adapter in each hemifield.

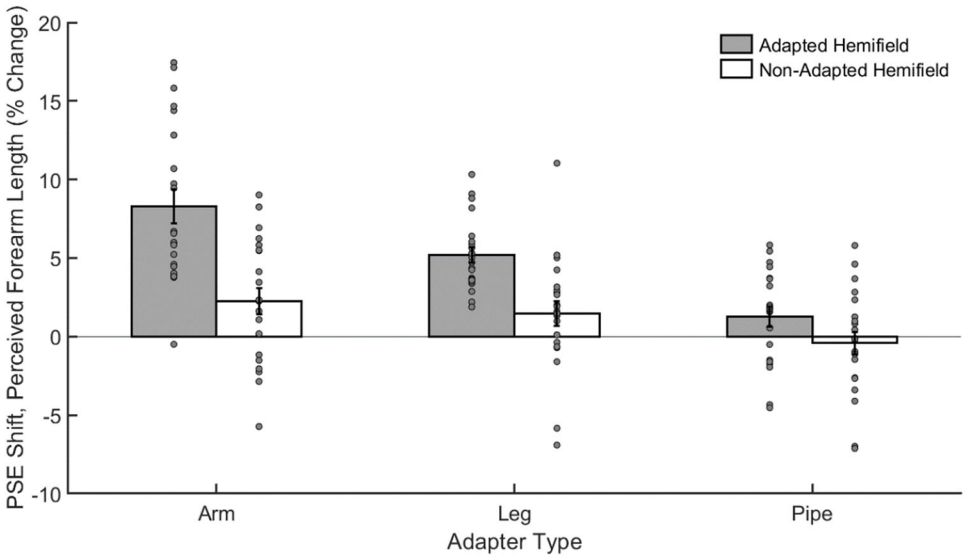

Figure 2.6. Results of Experiment 2. The average PSE shift (PSE at Baseline minus PSE at Post test) is shown for each adapter type in the adapted (gray bar) and non-adapted (white bar) hemifields. Datapoints for individual observers are shown as gray dots. Error bars represent SEM.

Adaptation was strongest for the arm adapter, intermediate for the leg adapter, and weakest for the pipe adaptor, and in all cases was stronger for the adapted hemifield than the non-adapted hemifield. The ANOVA revealed significant main effects of adaptation [$F(1, 21.00) = 38.47$, $p < 0.001$)], hemifield [$F(1, 21.01) = 5.13$, $p < 0.05$)], and adapter type [$F(2, 21.00) = 4.50$, $p < 0.05$)]. Furthermore, there were significant two-way interactions between hemifield and adaptation [$F(1, 146.99) = 55.47$, $p < 0.001$)], adaptation and adapter [$F(1, 146.99) = 30.10$, $p < 0.001$)], and hemifield and adapter [F(1,

146.99) = 7.30, $p < 0.001$)], as well as a significant three-way interaction between hemifield, adaptation, and adapter type [$F(1, 146.99) = 6.07$, $p < 0.01$)].

When adapting to a shortened forearm, observers perceived test arms in both the adapted hemifield and non-adapted hemifield as being significantly longer [adapted PSE shift = 8.29, $F(1, 94.42) = 121.97$, $p < 0.001$); non-adapted PSE shift = 2.24, $F(1, 94.42) = 8.86$, $p < 0.05$)]. Adaptation was greater in the adapted than non-adapted hemifields [PSE shift difference = 6.06, $F(1, 147) = 46.51$, $p < 0.001$)].

Adaptation from viewing a shortened leg produced a markedly smaller effect on the arm in the adapted hemifield than when adapting to an arm [PSE shift difference = 3.11, $F(1, 147) = 12.22$, $p < 0.01$)], though the former was significantly above zero within the adapted hemifield [PSE shift = 5.19, $F(1, 94.42) = 47.73$, $p < 0.001$)]. Contrary to the arm adapter, observers did not perceive arms as significantly longer in the non-adapted hemifield following adaptation to the shortened leg [1.47% PSE shift, $F(1, 94.42) = 3.84$, $p = 0.16$)], and this shift was not significantly different from the non-adapted hemifield effect seen with the arm adapter [0.77% PSE shift difference, $F(1, 147) = 0.74$, $p = 0.39$)]. As with arm, the effect was significantly larger in the adapted vs. non-adapted hemifield [PSE shift difference = 3.72, $F(1,147) = 17.51$, $p < 0.001$].

Finally, when adapting to the pipe, observers experienced no significant change in their perceived arm length in either the adapted hemifield [1.27 PSE shift, $F(1, 94.42) = 2.84$, $p = 0.19$)] or in the non-adapted hemifield [-0.42 PSE shift, $F(1, 94.42) = 0.31$, $p = 0.58$)], though there was a trend between the two hemifields [1.69 PSE shift difference, $F(1,147) = 3.60$, $p < 0.1$]. The observed effects were significantly lower than the effect for the arm adapter in both the adapted hemifield [7.03 PSE shift difference, $F(1,147) = 62.60$, $p < 0.001$] and non-adapted hemifield [2.66 PSE shift difference, $F(1,147) = 8.94$, $p < 0.01$]. The effect was also significantly lower for the leg adapter in the adapted hemifield [3.92 PSE shift difference, $F(1,147) = 19.48$, $p < 0.001$] and trend in the non-adapted hemifield [1.89 PSE shift difference, $F(1,147) = 4.53$, $p < 0.1$].

We also constructed an additional model, including hemifield of adaptation (left versus right). Here, we observed a trend for a main effect of hemifield of adaptation [$F(1,139.99) = 3.39$, $p < 0.1$)], but no associated interactions. Appendix Figure A1.1 shows division of the effects as a function of hemifield of adaptation. Given prior literature of

lateralization of body selective cortex (Downing et al., 2001; Peelen & Downing, 2005; Willems et al., 2010), future work is needed to investigate how this plays a role in these adaptation effects.

2.4 Discussion

The goal of the present study was to test for distinct high-level representations of body parts. The results across both experiments are consistent with high-level, body-part specific mechanisms that could be used to compute spatial relationship between parts.

Our key prediction was that adaptation should transfer across features for which higher-level neurons are less well-tuned and lower-level neurons are more tightly tuned, specifically retinal orientation and location. In Experiment 1, we found that when adapting to shortened forearms, observers perceived forearms as significantly longer in the adapted orientation. A trend in this direction was also observed in the non-adapted orientation, albeit with a significantly reduced magnitude relative to the adapted orientation. This effect was strengthened in reliability in Experiment 2; a significant adaptation effect was measured in both the adapted and non-adapted visual hemifield when observers adapted to a shortened forearm (once again, with a reduction in magnitude in the non-adapted hemifield). Together, these findings suggest that the effect is, at least in-part, arising from non-retinotopic, high-level neurons.

Another prediction was that adaptation should be greater for the same body part as the adapter than for other visually similar body parts and objects. Experiment 2 revealed that when observers adapted to legs with shortened lower legs, they once again perceived arms as longer, but the magnitude of the effect was reduced relative to arms in the adapted hemifield, and not significant in the non-adapted hemifield. In addition, no significant shifts in perception were found when observers adapted to a pipe adapter with an aspect ratio matched to the shortened forearm and leg adapters. Such a result suggests that not only does the effect observed in both Experiments 1 and 2 appear to have a high level component, but that the effect can even be differentiated at the level of specific body parts, indicating there maybe underlying mechanisms devoted to the processing of limb subsets.

Our findings and interpretations, specifically with respect to lower level, retinotopic phenomena, are consistent with other work on body adaptation, which has mainly focused on whole body adaptation effects. Past findings have shown that, for instance, adaptation to body size/weight could not be explained simply by adaptation to basic shapes of a similar aspect ratio (Hummel, Grabhorn, et al., 2012). Furthermore, these types of adaptation effects appear to transfer to different viewpoints as well as to different body poses (Sekunova et al., 2013), suggesting the engagement of body-specific mechanisms rather than low-level, retinotopic mechanisms.

Further work has also demonstrated that body size/weight effects transfers across identity (Hummel, Rudolf, et al., 2012). Such a finding helps to potentially elucidate a general location of these mechanisms within the visual hierarchy. While perceptual effects pertaining to basic body shape and size likely arise from a high level, body specific mechanisms, such mechanisms are likely distinct from and exist earlier in the visual hierarchy than mechanisms which process identity.

Consistent with this idea, recent evidence in the face perception domain has found that in both humans (Grill-Spector et al., 2017; D. Y. Tsao et al., 2008) and non-human primates (Freiwald & Tsao, 2010; Meyers et al., 2015), sensitivity to identity appears to increase throughout the progression in the visual hierarchy, peaking near the top (e.g., anterior temporal lobe), whereas sensitivity to basic within-category part relationships peaks earlier on (e.g., medial temporal lobe). In line with these intuitions on hierarchical location, fMRI investigations of the body size/weight adaptation effects have further revealed that higher level, body-selective visual cortical regions (e.g., EBA, FBA) but not lower level regions (e.g., V1) nor very high level regions (e.g., anterior temporal) appear to be involved with body size/weight adaptation (Hummel et al., 2013).

However, our work not only suggests an engagement of body-specific mechanisms but suggests one which appears to be sensitive to specific body *parts*. Consistent with our findings, as well as the fMRI findings noted above, recent studies have been able to further elucidate the level of representation of body parts within body selective regions of visual cortex. Using fMRI, it has been demonstrated that there are regions within lateral occipital cortex that have selective responsiveness to individual body parts (Orlov et al., 2010). Furthermore, it has been shown that neural activity within body selective visual cortical

areas yields distinct patterns of activity for individual body parts, suggesting fine grain representation for individual body parts within body selective cortex (Bracci et al., 2015).

2.5 Conclusions

Our results provide further evidence of specific high level representations for body stimuli and argue for a hierarchical arrangement in the representation of this stimulus class. The effects of adaptation appear to not only rely on representations specific to body stimuli, but mechanisms which are sensitive to the spatial relationships between individual parts. Future work should be able provide further detail into the specificity of this representation, as well as investigate the neural basis of the effect and its consistency with recent findings in the fMRI literature.

3. Sensitivity to subordinate spatial relationships in body selective visual cortex

From basic survival to engaging in complex social interactions, the ability to quickly identify and parse the spatial relationships between human body features is both critical and one which human observers perform with relative ease. Two regions which underpin the perception of human bodies have been identified in human visual cortex: the extrastriate body area or EBA (Downing et al., 2001) and the fusiform body area or FBA (Peelen & Downing, 2005). However, how these cortical areas represent spatial relationships between body features is a question which has typically been examined using full body context. Recently, computer vision work has suggested that even basic, pairwise spatial relationships are sufficient for making complex inferences about whole body spatial relationships (Chen & Yuille, 2014). Here, we examined whether human body-selective cortical areas are sensitive to these basic relationships. We used fMRI to measure neural responses to pairs of body parts that were presented either in their "normal" connected positions or rotated within the apertures to induce the percept of disconnected arm parts. We found that both the right EBA and right FBA were sensitive to these stimulus manipulations, suggesting that body-selective cortical areas represent these basic, subordinate spatial relationships. Portions of this work were presented at the 2017 Society for Neuroscience annual meeting (Bratch, Burton, et al., 2017) and 2018 Vision Science Society (VSS) annual meeting (Bratch, Engel, et al., 2018).

3.1 Introduction

Recognizing human figures and identifying their poses is an important function of our visual systems. However, recognizing bodies and their poses in images is difficult due to factors such as the wide range of joint articulations, the frequency of self-occlusion (where not all body parts are visible), and high degree of variation in appearance. These difficulties are compounded in multi-person images, where the body part from one person projects close to that of another person. Accordingly, the visual system must employ strategies for dealing with image ambiguity, and one potential mechanism to resolve these ambiguities is to use information about probable spatial relationships between pairs of parts.

Computer vision studies have shown that natural images of a single body part can be highly predictive of the location, orientation, and identity of another part. This allows sets of pairwise relationships to be sufficient for accurate whole body pose estimation without explicit recognition of the many higher order relationships of body parts (Chen & Yuille, 2014). For example, recovering the pairwise spatial relationships between hand and wrist, wrist and forearm, forearm and upper arm, etc., can allow for recognition of arm pose without explicitly considering all combinations of the relative positions of each individual part. In addition, computing pairwise relationships can also be used to detect whether two parts are connected or not in multi-person images (Chen & Yuille, 2014; Insafutdinov et al., 2016).

Here we examined whether the human brain encodes these pairwise relationships between body parts. In recent years, two anatomically distinct regions of visual cortex have been identified as selective for static human body stimuli: the extrastriate body area (EBA, (Downing et al., 2001)) and the fusiform body area (FBA, (Peelen & Downing, 2005)). While previous studies have investigated these areas' sensitivity to spatial relationships between body parts, they have only done so by coarsely manipulating the spatial relationships (e.g., scrambling vs whole) using whole body stimuli and binarized stimulus categories (Bauser & Suchan, 2015; Brandman & Yovel, 2016). Thus, it remains unknown the extent to which these body-selective areas are sensitive to spatial relationships on a more local, fine-grained scale (e.g., to pairs of parts) and across smaller, parametric variations in these relationships.

Specifically, we examined whether body-selective cortical areas show sensitivity to the configuration between pairs of arm parts. Observers were presented with two images, one of a hand with wrist, and a second of an elbow, seen through two circular apertures (Figure 3.1). The spatial configuration of the parts was parametrically manipulated by varying the relative orientations of the images, resulting in varying probability of perceived connectedness between the parts. We predicted that responses in regions sensitive to body-part configurations would be modulated by the cues to connectedness in the image, which, notably, are very small in terms of low-level image features present in each patch. We additionally tested whether such sensitivity to spatial relationships depended on task, by having observers perform two separate tasks: 1) a stimulus relevant task, in which observers judged whether the arm parts appeared connected or disconnected or 2) a stimulus distracted task, in which observers performed a 1-back task based on the angle of the arm parts. Responses were then assessed across the varying degrees of stimulus orientation and as a function of task in body-selective cortical regions identified using independent localizer scans, as well as stimulus regions in early visual cortex (V1, V2, and V3).

3.2 Methods

3.2.1 Observers

Fourteen observers with normal or corrected-to-normal vision participated in the present study. Observers provided written informed consent and participated in a protocol approved by the University of Minnesota Institutional Review Board and in accordance with safety guidelines for MRI research from the Center for Magnetic Resonance Research. Two observers were excluded from the analysis due to data acquisition issues.

3.2.2 Stimuli & Paradigm

To localize body areas, we contrasted responses to images of bodies and chairs using the procedures of Taylor, Wiggett, & Downing (2007). Grayscale images of chairs and bodies with heads cropped out were presented in the framework of a block design. Images were presented on a gray background for 350 ms, separated by a 450 ms inter-

stimulus interval, within a 15 sec block. Observers viewed a total of 21 blocks: eight blocks of bodies, eight blocks of chairs, and five "baseline" blocks in pseudo-random order. During the stimulus blocks, observers performed a 1-back task and fixated on a central cross throughout the run.

Three additional runs were used to localize the retinotopic representation of the stimulus apertures used in the main experiment. While maintaining fixation, observers viewed contrast reversing checkerboard patterns (8 Hz) in the hand/wrist aperture (left of fixation) and the elbow aperture (right of fixation). A block design was used, consisting of 18 blocks with a 12 second block length. Three blocks of each stimulus area were presented per run, each being preceded by a fixation block.

In the main experiment, observers viewed apertured images derived from a single 500 x 500 pixel photo of a left arm, with the elbow bent at approximately 90 degrees (Figure 3.1). A color image was converted to grayscale and two 100 pixel circular apertures (4.1 degrees of visual angle in diameter) were centered over the hand and the elbow. To manipulate stimulus alignment, six images of apertured stimuli were generated. In one condition, the image fragments in the two apertures were properly aligned, while in the remaining five conditions the pixels in each aperture were parametrically varied by rotating each aperture counter-clockwise by a specified amount (from 1^{o} to 5^{o}, in 1^{o} increments; see Figure 3.1). Outside the apertures, the image was uniform gray.

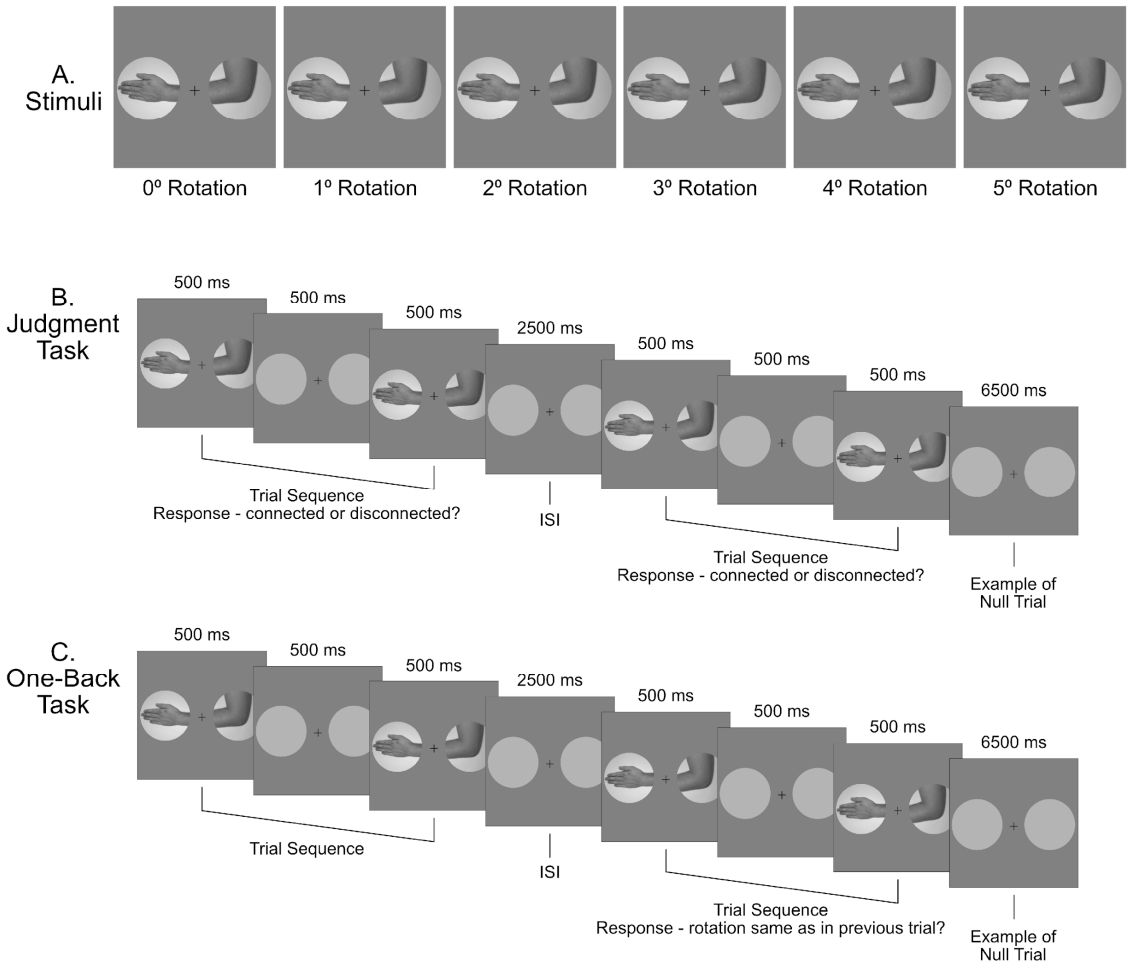

Figure 3.1. Stimuli and Task. A) The 6 stimuli created using an apertured image of an arm and rotating both apertures counter-clockwise at 1 degree increments. B) The Judgment Task. Observers saw a flickered presentation of each stimulus and responded whether a stimulus on a given trial appeared "connected" or "disconnected". C) The One-Back Task. Observers saw a flickered presentation of each stimulus and responded whether the angle of the arm components within the apertures were the same as in the previous trial.

Images in the main task were presented in a rapid event-related design, the order of which was optimized using an M-sequence (Buracas & Boynton, 2002; T. T. Liu, 2004). During each trial, the aperture image was presented twice for 500 ms, separated by a 500 ms interval, and followed by a 2500 ms inter-trial interval. To strengthen the impression

of viewing a single connected arm through apertures, the apertures were filled with gray at the average intensity of the arm stimulus during the ISIs and ITIs. During judgment task runs, observers judged whether the hand and elbow appeared "connected" (i.e., as part of the same arm) or "disconnected" (i.e., as two distinct arm parts). During one-back task runs, observers judged whether the orientation of the parts was the same as in the previous trial. Responses were collected using a fiber optic button box. Each observer completed 6 runs of each task. Throughout each run, observers fixated a small cross centered between the apertures.

3.2.3 Apparatus & Acquisition

Data were acquired on a Siemens Prisma 3T scanner (Siemens, Erlangen, Germany), equipped with a 32-channel head coil, at the University of Minnesota's Center for Magnetic Resonance Research. Functional runs were acquired using a T2* weighted, slice accelerated multiband (J. Xu et al., 2013) echo-planar imaging sequence (TR = 2 s, TE = 30.4 ms, flip-angle = 80^o, matrix = 86 x 86, multiband Factor = 3, FoV = 208 x 208 mm, voxel size = 2.4 mm isotropic, phase encoding direction = AP) in 60 interleaved slices covering the whole brain. A T1 weighted anatomical data set was also collected (MP-RAGE, 1mm isotropic, (Mugler & Brookeman, 1990)) for each observer. At the end of each session, a 15-volume reverse phase encoded EPI sequence was collected for the purpose of spatial distortion correction.

Stimuli were back-projected onto a translucent screen placed in the scanner bore (Sony projector; 1024x768 pixels, 60 Hz, ~120 cd/m^2 mean luminance). Observers viewed the stimuli through a mirror attached to the head coil from a distance of approximately 100 cm. The total image area was approximately 26^{o}x20^o. Stimuli were presented and responses collected using custom scripts written in Matlab (version 2016a) with the extensions of the Psychophysics toolbox (Brainard, 1997).

3.2.4 Pre-processing and GLMs

All functional data were analyzed with the AFNI (Cox, 1996) and Freesurfer (Fischl, 2012) software packages. Data were aligned to the first volume of the first run and

remained in native subject space for analysis. Slice time correction, regression of subject motion, and distortion correction were performed in data preprocessing. Spatial smoothing was performed for the localizers, using a 4mm FWHM Gaussian kernel. ROIs and tSNR maps were converted to MNI space using @SSwarper for the purposes of visualization.

Functional data were analyzed in the framework of the general linear model (GLM) using AFNI's 3dDeconvolve. For the localizers, block responses were modeled as the stimulus time course convolved with an incomplete gamma function (BLOCK function in 3dDeconvolve). For task runs, GLM was created for each run of the task data (6 runs per task, 12 runs total). Individual events were modeled using a canonical HRF (GAM function in 3dDeconvolve).

3.2.5 ROI definition

Identification of retinotopic areas was performed using a probabilistic cortical topology mapping algorithm developed by (Benson et al., 2012). The T1-weighted anatomical data was first processed using Freesurfer (Fischl, 2012) to segment white and gray matter and to define and inflate the cortical surface. The retinotopic templates, defining polar angle, eccentricity, and visual area, were then mapped to native space. Visual area surface data were then transformed to volumetric data using 3dSurf2Vol in AFNI. Left and right stimulus apertures as well as the area between the two apertures (Figure 3.1) were defined as the maximally activated single cluster (between 50 and 100 voxels) in each hemisphere of V1, V2, and V3 meeting a minimum threshold of $p < 0.05$ (FDR corrected).

For body areas, a contrast of bodies > chairs was used to define the ROIs. The left and right extrastriate body areas (lEBA and rEBA) were defined as the cluster(s) of voxels on the middle temporal gyrus/inferior temporal sulcus/lateral occipital gyrus. The left and right fusiform body areas (lFBA and rFBA) were defined as the cluster(s) of voxels on each of the left and right fusiform gyri. All ROIs were restricted to a single cluster of the maximally activated voxels (between 50 and 100 voxels) meeting a minimum threshold of $p < 0.05$ (FDR corrected). Figure 3.2 shows a location heatmap observers' body ROIs when converted to MNI space.

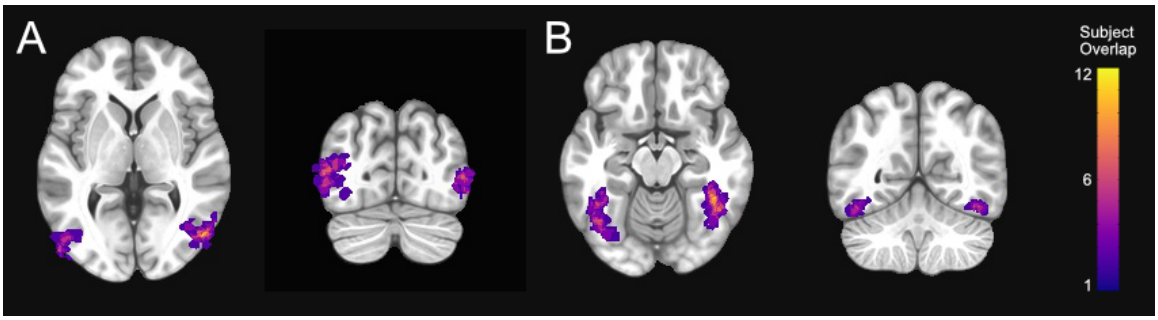

Figure 3.2. Heatmap of ROIs projected into MNI space. A) Location of EBA in the axial (left) and coronal (right) planes. B) Location of FBA in the axial (left) and coronal (right) planes. Note: this figure is to illustrate the overlap of locations of the target ROIs when examined in standard space. ROI analysis was conducted in native subject space.

3.2.6 ROI Analysis

For each condition, t values were extracted for each run from the 4 body ROIs (lEBA, rEBA, lFBA, and rFBA) as well as the stimulated regions of V1, V2, and V3. To test for stimulus driven differences across conditions, linear fits calculated across conditions for each run of each task and ROI on a subject-by-subject basis. The coefficients (i.e., slope) of these linear fits were then analyzed within the context of a linear model, constructed in the R programming environment using the LME4 package (Bates et al., 2015). The model was then assessed with a Type III analysis of variance using the car package (Fox & Weisberg, 2019). Post hoc assessments were then examined with F-tests using the phia package (De Rosario-Martinez, 2015) with p-value correction via the Benjamini-Hochberg (FDR) method. Fixed effects included ROI, task, and the associated interaction between the two. Random effects included intercepts for each individual observer.

3.3 Results

3.3.1 ROI Analysis

Figure 3.3 shows the responses to each stimulus condition as a function of task, with the associated linear fits overlayed, are shown for each ROI. Averages of the linear fits for each task and each ROI are shown in Figure 3.4.

We found a significant main effect of ROI [$F(6, 983) = 2.90$, $p < 0.01$], but no significant main effect of task [$F(1, 983) = 0.28$, $p > 0.05$] nor a significant interaction between ROI and task [$F(6, 983) = 0.42$, $p > 0.05$]. Post-hoc tests assessing each ROI found that there was a significant effect of stimulus alignment in the right EBA [linear coefficient = -0.43, $F(1, 30.21) = 17.10$, $p < 0.01$] and right FBA [linear coefficient = -0.27, $F(1, 30.21) = 6.82$, $p < 0.05$], indicating that responses in these two body-selective areas decreased significantly as alignment cues to part connectedness decreased.

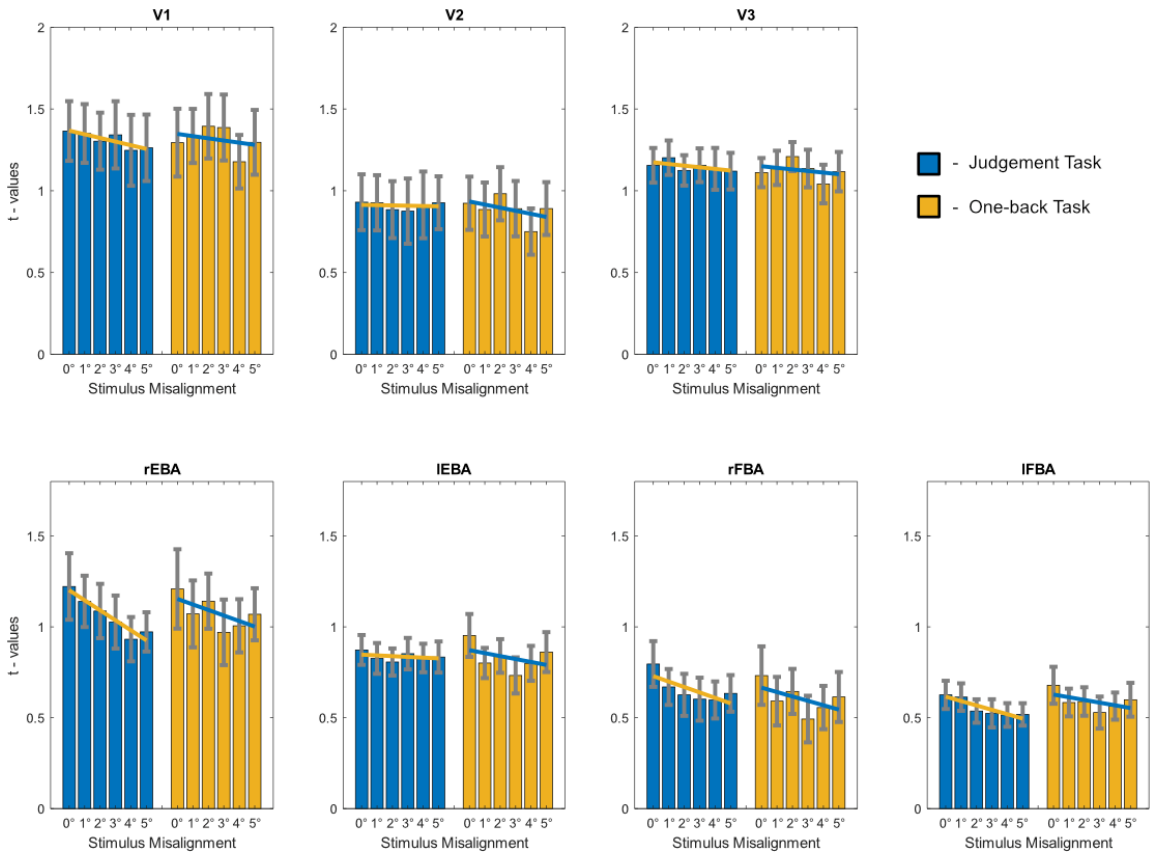

Figure 3.3. Average response to each condition as a function of ROI and task. The average best fit line for each ROI is plotted over each task. Error bars represent standard error of the mean (SEM).

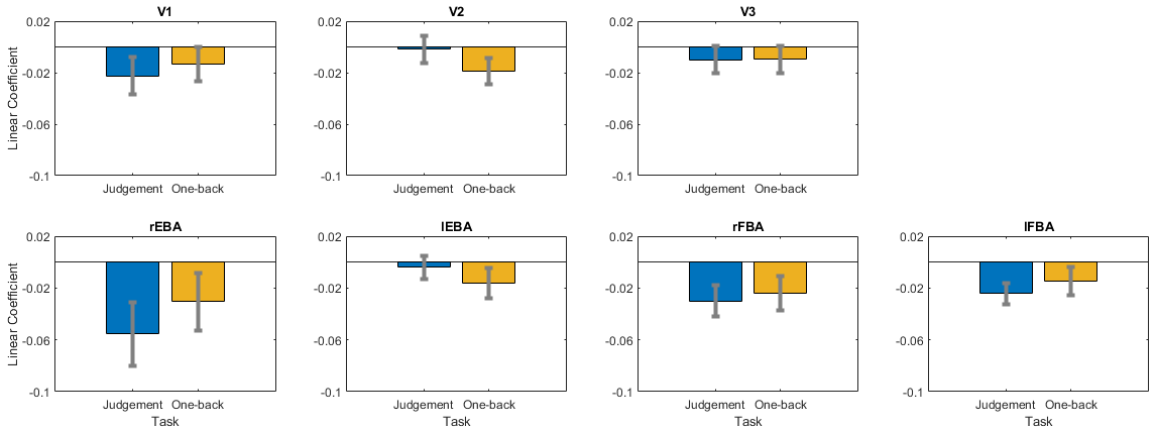

Figure 3.4. Average of the linear fit coefficients as a function of ROI and task. Error bars represent standard error of the mean (SEM).

3.4 Discussion

The goal of the present study was to advance the understanding of how body sensitive regions of cortex, in conjunction with early visual areas, process spatial relationships between pairs of body parts. Observers viewed pairs of arm parts (hand/wrist and elbow) which were parametrically varied in their alignment to alter their perceived connectedness. Observers either actively judged the perceived connectedness of the arm parts or performed a one-back task. In the right EBA and right FBA, we observed a significant negative linear trend associated with decreasing connectedness of the stimuli. Thus, stimuli which are more likely to be perceived as connected yielded a larger response.

Previous work has investigated the question of whether body-selective areas are sensitive to configuration/spatial relationships. Sensitivity to inverting the image has been demonstrated in both the EBA and FBA using fMRI (Brandman & Yovel, 2010), consistent with behavioral impacts of body inversion (Reed et al., 2003). Furthermore, it has been shown that the EBA (the FBA was not investigated) is sensitive to typical configurations with respect to visual field location, where the presence of a body part in the visual hemifield which it is typically viewed (e.g., another person's left arm typically falls in one's right visual hemifield) yields higher activity (Chan et al., 2010). More recent investigations have compared responses to whole bodies versus scrambled body parts. Using this approach, Bauser & Suchan demonstrated that scrambling yields lower activity than intact bodies in FBA (2015). Using a similar paradigm, they showed that, in addition to the FBA, this effect was also noted in the EBA (Brandman & Yovel, 2016), suggesting that both EBA and FBA may be sensitive to the spatial relationships between parts.

However, both of these recent scrambling studies used full bodies, which limits the interpretation of sensitivity to spatial relationships to whole body context. Here, we have demonstrated the same sensitivity to spatial relationships using pairs of arm parts, suggesting that sensitivity to these relationships exists for relationships subordinate to whole bodies/poses. Furthermore, rather than using binarized categories of stimuli (i.e., scrambled vs. unscrambled), we utilized stimulus conditions which have been parametrically varied in their connectedness, demonstrating a linear trend as a function of

this connectedness, further emphasizing the apparent sensitivity to spatial relationships within these areas.

Interestingly, we did not observe a significant main effect of task nor a task/ROI interaction. Prior work has found evidence of modulation as a function of task in face- and object-selective regions (Harel et al., 2010; Thoma & Henson, 2011; Vuilleumier et al., 2001; Wojciulik et al., 1998). However, the difference between the stimulus relevant versus stimulus distracted task in these studies was typically quite dramatic; often observers fully switched their attention away from the target stimulus (e.g., using a fixation task or attending to an alternative stimulus being presented simultaneously). Here, we used a one-back procedure as the stimulus distracted task, which still necessitated that observers attend to the stimulus, but to focus on the trial-to-trial variation of the components rather than the wholistic percept (i.e., connected or disconnected). Thus, it is possible this task does not reduce attention enough to yield a significant modulatory effect. Consistent with this notion are findings showing that a one-back task typically yields more stimulus-relevant activation patterns than a fixation task (Kay & Yeatman, 2017). The statistical power to detect interactions may also have been limited in our study in part due to the subtle nature of our stimulus manipulation. Thus, it is still possible that body-selective cortical areas are sensitive to these task effects. Future work investigating this phenomenon should consider using a task with a more robust shift in attention as well as paradigms which use less subtle stimulus manipulations as our own.

An additional noteworthy finding is the minimal impact of arm alignment in the stimulus regions of V1, V2, and V3. As these are early, retinotopic regions of visual cortex, one would not expect categorical sensitivity to these stimuli and thus an absence of any linear trend as a function of condition is not entirely unexpected. However, previous literature would suggest a possibility of a positive linear trend, where misalignment increases activity, resulting from predictive coding in early visual cortex (Fang et al., 2008; Murray et al., 2002). One argument for the absence of this effect is that individual body parts are often seen without full context of their spatial relationships to other body parts, in the case of self-occlusion. Furthermore, multiple body parts/wholes without any spatial relationships to one another are often experienced in crowd settings, where only a few portions of an individual person are visible. Thus, two disjointed body parts does not

necessarily reflect an uncommon configuration, but rather provides evidence towards an alternative hypothesis (e.g., 2 people versus 1).

3.5 Conclusions

In summary, we have used a paradigm in which the spatial relationships between pairs of body parts are manipulated to investigate sensitivity to spatial relationships between subordinate sets of body parts within body-selective visual cortex. We have shown that both the right EBA and right FBA are sensitive to these spatial relationships, and that this sensitivity appears independent of task. Future work should examine the types of spatial relationships to which these body-selective cortical areas may be tuned and should further evaluate the sensitivity of these areas to task effects.

4. High resolution exploration of the right extrastriate body area reveals hand-preferential voxel clusters

In the past 20 years, distinct cortical areas have been identified in human visual cortex which appear to process body stimuli (Downing et al., 2001; Peelen & Downing, 2005) much has been learned regarding the function of these areas, very few studies have investigated whether these areas contain subordinate representations of body stimuli (e.g., representations of individual body parts). Recent advancements in sub-millimeter functional MRI have enabled the delineation of sub-populations of voxels in sensory cortex which appear to respond preferentially to various subordinate elements of their tuned feature space (see Lawrence et al., 2019 for review). Here, we applied these sub-millimeter fMRI techniques to explore subordinate representations of body parts within the right EBA, an area reported to be selective for individual body parts (Taylor et al., 2007). In our study, subjects viewed images of 5 different body parts (hands, arms, feet, legs, and torsos) in the context of a block design. Laminar profiles of the underlying anatomy were then generated to enable the assessment of responses to these stimuli as a function of cortical depth. We found that, of the 5 body parts tested, hands generally yielded the largest response, and that the relative amplitudes to each of the 5 body parts were consistent across cortical depths. Spatial mapping further revealed large spatial clusters of voxels which preferentially respond to hands, and that the location of these clusters remained constant as a function of cortical depth. Portions of this work was presented at the 2018 Society for Neuroscience conference (Bratch, Vizioli, et al., 2018) and the 2019 Organization for Human Brain Mapping conference (Bratch et al., 2019)

4.1 Introduction

The ability to quickly and accurately process information related to other humans is one of both critical importance and one that the human visual system performs with relative ease. From the perspectives of survival, social interaction, and skillful engagement with the natural world, such a feat arguably requires dedicated, highly specialized neural mechanisms. While much work has been done to investigate the neural mechanisms underpinning face processing (for review, see: Duchaine & Yovel, 2015; Grill-Spector et al., 2017), the mechanisms involved in the processing of the human body have been comparatively underexplored.

The ability to an interpret the image of a person requires the detection and integration of information about body parts and how they should be integrated. The vast range of appearance of different of individual body parts and the large range of joint articulations presents a challenging computational problem, requiring the ability to process individual parts as well as whole bodies. Since the advent of functional MRI (fMRI), two regions which appear responsible for processing these stimuli have been identified in human visual cortex. In the lateral occipital region the extrastriate body area (EBA, (Downing et al., 2001)) has been identified, which appears to represent individual body features (Taylor et al., 2007). Additionally, in the fusiform gyrus, the fusiform body area (FBA, (Peelen & Downing, 2005)) has been identified, which seems to play a stronger role in processing whole, configured bodies (Bauser & Suchan, 2015; Taylor et al., 2007).

To date, much work has been done to further elucidate the functional roles of these areas in the processing body information. These investigations have revealed sensitivity to various mid and high level features, such as perceived body size (Carey et al., 2019; Hummel et al., 2013), viewpoint (Chan et al., 2004; Taylor, Wiggett, et al., 2010), gender (Aleong & Paus, 2009), identity (Hodzic et al., 2009; Urgesi et al., 2007), configuration (Bauser & Suchan, 2015; Talia Brandman & Yovel, 2016a), and pose (Abassi & Papeo, 2020; Cross et al., 2010). However, how these regions encode subordinate representations of bodies (e.g., their individual body parts) has been less studied. Current work has suggested that there may be sub-populations of voxels (Bracci et al., 2010; Op de Beeck et al., 2010; Orlov et al., 2010) as well as differential patterns of activation (Bracci et al.,

2015) for various subordinate body stimulus features, specifically with respect to the individual parts comprising the human body.

Recent advancements in high-field MRI have allowed for much greater precision in understanding stimulus representation in sensory cortices. Specifically, the use of sub-millimeter acquisition techniques can be employed to examine the spatial distribution of responses across a give patch of cortex, and as a function of cortical depth. These techniques have been used to reveal preference maps for ocular dominance (Yacoub et al., 2007) and orientation (Yacoub et al., 2008) in early visual cortex, axis of motion (Zimmermann et al., 2011) in motion selective visual cortex, and tone/pitch (De Martino et al., 2015) in auditory cortex. Such studies have not only found preference maps of their stimulus features but have further established consistency of these maps as a function of cortical depth, suggesting columnar representation.

Here we used sub-millimeter fMRI techniques to test whether we could resolve representations of individual body parts. We used a paradigm in which subjects viewed blocks of individual body parts (hands, arms, feet, legs, and torsos) across a range of viewpoints. Given its suggested role in processing individual body components (Taylor et al., 2007) as well as its apparent right dominance (Downing et al., 2001; Peelen & Downing, 2005; Willems et al., 2010), we assessed responses to these stimuli in the right EBA. Individual response profiles for each body component were assessed as a function of cortical depth, revealing strong preferences for hand stimuli and a consistency of this trend through cortical depths. Using techniques enabling the spatial assessment of activity as a function of cortical depth, body part preference maps revealed large clusters of hand-preferential voxels that were consistent across depth.

4.2 Methods

4.2.1 Subjects

Four subjects with normal or corrected-to-normal vision participated in the present study. Subjects provided written informed consent and participated in a protocol approved by the University of Minnesota Institutional Review Board and in accordance with safety guidelines for MRI research from the Center for Magnetic Resonance Research.

4.2.2 Stimuli & Paradigm

For both the functional localizer and body part localizer, stimuli were presented using a standard block design paradigm. Stimuli were back-projected onto a translucent screen placed in the scanner bore (NEC NP4000 projector; 1920x1080 pixels, 60 Hz). Subjects viewed the stimuli through a mirror attached to the head coil from a distance of approximately 85 cm. Stimuli were presented using Matlab with the extensions of the Psychophysics toolbox (Brainard, 1997).

4.2.2.1 Functional Localizer

To localize visual areas, we used a stimulus set consisting of grayscale images taken from the functional localizer paradigm developed by The Stanford Vision & Perception Neuroscience Lab (Stigliani et al., 2015). Our localizer consisted of 5 categories: phase scrambled noise, objects, limbs, whole bodies (without faces), and adult faces. Images from each category were presented on a phase scrambled background and subtended approximately 8 x 8 degrees of visual angle.

Stimuli were presented within a block design framework. Each run began with 12 seconds of a gray screen with a fixation cross in the center of the screen, followed by 12 second blocks of stimulus images (10 total stimulus blocks, 2 blocks per stimulus category, each separated by a 12 second fixation block). Within each 12 second stimulus block, 16 images were presented. Each image was presented for 500 ms with a 250 ms interstimulus interval (ISI). To ensure attention was directed to the stimuli, subjects performed a 1-back task, in which they would respond if they saw a repetition of two stimuli within a block (consisting of ~10% of trials).

4.2.2.2 Body part localizer

A body part localizer was developed using digital renders of individual body parts. We first generated a normally proportioned, gender neutral human avatar using the MakeHuman 3D character design software package. We then imported this avatar into Blender, where it was segmented into 5 different body parts: hand, arm, foot, leg, and torso.

For the 4 limbs, only right-side limbs were segmented. We then placed these individual parts into a custom camera/lighting rig in Blender, in which the camera was aimed directly at each part, while rotating around the part at 45^{o} increments such that 8 viewpoints were captured for each individual part (Figure 4.1). Each of these limb images were then mirrored, such that the stimulus set for each limb category consisted of a balanced set of 16 images (8 left and 8 right sided limbs). Images were presented to subjects in color on a gray background, where each limb subtended approximately 5-6 degrees of visual angle vertically.

The presentation paradigm followed the same procedures as the functional localizer. Stimuli were presented in a block design paradigm (10 total stimulus blocks, 2 blocks per stimulus category, each separated by a 12 second fixation block). Subjects performed a 1-back task on the viewpoint the body part category within a given block, responding if they saw a repetition of a viewpoint within that block.

Figure 4.1. Stimuli used in the body part localizer. Each column shows one of the 5 body parts (hands, arms, feet, legs, and torsos). Each row shows one of the 8 viewpoints used, starting at the top with the 'front' facing viewpoint. Note: this figure only shows right-sided parts. In the experimental paradigm, these stimuli were also mirrored such that there was a balanced left-right set.

4.2.3 MR Acquisition & Processing

Functional data were acquired on a 7T system (Magnex Scientific Limited, Abington, UK) equipped with a Siemens console (Siemens Healthcare, Erlangen, Germany) and using a custom head coil (4 channel transmit, 32 channel receive). Functional data were acquired using a gradient echo pulse sequence covering the back ~1/3 of the head (84 slices, Resolution: 0.8 mm isotropic, TR = 2.2 s, TE = 26.4 ms, iPat = 3,

multiband = 2). B0 shimming was adjusted manually to achieve optimal homogeneity within the lateral occipital cortices. Flip angles and B1 solutions were adjusted on a subject-by-subject basis for improved SNR.

Anatomical data were acquired on a Siemens Prisma 3T scanner (Siemens, Erlangen, Germany), equipped with a 32-channel head coil. A total of 8 T1 weighted MPRAGE volumes were acquired for each subject (192 slices, Resolution: 0.8 mm isotropic, TR: 1900 ms, TE: 2.52 ms, FoV, 256 x 256 mm; flip angle, 9°).

4.2.3.1 Anatomical data processing

The 8 volumes of 0.8 mm T1 weighted data were first co-registered and averaged using components of the cortical reconstruction routine in Freesurfer (Fischl, 2012). The averaged T1 was then converted to NIFTI and brought into BrainVoyager (Brain Innovation, Maastricht, The Netherlands). This volume was then corrected for intensity inhomogeneities and up-sampled to 0.4 mm for the purpose of improving segmentation. The volume was then manually converted to ACPC space and passed through the BrainVoyager advanced segmentation analysis toolset. To establish laminar profiles for the rEBA in each subject, manual optimization of the initial automatic segmentation was first performed in the cortical regions around the right EBA defined using the functional localizer (see ROI definition procedure below). We then established layer profiles using an equi-volume approach (Kemper et al., 2018; Waehnert et al., 2014), creating grids at 6 cortical depths (from inner to outer 10%, 26%, 42%, 58%, 74%, 90%) with a resolution of 0.2 mm per grid voxel. Time courses of the body localizer functional data were then extracted using these grids both constrained within the rEBA for data quality univariate analysis, and within a large 2 x 4 cm grid centered on the rEBA for spatial analysis. Data presented as a function of layer are labeled using anatomical convention: 1 as the most superficial (i.e., nearest to cortical surface) through 6 as the deepest (i.e., nearest to white matter).

4.2.3.2 Functional data preprocessing

First, to ensure no residual steady-state artifacts remained following the scanner's automated exclusion procedure, an additional two volumes were removed from the beginning of each run. Next, prior to applying standard fMRI preprocessing methods, the functional data were then passed through a version of the NORDIC denoising algorithm (Moeller et al., 2020) designed for use with magnitude-only data (see Appendix 2 for data comparisons). Functional data were then preprocessed using BrainVoyager (Brain Innovation, Maastricht, The Netherlands). Preprocessing steps consisted of (in order) slice time correction, motion correction, and temporal filtering (using a 2-parameter discrete cosine transform). All interpolation steps were performed using sinc interpolation to preserve spatial precision. Furthermore, to preserve this spatial precision and to improve anatomical registration, no distortion correction was applied. Registration of the functional to the anatomical data was performed using the high contrast single band reference (SBRef) volume acquired at the start of each functional run for coil sensitivity calibration in multiband imaging sequences. Inspection and manual adjustments were made to the registration to ensure highly accurate registration in the target region of interest.

4.2.4 Visual Localizer analysis and ROI definition

The preprocessed runs of the functional localizer were concatenated and entered into a GLM to determine the responses to each of the 5 localizer categories. A 12 second box car convolved with a double gamma function was used to model each event. To localize the right EBA, statistical maps were computed by contrasting the joint response to whole bodies and limbs > noise + objects + faces in conjunction with bodies > 0 and limbs > 0. The largest significant (minimum $p < 0.05$ FDR corrected) cluster of voxels from this contrast, falling within the typically reported location of EBA and avoiding areas of high distortion or large venous contamination, was then used to define the ROI. Figure 4.2 shows the overlay of the contrast used to define the right EBA for each subject.

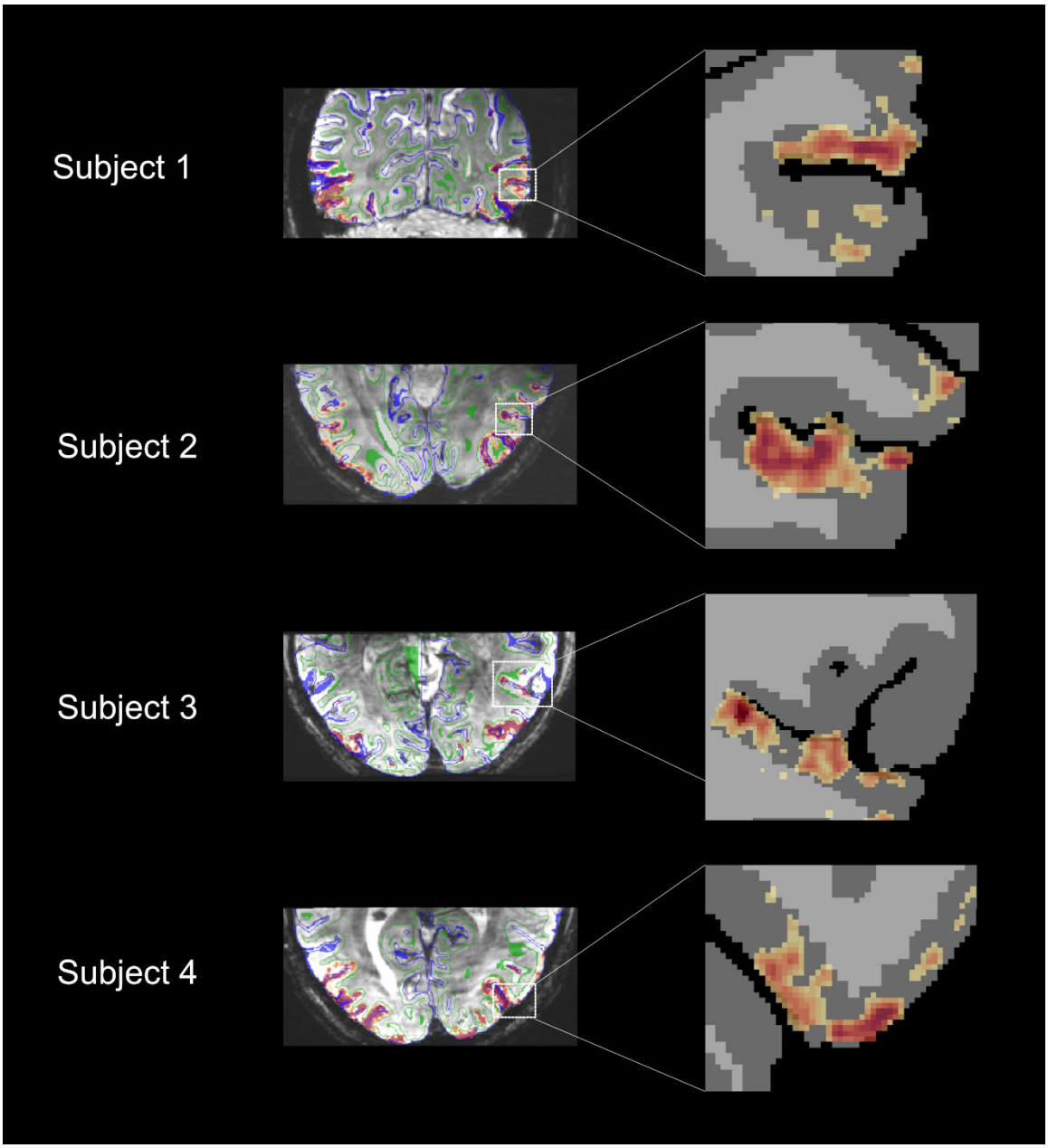

Figure 4.2. Localization and segmentation for each subject. The middle column shows one volume of the EPI for each subject. Borders for the gray matter/white matter and gray matter/CSF are shown in green and blue, respectively. Overlayed on this is the mean activation to all conditions of the body part localizer, shown here to demonstrate the well localized responses within the gray matter, thus suggesting reasonable alignment and segmentation. The right column shows a close-up view of the binarized gray matter/white matter, generated via automated and manual segmentation, overlayed with the contrast used to define the right EBA for each subject.

4.2.5 Body localizer analysis: response amplitude

To inspect data quality, a GLM was performed on the ROI data using a finite impulse response (FIR) deconvolution, which makes no assumption as to the shape of the hemodynamic response function (HRF). For this GLM, 14 bins (30.8 secs) were used to estimate the response profile for each condition on a run-by-run and layer-by-layer basis. In order to assess the response amplitude to each condition, a GLM was created using a standard 12 second box car convolved with a double gamma function, estimating the response to each trial of each condition on a run-by-run and layer-by-layer basis[1].

To assess the response amplitude to each condition, data were analyzed on the individual subject level. Response amplitudes for each trial of each condition were entered into a linear model built in the R programming language using the LME4 package (Bates et al., 2015). The model was then assessed with a Type III analysis of variance using the car package (Fox & Weisberg, 2019) to test for the fixed effects of condition and layer, and the associated interaction between the two. Post hoc tests were conducted with F-tests with p-value correction via the Benjamini-Hochberg (FDR) method using the phia package (De Rosario-Martinez, 2015).

4.2.6 Body localizer analysis: spatial mapping

In order to investigate potential spatial representations of body part stimuli in the right EBA, we first entered the spatial grid data into a GLM using a standard 12 second box car convolved with a double gamma function, again estimating the response to each trial of each condition on a run-by-run, layer-by-layer basis.

The resulting data were then entered into a voxel-wise selectivity analysis procedure. In this procedure, a voxel was defined as selective for a given condition using a conjunction analysis; that is, if a voxel responded significantly higher ($p < 0.05$,

[1] Principally, response amplitude could be assessed by either extracting the peak timepoint of the FIRs or an average of several time points representing the peak. However, because of the large number of time bins required to estimate the response of this block design paradigm (5 conditions x 14 bins + 1 study constant = 71 total bins) relative to the total number a TRs per run (115 TRs), the FIR model constructed here results in a fairly overfit model. While this is still useful for assessing data quality, it can result in a poor estimate of the peak amplitudes. Given this issue, as well as the well-behaved nature of the FIRs observed in our data, we used the standard double-gamma deconvolution in order to add greater precision to the estimate of the peak amplitudes for each condition.

uncorrected) than each other condition independently (i.e., [hand > arm] & [hand > foot] & [hand > leg] & [hand > torso]), then that voxel was labeled as selective for that condition. To assess the stability of the generated maps, the data were additionally split into odd and even runs and passed through the same procedure.

To correct these maps for multiple comparisons, a cluster-based correction procedure was used. In short, 500 iterations of data, where the mean of each condition had been removed, were used to define a distribution of maximum cluster sizes using the same selectivity procedure described above. From this distribution, a 95% confidence interval was derived, which was then used to threshold the selectivity maps.

4.3 Results

4.3.1 ROI analysis

In order to assess the quality of the data extracted from the laminar profiles within the right EBA, we first examined the hemodynamic responses derived using the FIR GLM to each of the body part stimuli as a function of cortical depth. Figure 4.3 shows the responses for each subject individually, with error bars indicating the standard error of the mean (SEM) for each time point across runs.

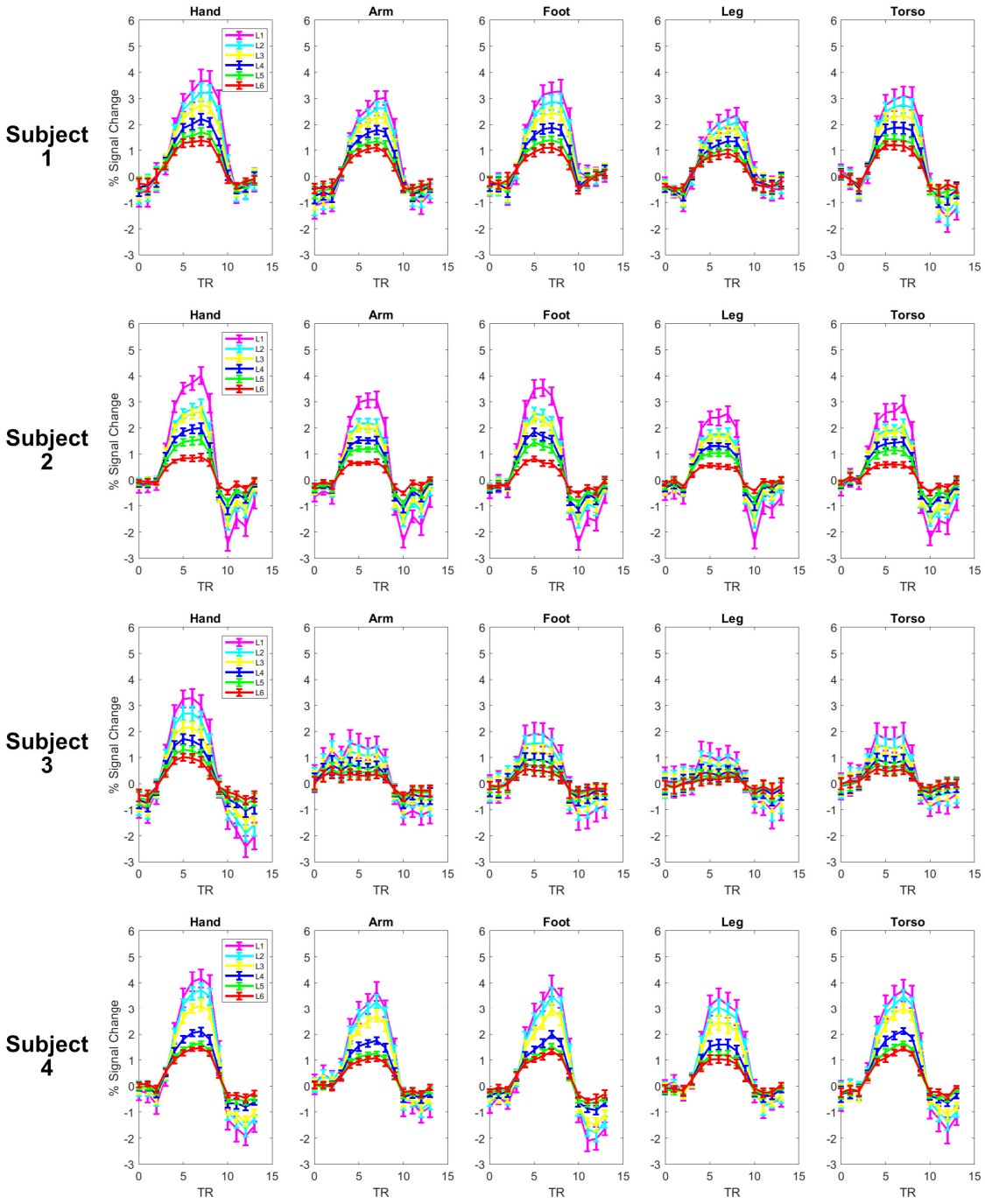

Figure 4.3. FIR plots as a function of condition and layer for each subject. Error bars represent standard error of the mean (SEM) of the responses across acquisition runs.

We found that the responses to each condition reasonably conformed to the expected shape of the hemodynamic response for each of the 4 subjects. Furthermore, a strong degree of run-to-run response consistency can be noted by the low SEM across runs

for each individual time point. Finally, an increase in the response amplitude as a function of cortical depth (due to the increasing proximity to pial veins) can be noted. While such an effect suggests the response profiles are somewhat biased by draining veins, the strong delineation of each layer's response nonetheless suggests a reasonable degree of independence of the data as a function of cortical depth.

Next, we examined the peak amplitude of response to each body part stimulus as a function of cortical depth. Figure 4.4 shows the response peak amplitudes for each individual subject. Detailed results of the single subject ANOVAs and associated post-hoc tests can be found in Appendix Tables A2.2 through A2.5.

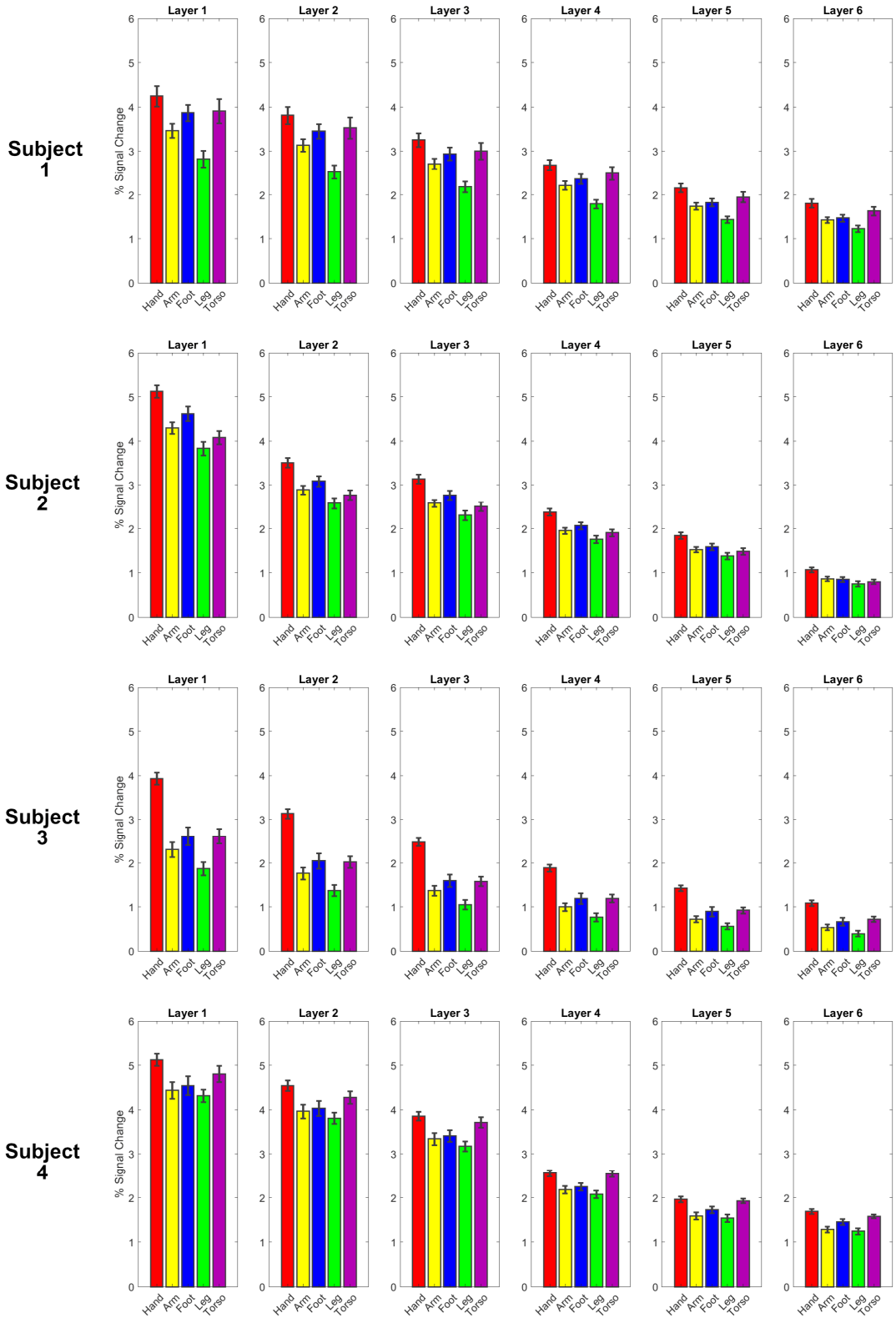
Subject 1
Subject 2
Subject 3
Subject 4
Layer 1
Layer 2
Layer 3
Layer 4
Layer 5
Layer 6
% Signal Change
Hand
Arm
Foot
Leg
Torso

Figure 4.4.Response amplitudes for each condition as a function of cortical depth, shown for each individual subject. Error bars correspond to the standard error of the mean (SEM) across individual trials.

For all subjects, we found a significant main effect of stimulus condition. Post hoc tests revealed that for all subjects, hands elicited significantly stronger responses than all other limb/appendage conditions (arm, foot, and leg). Hand also elicited a stronger response than torsos (and thus, for all other conditions) in three of the four subjects (subjects 1 through 3). Additionally, both foot and torso elicited significantly higher responses than leg in all subjects (see Appendix Tables A2.2 and A2.3 for details).

Additionally, a main effect of layer was also noted for all subjects. Post hoc tests showed that responses increased significantly as a function of cortical depth, which is consistent with rising amplitude of responses from deepest (layer 6, near white matter) to most superficial (layer 1, near CSF) cortical layers when using a vasculature-sensitive pulse sequence, such as the GRE sequence used in the present study (see Appendix Tables A2.2 and A2.4 for details).

We also found a significant interaction effect as a function of cortical depth in two of the four subjects. The results of a condition x layer post hoc assessment for these two subjects revealed that the differences between condition noted in the above post hoc assessments were either smaller or non-significant in deeper layers of cortex, with increasing reliability noted when moving from deeper to superficial layers. Such a finding is likely the result of overall low stimulus amplitudes typical of deeper cortical layers, and does not necessarily suggest a change in the response profile (e.g., one condition relative to another) as a function of cortical depth (see Appendix Tables A2.2 and A2.5 for details).

In summary, we found that hands generally elicit a dominant response relative to the other body part conditions examined. Furthermore, we see a consistency of the general response profiles of all conditions across cortical depths (albeit with an expected increase in amplitude when moving toward superficial layers). Such a finding argues in favor of columnar organization, wherein one would expect stability of responses as one moved vertically through a given columnar unit.

4.3.2 Preferential responses: spatial representation

To further understand the response profiles noted above in section 4.3.1, we constructed preference maps using Laplacian-transformed, equi-volume cortical grids (Kemper et al., 2018; Waehnert et al., 2014) generated for each layer of cortex, centered on the right EBA. We then assessed, for a given grid voxel, whether that voxel elicited a stronger response for a given body part condition, using a cluster corrected, conjunction base approach to generate preference maps over the entire grid (see section 4.2.6 for details). Figure 4.5 shows these preference maps overlayed on a binarized mask showing the contrast used to define the right EBA.

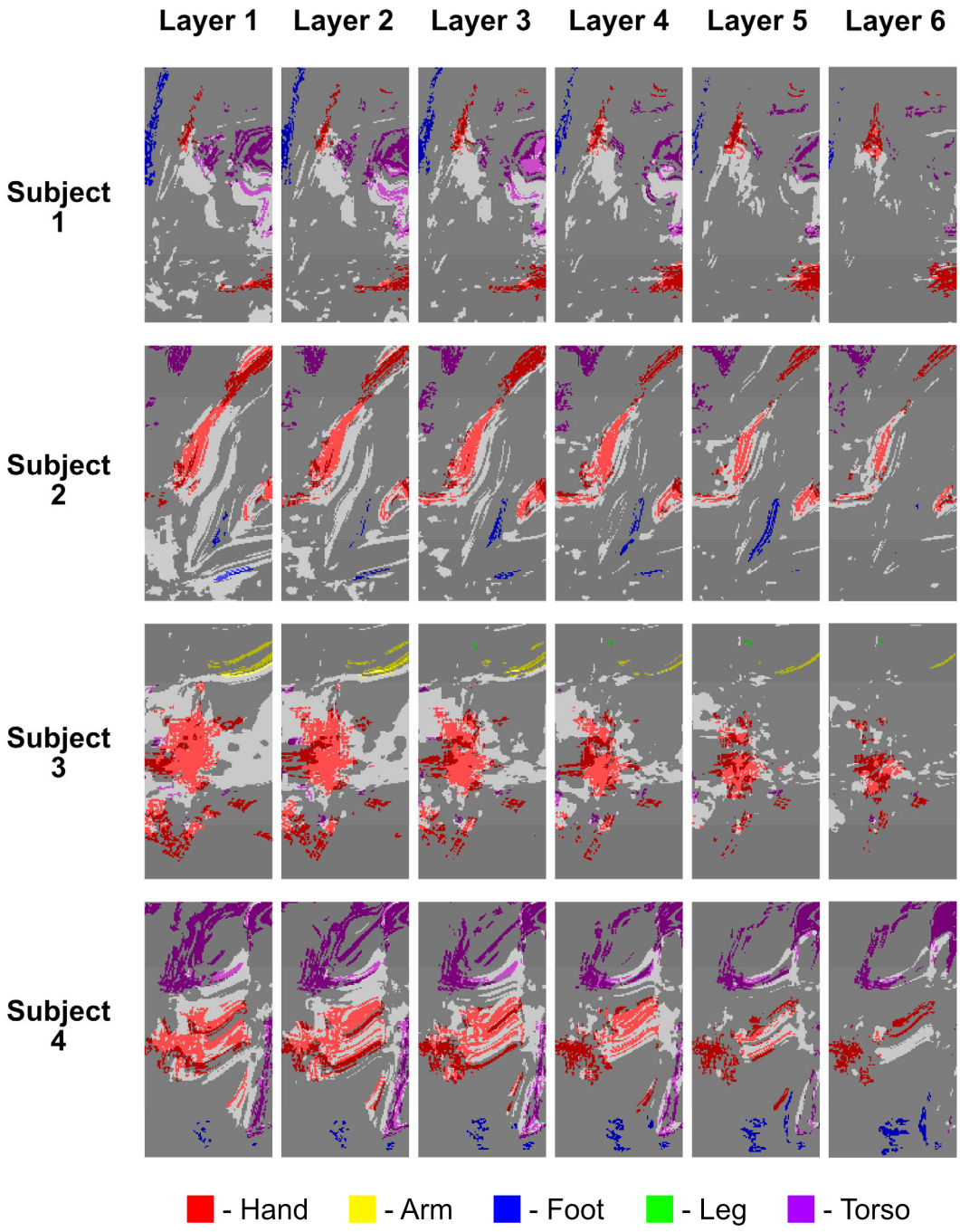

Figure 4.5. Body part preference maps for each subject, overlayed on a binarized map (binarization threshold: $t > 6$) of the contrast used to localize the right EBA, which appears white in the underlay. Color legend at the bottom of the figure shows the colors corresponding to each body part category.

For all four subjects, we found large clusters of voxels with preferences for hands within the right EBA. Furthermore, we observed a high degree of consistency of these

clusters as a function of depth, with a slight but expected reduction in cluster size in lower layers, presumably owing to lower signal. These results are convergent with the univariate findings described in section 4.3.1; taken together, these results suggest columnar representation of hand stimuli within the right EBA. We did observe other clusters showing preferences to other body parts, specifically torso being the most common. However, both the sizes of the torso clusters across subjects, as well as their overlap with the EBA-defining contrast, was less consistent.

4.3.3 Controls for preference maps

While these results provide encouraging evidence favoring hand dominant clusters of voxels with a columnar arrangement in right EBA, the stability of these results must be explored. Furthermore, alternative explanations for the depth-consistent results must also be considered. To assess the stability of the preference maps, we conducted the same preference mapping procedure described above, but did so on separate splits of the data (odd versus even runs).

With respect to alternative explanations for columnar arrangement, it could easily be the case that large draining veins happen to traverse upward through the cortex in the areas we find hand-selective clusters, thus giving the appearance of columnar organization. Accordingly, we examined the mean EPI images as well as the mean amplitudes of the task data, in an effort to identify venous contamination. Figure 4.6 shows the preference maps for each data split, the EBA localizer contrast, the mean task activation, and the mean EPI images. Additionally, overlays of the preference maps on the mean EPI images can be found in Appendix Figure A2.2.

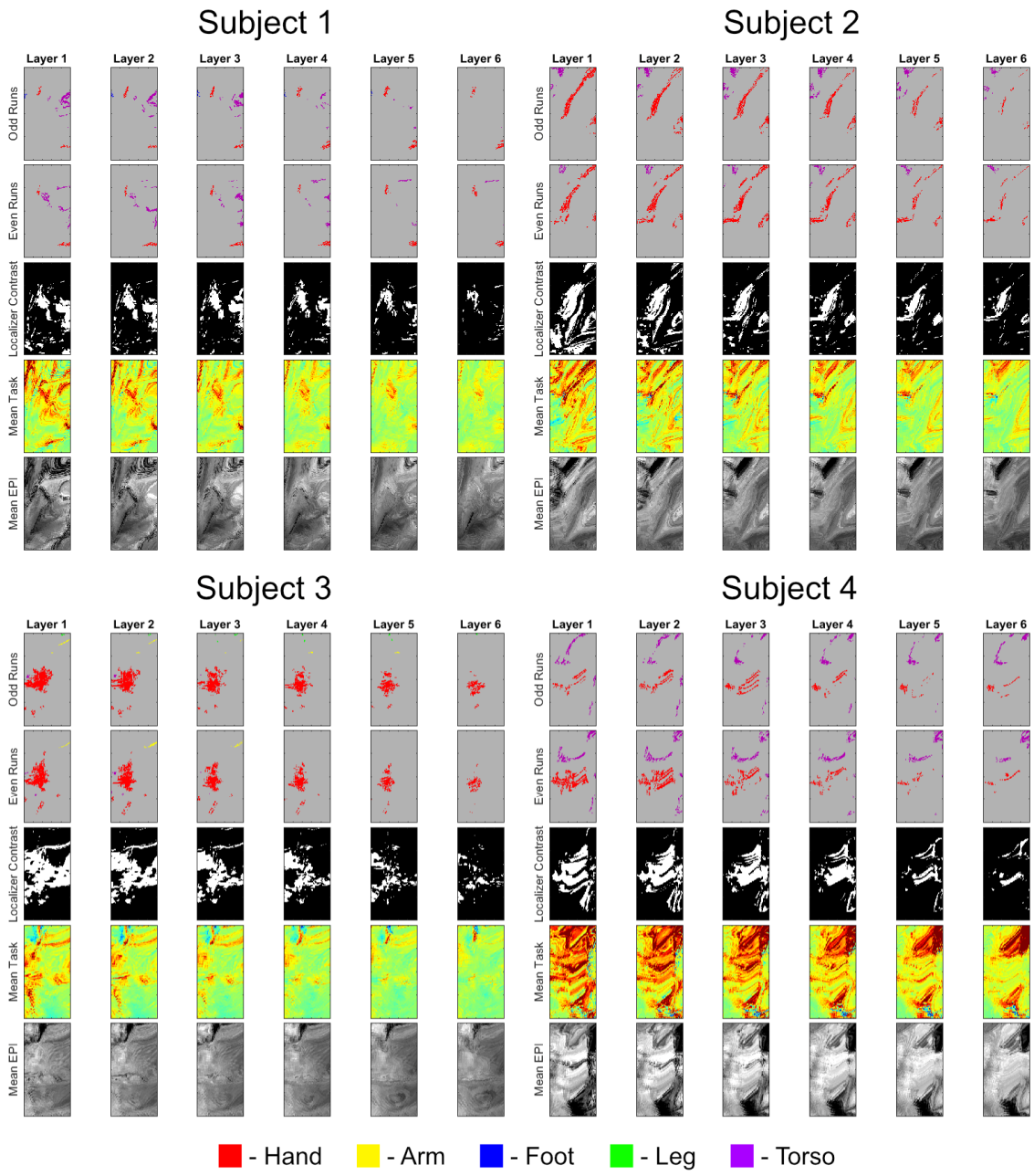

Figure 4.6. Results of the split half analysis of the spatial data, showing strong consistency of the preference maps. The bottom three rows show the localizer contrast, the mean task response profile, and the mean EPI, respectively.

Our assessment of the two splits of the data showed a strong degree of consistency in the respective preference maps; the results converged with the full data preference maps and only minimal changes in the spatial distribution of responses were noted between each

split, most of which are likely the result lower statistical power resulting from the halved data.

Furthermore, examination of the mean EPI and mean task responses suggested that, for hand-preferential voxel clusters, the depth-consistent results cannot be attributed to large draining veins; these large veins, which will appear as dark spots on the mean EPI or potentially as areas of strong positive or negative activation in the response amplitude data, do not appear to overlap with the hand-preferential voxel clusters. However, it should be noted that in subjects 2 and 4, their torso-preferential clusters appear to be adjacent to and, in some cases, overlapping with potential veins, thus further restricting columnar interpretations to the hand-preferential clusters within this dataset.

4.4 Discussion

We have shown that the right extrastriate body area shows a strong preference for hand stimuli. ROI analyses indicate that throughout the right EBA, hands elicit stronger responses than all other limb/appendage categories (arm, foot, and leg). Additionally, spatial preference mapping shows that, within the EBA, there are large clusters of voxels that preferentially respond to hands above all other body part categories. Furthermore, both ROI and spatial preference analyses reveal a consistency of these trends as a function of cortical depth, providing preliminary evidence in favor of columnar arrangement.

4.4.1 Subordinate representations, with preferences for hands

The few prior studies which have examined the question of subordinate representation in body selective cortex have found evidence consistent with our findings. Orlov and colleagues (2010) found that, within the entirety of lateral occipital cortex (not just in the EBA), there were large clusters of voxels showing selectivity to all of the individual body and face parts they examined. However, hand/arm-selective voxels consistently showed the most overlap with their predefined EBA. In line with these results, Op de Beeck and colleagues (2010) were able to isolate distinct, large populations of voxels within the EBA that were sensitive to hands, as well as those sensitive to torsos. They, as well as Bracci and colleagues (2015), additionally showed that the pattern of responses

(identified using MVPA and RSA, respectively) was dissociable for all subordinate body parts examined.

One study, which directly examined the question of hand representation in body selective areas, failed to find clusters of voxels within EBA selective for hands, instead finding large hand-selective areas, distinct from EBA, in the left lateral occipital sulcus (Bracci et al., 2010). However, this study used a set of contrasts, which included whole bodies (with visible hands), and non-categorized body part sets to establish these hand preferential areas. Given our results and the results of Op de Beeck (2010) and Orlov (2010), which suggest that hands represent only a sub-population of voxels within the EBA, it is possible that the contrast procedure used in this study may have diminished or negated hand selective voxel populations in EBA.

One noteworthy finding is the variability of torso preferences found in our dataset – two of the four subjects showed fairly large spatial clusters of torso-preferential voxels, while one subject showed much smaller clusters, and one only showed clusters outside of the right EBA. While previous EBA literature has suggested that there is typically a higher response amplitude for whole bodies (without heads) as opposed to individual body parts (Downing et al., 2001; Taylor et al., 2007) these paradigms inherently confound the stimulus category of torso with all other body parts.

Few studies which have directly examined torsos in isolation have found similar results to what we report here. In the studies subordinate representation previously noted above, Orlov and colleagues (2010) found similar variability in their body part mapping; some but not all subjects showed torso selective clusters overlapping with predefined their EBA. Consistent with this, Op de Beeck and colleagues (2010) found that, of the hand and torso sub-populations found within EBA, the torso subpopulation was much smaller on average (248 vs 74 voxels for hands and torsos, respectively, averaged across subjects). They also noted that these torso selective subpopulations were still strongly active for hands. Finally, Bracci and colleagues (2015) found that responses to torsos were lower than all other body parts, except for legs. However, the torso stimuli used were split into chest versus waist. Thus, it is possible that removal of context/splitting of this stimulus results in a reduction of activity. In light of these findings, it is conceivable that the variability noted

in our dataset may be consistent with previously reported subject-to-subject variability of torso representation in the EBA.

4.4.2 Hands as a Special Stimulus Category for Visual Representation

The fact that hand appears to be the dominant body part represented in the right EBA may not necessarily come as a surprise. The hand is, arguably, the most crucial body part of the 5 body parts assessed in this study. Hands are the primary means by which we can interact with the world using a high degree of motor precision. Thus, from the perspective of developing and monitoring basic motor skills (e.g., grasping) to acquiring and developing complex actions, a strong visual representation of the hand seems absolutely necessary.

Consistent with this idea, it has been demonstrated that the EBA plays a role in both perceiving (Takahashi et al., 2008), imagining (Tomasino et al., 2012), performing (Astafiev et al., 2004) goal-directed actions, all of which used actions necessitating the engagement of hands. Furthermore, the use of TMS has causally implicated EBA in the planning of hand-based actions (Zimmermann et al., 2016). In light of these findings, it has been proposed that the EBA may be integrated within the network of brain areas responsible for action planning and associated visual feedback (Amoruso, 2011; M. Zimmermann et al., 2018).

Additionally, hands are also used extensively for social interaction and communication, frequently used for emphasis of critical points when speaking, to signal one's intentions/emotional state, and to direct the spatial attention of others. While there is sparse literature on EBA's role in hand-specific communication, recent evidence has suggested that EBA plays a role in the comprehension of semantically meaningful gestures (Kubiak & Króliczak, 2016; Proverbio et al., 2015).

4.4.3 Columnar organization: past findings, limitations, and implications

Columnar organization is a long-studied principle of cortical organization, with the intuition being that cells arranged in a column spanning the cortical depths represent a distinct functional unit, with its own stimulus response properties (Buxhoeveden &

Casanova, 2002; Hubel & Wiesel, 1959; Mountcastle, 1957). This principle has since been demonstrated using electrophysiology within various sensory cortices throughout the past several decades (Albright et al., 1984; D. H. Hubel & Wiesel, 1959; David H Hubel & Wiesel, 1977; Merzenich & Brugge, 1973; Tootell et al., 1988).

The advent of sub-millimeter fMRI acquisition strategies has now enabled non-invasive investigations of columnar representation, allowing for the exploration of these fundamental organizational principles in human subjects. Such investigations have mirrored the findings of animal electrophysiology, revealing columnar representation of various stimulus features in visual cortex (Yacoub et al., 2007, 2008; Zimmermann et al., 2011), auditory cortex (De Martino et al., 2015), and somatosensory cortex (Yang et al., 2019).

The results of both our ROI analysis and particularly our spatial preference mapping suggests that the representations in the right EBA, specifically to hands, may be arranged in a columnar fashion. However, it is worth considering that relative to other columnar organization found in visual cortex, this represents a somewhat atypical case. Generally, it has been found that across the surface of cortex, there is a fairly well distributed representation for all dimensions of the stimulus of interest. For instance, with orientation, the longstanding finding is a widespread distribution of columns tuned to the full range of orientations, and clusters of larger 'hypercolumns', each containing a relatively even distribution of columns for each orientation (see Swindale, 1996 for review). Thus, to have a very large cluster of columnar representation for only one element of a theorized feature space is somewhat unprecedented in visual cortex. Nevertheless, the idea of columnar representation with large spatial clusters for a given element of the feature space isn't itself unprecedented; tonotopic representations often appear demonstrate a slow varying spatial extent with respect to their frequency preferences (De Martino et al., 2015; Formisano et al., 2003; Leaver & Rauschecker, 2016). In short, while the current findings demonstrate evidence suggesting columnar structure, further work is needed to reconcile our findings with the current theories and literature surrounding columnar representation.

Furthermore, additional care must be taken when interpreting the apparent columnar profiles noted in this study due the methodology employed. Specifically, given our choice of a gradient echo pulse sequence, it is possible that the observed consistency

across depths may be the result of draining veins which traverse through the layers. While our examination of the mean EPI data suggests that the results we observed are unlikely due to large draining veins, we cannot rule out smaller vasculature that would not be visible in the EPI data. Previous investigations of columnar representation, noted above, typically utilized pulse sequences that were less biased to vasculature; future explorations should highly consider the use of such sequences in an effort to mitigate this confound.

Nonetheless, that fact that our findings preliminary suggest columnar representation for hands is quite novel, in that it reflects the existence of columnar representation for high level stimuli within visual cortex. Furthermore, if such a finding is indeed valid, it would enable numerous opportunities for exploration of intriguing neuroscientific questions. Particularly, given the well-established principle that feedback versus feedforward connections are made differentially throughout the cortical depths (for review, see: Lawrence et al., 2019), one could conceive of experiments involving hand perception which may differentially necessitate feedback versus feedforward processing. Responses could then be assessed both within and outside of the 'hand columns' in the EBA, with the assumption being that 'hand columns' should better delineate the predicted feedback/feedforward response profiles.

4.5 Conclusions

Here, we have demonstrated hand preferential response profiles in the right EBA, a finding which is not only consistent with previous literature but falls in-line with the intuition of the important role hands have in our perceptual environment. Furthermore, we demonstrate the existence of spatial clusters of hand-preferential voxels within the right EBA, and a consistency of these spatial clusters through the cortical depths. This finding provides preliminary evidence for columnar arrangement of these hand populations and suggests the potential of columnar arrangement for high-level visual stimuli.

5. Summary, Future Directions, and Final Thoughts

The preceding chapters have served to outline the existing literature on the visual perception of human bodies and to contribute a series of experiments to help address current gaps in knowledge. Specifically, the representation of more basic elements (e.g., individual body parts) and the relationships between them was explored.

5.1 Adaptation to limb length

In the scope of Chapter 2, a set of experiments found sensitivity to basic length relationships between body parts (i.e., the length of one part relative to another) using an adaptation paradigm. Furthermore, it was demonstrated that this sensitivity appears to be based on not only high level, body selective mechanisms, but to limb specific mechanisms.

This set of findings opens the door to several potential avenues of investigation. One of particular interest is the role of context. For instance, one can imagine that including additional body parts, the whole body, or even additional human figures, may have an impact on the effects we have seen. Consistent with this, it has been shown that when observers are required to assess differences in the length of limbs in point light walkers, configural cues given by a wholly configured point light walker elevates the length discrimination threshold (Lu et al., 2006). Such a finding suggests that the underlying knowledge of typical part relationships may override sensory inputs when enough context is present. Thus, it is possible that the effects we have seen may be impacted similarly (i.e., a reduction in the adaptation effect) with the addition of whole body context.

There is also an additional question of 2D versus 3D representation. The experiments described in Chapter 2 presented stimuli from a view that maximized the projected size of the limbs, which suggests minimal depth change across the limb. But the image size of a given limb depends, in part, on rotation in depth. Thus, whether these representations are based on image-based, 2D information or based on a deeper level of 3D representation remains an open question. Given the current findings suggest a high level, body/limb specific mechanism, as well as the fact that limbs are highly kinematic elements, moving greatly within 3D space, it seems likely that there may be an underlying 3D basis of representation. One, therefore, could conceive of experiments using either static images

with 3D cues, or animations which move the stimuli in 3D space, to assess whether these sensitivities to limb length relationships rely on a 3D component.

5.2 Sensitivity to pairwise spatial relationships

Within Chapter 3, an experiment was conducted investigating the sensitivity to basic pairwise spatial relationships between pairs of body parts in body-selective cortical areas. This investigation revealed that these cortical areas are in fact sensitive to these basic pairwise relationships, responding more strongly when pairs of parts were presented in their typical configuration (i.e., when the two parts were aligned to appear as one contiguous part).

Given these findings were derived using a hand/wrist and an elbow as the part pairs, it remains an open question of whether the same sensitivities could be found using pairs of other parts, such as foot/ankle and knee or two limb components without the appendage visible (e.g., upper arm/shoulder and knee). Given the findings of Chapter 4, perhaps it should not be a surprise that body-selective areas are sensitive to even small spatial manipulations of hand and hand-related stimuli. As such, it is possible that the sensitivity to non-hand pairwise relationships might be relatively smaller.

Another open question is the impact of context, both body-based, and background based. For body-based contexts, adding additional body part patches (i.e., beyond simple pairwise relationships) could provide a useful window into how the visual system begins incorporating ever-increasing information needing assembled into a whole-body representation. Furthermore, such a design could also be useful for further exploring the question of task/attentional differences; one could imagine a design with multiple body patches, where observers selectively attend to and judge the alignment of only two patches (as in Chapter 3). The impact of manipulating the alignment of the target versus non-target patches could then be assessed. Previous literature on faces (Vuilleumier et al., 2001) would suggest that the attended versus un-attended stimuli would likely yield a larger effect.

In addition to body context, one could also consider the impact of non-body context (e.g., patches containing not body information, such as background, clutter, etc.). Recent

work has demonstrated that when perceiving aligned versus unaligned Gabor patches, modulation of early visual cortex as a function of alignment was only noted in the presence of irrelevant context (Qiu et al., 2016). With respect the design in Chapter 3, it suggests that the addition of such context may yield a modulatory effect that, in the present design, was not noted in early visual cortex. Furthermore, it begs the question of whether such a manipulation would have a similar impact on the responses in high level, body-selective areas.

Finally, from a more practical perspective, it is worth noting some improvements that could be made on our design when considering future work. The degree to which alignment of the stimuli was manipulated (increments of 1 degree) was very fine, which not surprisingly yielded small differences between the amplitudes of each condition. Thus, future designs could consider a higher degree of separation between stimulus conditions, a higher SNR acquisition scheme.

5.3 Subordinate representation of body parts, and the dominance of hands

Chapter 4 presented a study which used sub-millimeter fMRI techniques to explore whether subordinate body features (e.g., their individual parts) were represented independently in body-selective cortex (specifically, the right EBA). It was found that, generally, hands yielded the highest response of all categories tested. Furthermore, spatial mapping techniques revealed large spatial clusters of hand-preferential voxels. Such clusters additionally appeared to be consistent through the cortical depths, providing preliminary evidence supporting the idea of columnar representation.

The notion of a hand-dominant representation in visual cortex is one which seem rather sensible, given the perhaps disproportionality high level of importance of hands relative to other body parts (see section 4.4.2 for details). This, in turn, suggests many directions for future experimentation. Given what has been shown to be a large areas of cortex dedicated to processing hands, one may anticipate that humans should be able to make finer discriminations about hands rather than other body parts, similar to what we see in early visual cortex regarding cortical magnification for foveal versus peripheral representation (Cowey & Rolls, 1974; Rovamo & Virsu, 1979).

Given that the spatially localized clusters of voxels dedicated to hand processing appear to be spatially consistent through the cortical depths, further sub-millimeter fMRI experiments could also seek to address more detailed questions regarding the flow hand-related information throughout the visual system. Section 4.4.3 discusses the concept of differential laminar processing, in that certain layers of the cortex serve as either input/output layers for either feedback or feedforward information (see Lawrence et al., 2019 for review). Thus, there are numerous experiments one could conduct investigating tasks that necessitate feedback versus feedforward information related to hands and examine the responses within these hand-preferential voxel clusters as a function of cortical layer. Furthermore, recent work has applied laminar fMRI to functional connectivity methods, enabling the assessment of functional connectivity as a function of cortical layer and thus as a function of feed forward versus feedback information flow (Huber et al., 2017, 2020). A such, one could examine how other brain regions integrate with these hand-preferential clusters.

Finally, when examining our findings, as well as the findings of others (notably Op de Beeck et al., 2010 and Orlov et al., 2010), it must be noted that there are large populations of voxels within the right EBA which appear uninvolved in the representation of hands or any other individual body part. Given the involvement of the EBA in numerous aspects of body perception (see Chapter 1, as well as Amoruso, 2011 and Downing & Peelen, 2011 for review), it is possible that there is a modular structure within the EBA, with different subsets of voxel populations serving different functions. Such a theory could again be addressed using sub-millimeter fMRI methodology and would help to clarify not only the organization of the EBA but, more generally, the organizing principle for high-level visual areas of the brain.

5.4 Final thoughts

The ultimate goal of this dissertation was to shed a bit more light on questions surrounding the visual representation of the human body. Specifically, within the scope of the preceding chapters, questions about more basic elements of body representation (sensitivity to different spatial relationships, subordinate representation, etc.) have been

answered. But as with many questions, once they are answered, a good many more arise. It is the hope that this work, its implications, and associated suggests for additional research, may help to guide future work seeking to understand and, ultimately, build a comprehensive theoretical framework for the visual perception of human bodies.

Bibliography

Abassi, E., & Papeo, L. (2020). The Representation of Two-Body Shapes in the Human Visual Cortex. *The Journal of Neuroscience*, *40*(4), 852–863. https://doi.org/10.1523/JNEUROSCI.1378-19.2019

Albright, T. D., Desimone, R., & Gross, C. G. (1984). Columnar organization of directionally selective cells in visual area MT of the macaque. *Journal of Neurophysiology*, *51*(1), 16–31. https://doi.org/10.1152/jn.1984.51.1.16

Aleong, R., & Paus, T. (2009). *Neural Correlates of Human Body Perception*. 482–495.

Ambroziak, K. B., Azañón, E., & Longo, M. R. (2019). Body Size Adaptation Alters Perception of Test Stimuli, Not Internal Body Image. *Frontiers in Psychology*, *10*, 2598. https://doi.org/10.3389/fpsyg.2019.02598

Amoruso, L. (2011). Beyond extrastriate body area (EBA) and fusiform body area (FBA): Context integration in the meaning of actions. *Frontiers in Human Neuroscience*, *5*(November), 1–3. https://doi.org/10.3389/fnhum.2011.00124

Astafiev, S. V., Stanley, C. M., Shulman, G. L., & Corbetta, M. (2004). Extrastriate body area in human occipital cortex responds to the performance of motor actions. *Nature Neuroscience*, *7*(5), 542–548. https://doi.org/10.1038/nn1241

Avidan, G., & Behrmann, M. (2009). Functional MRI Reveals Compromised Neural Integrity of the Face Processing Network in Congenital Prosopagnosia. *Current Biology*, *19*(13), 1146–1150. https://doi.org/10.1016/j.cub.2009.04.060

Bao, P., & Tsao, D. Y. (2018). Representation of multiple objects in macaque category-selective areas. *Nature Communications*, *9*(1), 1–16. https://doi.org/10.1038/s41467-018-04126-7

Barton, J. J., Press, D. Z., Keenan, J. P., & O'connor, M. (2002). Lesions of the fusiform face area impair perception of facial configuration in prosopagnosia. *Neurology*, *58*(1), 71–78.

Bates, D., Maechler, M., Bolker, B., Walker, S., & Haubo Bojesen Christensen, R. (2015). *Lme4: Linear mixed-effects models using Eigen and S4. R package version 1.1–7. 2014*.

Bauser, D. S., & Suchan, B. (2015). Is the whole the sum of its parts? Configural processing of headless bodies in the right fusiform gyrus. *Behavioural Brain Research*, *281*, 102–110.

Behrmann, M., & Avidan, G. (2005). Congenital prosopagnosia: Face-blind from birth. *Trends in Cognitive Sciences*, *9*(4), 180–187. https://doi.org/10.1016/j.tics.2005.02.011

Bell, A. H., Hadj-Bouziane, F., Frihauf, J. B., Tootell, R. B. H., & Ungerleider, L. G. (2008). Object Representations in the Temporal Cortex of Monkeys and Humans as Revealed by Functional Magnetic Resonance Imaging. *Journal of Neurophysiology*, *101*(2), 688–700. https://doi.org/10.1152/jn.90657.2008

Benson, N. C., Butt, O. H., Datta, R., Radoeva, P. D., Brainard, D. H., & Aguirre, G. K. (2012). The retinotopic organization of striate cortex is well predicted by surface topology. *Current Biology*, *22*(21), 2081–2085. https://doi.org/10.1016/j.cub.2012.09.014

Bentin, S., Allison, T., Puce, A., Perez, E., & McCarthy, G. (1996). Electrophysiological studies of face perception in humans. *Journal of Cognitive Neuroscience*, *8*(6), 551–565. https://doi.org/10.1162/jocn.1996.8.6.551

Bernstein, M., Oron, J., Sadeh, B., & Yovel, G. (2014). An Integrated Face–Body Representation in the Fusiform Gyrus but Not the Lateral Occipital Cortex. *Journal of Cognitive Neuroscience*, *26*(16), 2496–2478. https://doi.org/10.1162/jocn

Biotti, F., Gray, K. L. H., & Cook, R. (2017). Impaired body perception in developmental prosopagnosia. *Cortex*, *93*, 41–49. https://doi.org/10.1016/j.cortex.2017.05.006

Blakemore, C., & Campbell, F. W. (1969). On the existence of neurones in the human visual system selectively sensitive to the orientation and size of retinal images. *The Journal of Physiology*, *203*(1), 237–260. https://doi.org/10.1113/jphysiol.1969.sp008862

Booth, M. C. A., & Rolls, E. T. (1998). View-invariant representations of familiar objects by neurons in the inferior temporal visual cortex. *Cerebral Cortex*, *8*(6), 510–523. https://doi.org/10.1093/cercor/8.6.510

Bötzel, K., Schulze, S., & Stodieck, S. R. G. (1995). Scalp topography and analysis of intracranial sources of face-evoked potentials. *Experimental Brain Research*, *104*(1), 135–143. https://doi.org/10.1007/BF00229863

Bracci, S., Caramazza, A., & Peelen, M. V. (2015). Representational Similarity of Body Parts in Human Occipitotemporal Cortex. *The Journal of Neuroscience*, *35*(38), 12977–12985. https://doi.org/10.1523/JNEUROSCI.4698-14.2015

Bracci, S., Ietswaart, M., Peelen, M. V., & Cavina-Pratesi, C. (2010). Dissociable neural responses to hands and non-hand body parts in human left extrastriate visual cortex. *Journal of Neurophysiology*, *103*(6), 3389–3397. https://doi.org/10.1152/jn.00215.2010

Brainard, D. H. (1997). The Psychophysics Toolbox. *Spatial Vision*, *10*, 433–436.

Brandman, T., & Yovel, G. (2010). The Body Inversion Effect Is Mediated by Face-Selective, Not Body-Selective, Mechanisms. *Journal of Neuroscience*, *30*(31), 10534–10540. https://doi.org/10.1523/JNEUROSCI.0911-10.2010

Brandman, Talia, & Yovel, G. (2016a). Bodies are Represented as Wholes Rather Than Their Sum of Parts in the Occipital-Temporal Cortex. *Cerebral Cortex*, *26*(2), 530–543. https://doi.org/10.1093/cercor/bhu205

Brandman, Talia, & Yovel, G. (2016b). Bodies are Represented as Wholes Rather Than Their Sum of Parts in the Occipital-Temporal Cortex. *Cerebral Cortex*, *26*(February), 530–543. https://doi.org/10.1093/cercor/bhu205

Bratch, A., Burton, P., Engel, S. A., & Kersten, D. J. (2017, November 11). Cortical Representation of Body Part Relationships. *Society for Neuroscience Annual Meeting*. Society for Neuroscience Annual Meeting, Washington DC, USA.

Bratch, A., Engel, S., Burton, P., & Kersten, D. (2018). The Fusiform Body Area Represents Spatial Relationships Between Pairs of Body Parts. *Journal of Vision*, *18*(10), 408–408. https://doi.org/10.1167/18.10.408

Bratch, A., Engel, S., & Kersten, D. (2017). Relational Representation of Body Parts Revealed by Adaptation. *Journal of Vision*, *17*(10), 1238–1238. https://doi.org/10.1167/17.10.1238

Bratch, A., Vizioli, L., Yacoub, E., Engel, S., Burton, P., & Kersten, D. (2018, November 3). Selectivity for Individual Body Parts within Body Selective Visual Cortex. *Society for Neuroscience Annual Meeting*. Society for Neuroscience Annual Meeting, San Diego, CA, USA.

Bratch, A., Vizioli, L., Yacoub, E., Engel, S., Burton, P., & Kersten, D. (2019, June 9). Selectivity for Individual Body Parts within Body Selective Visual Cortex. *Organization for Human Brain Mapping Annual Meeting*. Organization for Human Brain Mapping Annual Meeting, Rome, Italy.

Brooks, K. R., Clifford, C. W. G., Stevenson, R. J., Mond, J., Stephen, I. D., & Brooks, K. R. (2018). *The high-level basis of body adaptation Subject Category: Subject Areas: Author for correspondence :*

Buracas, G. T., & Boynton, G. M. (2002). Efficient Design of Event-Related fMRI Experiments Using M-Sequences. *NeuroImage*, *813*(3), 801–813. https://doi.org/10.1006/nimg.2002.1116

Buxhoeveden, D. P., & Casanova, M. F. (2002). The minicolumn hypothesis in neuroscience. *Brain*, *125*(5), 935–951. https://doi.org/10.1093/brain/awf110

Cao, Z., Hidalgo, G., Simon, T., Wei, S.-E., & Sheikh, Y. (2019). OpenPose: Realtime Multi-Person 2D Pose Estimation using Part Affinity Fields. *ArXiv:1812.08008 [Cs]*. http://arxiv.org/abs/1812.08008

Carey, M., Knight, R., & Preston, C. (2019). Distinct neural response to visual perspective and body size in the extrastriate body area. *Behavioural Brain Research*, *372*, 112063. https://doi.org/10.1016/j.bbr.2019.112063

Carlson, T., Tovar, D. A., Alink, A., & Kriegeskorte, N. (2013). Representational dynamics of object vision: The first 1000 ms. *Journal of Vision*, *13*(10), 1–1. https://doi.org/10.1167/13.10.1

Caspari, N., Popivanov, I. D., De Mazière, P. A., Vanduffel, W., Vogels, R., Orban, G. A., & Jastorff, J. (2014). Fine-grained stimulus representations in body selective areas of human occipito-temporal cortex. *NeuroImage*, *102*(P2), 484–497. https://doi.org/10.1016/j.neuroimage.2014.07.066

Chan, A. W.-Y., Kravitz, D. J., Truong, S., Arizpe, J., & Baker, C. I. (2010). Cortical representations of bodies and faces are strongest in commonly experienced configurations. *Nature Neuroscience*, *13*(4), 417–418. https://doi.org/10.1038/nn.2502

Chan, A. W.-Y., Peelen, M. V., & Downing, P. E. (2004). The effect of viewpoint on body representation in the extrastriate body area. *Neuroreport*, *15*(15), 2407–2410. https://doi.org/10.1097/00001756-200410250-00021

Chen, X., & Yuille, A. L. (2014). Articulated Pose Estimation by a Graphical Model with Image Dependent Pairwise Relations. *Advances in Neural Information Processing Systems (NIPS)*, 1736–1744.

Cichy, R. M., Pantazis, D., & Oliva, A. (2014). Resolving human object recognition in space and time. *Nature Neuroscience*, *17*(3), 455–462. https://doi.org/10.1038/nn.3635

Contini, E. W., Wardle, S. G., & Carlson, T. A. (2017). Decoding the time-course of object recognition in the human brain: From visual features to categorical decisions. *Neuropsychologia*, *105*(October 2016), 165–176. https://doi.org/10.1016/j.neuropsychologia.2017.02.013

Cowey, A., & Rolls, E. T. (1974). Human cortical magnification factor and its relation to visual acuity. *Experimental Brain Research*, *21*(5). https://doi.org/10.1007/BF00237163

Cox, R. W. (1996). AFNI: software for analysis and visualization of functional magnetic resonance neuroimages. *Computers and Biomedical Research*, *29*(29), 162–173. https://doi.org/10.1006/cbmr.1996.0014

Cross, E. S., MacKie, E. C., Wolford, G., & Antonia, A. F. (2010). Contorted and ordinary body postures in the human brain. *Experimental Brain Research*, *204*(3), 397–407. https://doi.org/10.1007/s00221-009-2093-x

De Gelder, B., Bachoud-Lévi, A. C., & Degos, J. D. (1998). Inversion superiority in visual agnosia may be common to a variety of orientation polarised objects besides faces. *Vision Research*, *38*(18), 2855–2861. https://doi.org/10.1016/S0042-6989(97)00458-6

De Martino, F., Moerel, M., Ugurbil, K., Goebel, R., Yacoub, E., & Formisano, E. (2015). Frequency preference and attention effects across cortical depths in the human primary auditory cortex. *PNAS*, *112*(52). https://doi.org/10.1073/pnas.1507552112

De Rosario-Martinez, H. (2015). phia: Post-hoc interaction analysis. *R Package Version 0.2-1*.

Desimone, R., Albright, T. D., Gross, C. G., & Bruce, C. (1984). Stimulus-selective neurons in the macaque. *Journal of Neuroscience*, *4*(8), 2051–2062.

DiCarlo, J. J., & Cox, D. D. (2007). Untangling invariant object recognition. *Trends in Cognitive Sciences*, *11*(8), 333–341. https://doi.org/10.1016/j.tics.2007.06.010

DiCarlo, J. J., Zoccolan, D., & Rust, N. C. (2012). How does the brain solve visual object recognition? *Neuron*, *73*(3), 415–434. https://doi.org/10.1016/j.neuron.2012.01.010

Downing, P. E., Jiang, Y., Shuman, M., & Kanwisher, N. (2001). A Cortical Area Selective for Visual Processing of the Human Body. *Science*, *293*(5539), 2470–2473.

Downing, P. E., & Peelen, M. V. (2011). The role of occipitotemporal body-selective regions in person perception. *Cognitive Neuroscience*, *2*(3–4), 186–203. https://doi.org/10.1080/17588928.2011.582945

Downing, P. E., Wiggett, A. J., & Peelen, M. V. (2007). Functional Magnetic Resonance Imaging Investigation of Overlapping Lateral Occipitotemporal Activations Using Multi-Voxel Pattern Analysis. *The Journal of Neuroscience*, *27*(1), 226–233. https://doi.org/10.1523/JNEUROSCI.3619-06.2007

Dubois, S., Rossion, B., Schlitz, C., Bodart, J. M., Michel, C., Bruyer, R., & Crommelinck, M. (1999). Effect of familiarity on the processing of human faces. *NeuroImage*, *9*(3), 278–289. https://doi.org/10.1006/nimg.1998.0409

Duchaine, B. C., & Nakayama, K. (2006). Developmental prosopagnosia: A window to content-specific face processing. *Current Opinion in Neurobiology*, *16*(2), 166–173. https://doi.org/10.1016/j.conb.2006.03.003

Duchaine, B., & Nakayama, K. (2005). Dissociations of face and object recognition in developmental prosopagnosia. *Journal of Cognitive Neuroscience*, *17*(2), 249–261. https://doi.org/10.1162/0898929053124857

Duchaine, B., & Yovel, G. (2015). A Revised Neural Framework for Face Processing. *Annual Review of Vision Science*, *1*(1), 393–416. https://doi.org/10.1146/annurev-vision-082114-035518

Ewbank, M. P., Lawson, R. P., Henson, R. N., Rowe, J. B., Passamonti, L., & Calder, A. J. (2011). Changes in "Top-Down" Connectivity Underlie Repetition Suppression in the Ventral Visual Pathway. *Journal of Neuroscience*, *31*(15), 5635–5642. https://doi.org/10.1523/JNEUROSCI.5013-10.2011

Ewbank, Michael P., & Andrews, T. J. (2008). Differential sensitivity for viewpoint between familiar and unfamiliar faces in human visual cortex. *NeuroImage*, *40*, 1857–1870. https://doi.org/10.1016/j.neuroimage.2008.01.049

Fang, F., & He, S. (2005). Viewer-Centered Object Representation in the Human Visual System Revealed by Viewpoint Aftereffects. *Neuron*, *45*(5), 793–800. https://doi.org/10.1016/j.neuron.2005.01.037

Fang, F., Kersten, D., & Murray, S. O. (2008). Perceptual grouping and inverse fMRI activity patterns in human visual cortex. *Journal of Vision*, *8*(7), 2–9. https://doi.org/10.1167/8.7.2.Introduction

Fang, F., Murray, S. O., & He, S. (2007). Duration-dependent fMRI adaptation and distributed viewer-centered face representation in human visual cortex. *Cerebral Cortex*, *17*(6), 1402–1411. https://doi.org/10.1093/cercor/bhl053

Farah, M. J. (1996). Is face recognition "special"? Evidence from neuropsychology. *Behavioural Brain Research*, *76*(1–2), 181–189. https://doi.org/10.1016/0166-4328(95)00198-0

Ferri, S., Kolster, H., Jastorff, J., & Orban, G. A. (2013). The overlap of the EBA and the MT/V5 cluster. *NeuroImage*, *66*, 412–425. https://doi.org/10.1016/j.neuroimage.2012.10.060

Fischl, B. (2012). FreeSurfer. *NeuroImage*, *62*, 774–781. https://doi.org/10.1016/j.neuroimage.2012.01.021

Formisano, E., Kim, D.-S., Di Salle, F., van de Moortele, P.-F., Ugurbil, K., & Goebel, R. (2003). Mirror-Symmetric Tonotopic Maps in Human Primary Auditory Cortex. *Neuron*, *40*(4), 859–869. https://doi.org/10.1016/S0896-6273(03)00669-X

Fox, J., & Weisberg, S. (2019). An R companion to applied regression (Third). *Thousand Oaks CA: Sage*.

Freiwald, W. A., & Tsao, D. Y. (2010). Functional Compartmentalization and Viewpoint Generalization Within the Macaque Face-Processing System. *Science*, *330*(6005), 845–851. https://doi.org/10.1126/science.1194908

Ghuman, A. S., McDaniel, J. R., & Martin, A. (2010). Face Adaptation without a Face. *Current Biology*, *20*(1), 32–36. https://doi.org/10.1016/j.cub.2009.10.077

Gilaie-Dotan, S., & Malach, R. (2007). Sub-exemplar shape tuning in human face-related areas. *Cerebral Cortex*, *17*(2), 325–338. https://doi.org/10.1093/cercor/bhj150

Glauert, R., Rhodes, G., Byrne, S., Fink, B., & Grammer, K. (2009). Body dissatisfaction and the effects of perceptual exposure on body norms and ideals. *International Journal of Eating Disorders*, *42*(5), 443–452. https://doi.org/10.1002/eat.20640

Gomez, J., Pestilli, F., Witthoft, N., Golarai, G., Liberman, A., Poltoratski, S., Yoon, J., & Grill-Spector, K. (2015). Functionally Defined White Matter Reveals Segregated Pathways in Human Ventral Temporal Cortex Associated with Category-Specific Processing. *Neuron*, *85*(1), 216–228. https://doi.org/10.1016/j.neuron.2014.12.027

Goodale, M. A., & Milner, D. A. (1992). Separate Visual Pathways for Perception and Action. *Trends in Neurosciences*, *15*(1), 20–25. https://doi.org/10.1016/0166-2236(92)90344-8

Grewe, P., Woermann, F. G., Bien, C. G., & Piefke, M. (2015). Disturbed spatial cognitive processing of body-related stimuli in a case of a lesion to the right fusiform gyrus. *Neurocase*, *21*(6), 688–696. https://doi.org/10.1080/13554794.2014.974619

Grill-Spector, K., Weiner, K. S., Kay, K., & Gomez, J. (2017). The Functional Neuroanatomy of Human Face Perception. *Annual Review of Vision Science*, *3*(1), 167–196. https://doi.org/10.1146/annurev-vision-102016-061214

Grimaldi, P., Saleem, K. S., & Tsao, D. (2016). Anatomical Connections of the Functionally Defined "Face Patches" in the Macaque Monkey. *Neuron*, *90*(6), 1325–1342. https://doi.org/10.1016/j.neuron.2016.05.009

Gross, C. G., Bender, D. B., & Rocha-Miranda, C. E. (1969). Visual Receptive Fields of Neurons in Inferotemporal Cortex of the Monkey. *Science*, *166*(3910), 1303–1306.

Gross, C. G., Roch-Miranda, C. E., & Bender, D. B. (1972). Visual Cortex Properties of Neurons in Inferotemporal of the Macaque. *Journal of Neurophysiology*, *35*(1), 96–111.

Grossman. (2010). FMR-adaptation reveals invariant coding of biological motion on human STS. *Frontiers in Human Neuroscience*, *4*(March), 1–18. https://doi.org/10.3389/neuro.09.015.2010

Grossman, E. D., & Blake, R. (2002). Brain areas active during visual perception of biological motion. *Social Neuroscience: Key Readings*, *9780203496*, 101–114. https://doi.org/10.4324/9780203496190

Halgren, E., Dale, A. M., Sereno, M. I., Tootell, R. B. H., Marinkovic, K., & Rosen, B. R. (1999). Location of human face-selective cortex with respect to retinotopic areas. *Human Brain Mapping*, *7*(1), 29–37. https://doi.org/10.1002/(SICI)1097-0193(1999)7:1<29::AID-HBM3>3.0.CO;2-R

Harel, A., Gilaie-Dotan, S., Malach, R., & Bentin, S. (2010). Top-Down Engagement Modulates the Neural Expressions of Visual Expertise. *Cerebral Cortex*, *20*(10), 2304–2318. https://doi.org/10.1093/cercor/bhp316

He, D., Kersten, D., & Fang, F. (2012). Opposite Modulation of High- and Low-Level Visual Aftereffects by Perceptual Grouping. *Current Biology*, *22*(11), 1040–1045. https://doi.org/10.1016/j.cub.2012.04.026

Henriksson, L., Mur, M., & Kriegeskorte, N. (2015). Faciotopy-A face-feature map with face-like topology in the human occipital face area. *Cortex*, *72*, 156–167. https://doi.org/10.1016/j.cortex.2015.06.030

Hirai, M., Chang, D. H. F., Saunders, D. R., & Troje, N. F. (2011). Body configuration modulates the usage of local cues to direction in biological-motion perception. *Psychological Science*, *22*(12), 1543–1549. https://doi.org/10.1177/0956797611417257

Hiris, E., Mirenzi, A., & Janis, K. (2016). Biological Form is Sufficient to Create a Biological Motion Sex Aftereffect. *Perception*, *45*(10), 1115–1136. https://doi.org/10.1177/0301006616652026

Hodzic, A., Kaas, A., Muckli, L., Stirn, A., & Singer, W. (2009). Distinct cortical networks for the detection and identification of human body. *NeuroImage*, *45*(4), 1264–1271. https://doi.org/10.1016/j.neuroimage.2009.01.027

Hu, Y., Baragchizadeh, A., & O'Toole, A. J. (2020). Integrating faces and bodies: Psychological and neural perspectives on whole person perception. *Neuroscience and Biobehavioral Reviews*, *112*(February), 472–486. https://doi.org/10.1016/j.neubiorev.2020.02.021

Hubel, D. H., & Wiesel, T. N. (1959). Receptive fields of single neurones in the cat's striate cortex. *The Journal of Physiology*, *148*(3), 574–591. https://doi.org/10.1113/jphysiol.1959.sp006308

Hubel, David H, & Wiesel, T. N. (1977). Functional architecture of macaque monkey visual cortex. *Procedings of the Royal Society of London*, *198*, 1–59.

Huber, L., Finn, E. S., Chai, Y., Goebel, R., Stirnberg, R., Stöcker, T., Marrett, S., Uludag, K., Kim, S.-G., Han, S., Bandettini, P. A., & Poser, B. A. (2020). Layer-dependent functional connectivity methods. *Progress in Neurobiology*, 101835. https://doi.org/10.1016/j.pneurobio.2020.101835

Huber, L., Handwerker, D. A., Jangraw, D. C., Chen, G., Hall, A., Stüber, C., Gonzalez-Castillo, J., Ivanov, D., Marrett, S., Guidi, M., Goense, J., Poser, B. A., & Bandettini, P. A. (2017). High-Resolution CBV-fMRI Allows Mapping of Laminar Activity and Connectivity of Cortical Input and Output in Human M1. *Neuron*, *96*(6), 1253-1263.e7. https://doi.org/10.1016/j.neuron.2017.11.005

Hummel, D., Grabhorn, R., & Mohr, H. M. (2012). Body-Shape Adaptation Cannot Be Explained by Adaptation to Narrow and Wide Rectangles. *Perception*, *41*(11), 1315–1322. https://doi.org/10.1068/p7197

Hummel, D., Rudolf, A. K., Brandi, M., Untch, K., Grabhorn, R., Hampel, H., & Mohr, H. M. (2013). Neural Adaptation to Thin and Fat Bodies in the Fusiform Body Area and Middle Occipital Gyrus: An fMRI Adaptation Study. *Human Brain Mapping*, *34*, 3233–3246. https://doi.org/10.1002/hbm.22135

Hummel, D., Rudolf, A. K., Untch, K. H., Grabhorn, R., & Mohr, H. M. (2012). Visual adaptation to thin and fat bodies transfers across identity. *PLoS ONE*, *7*(8), 1–6. https://doi.org/10.1371/journal.pone.0043195

Insafutdinov, E., Pishchulin, L., Andres, B., Andriluka, M., & Schiele, B. (2016). Deepercut: A deeper, stronger, and faster multi-person pose estimation model. *European Conference on Computer Vision*, *9910 LNCS*, 34–50. https://doi.org/10.1007/978-3-319-46466-4_3

Ishizu, T., Amemiya, K., Yumoto, M., & Kojima, S. (2010). Magnetoencephalographic study of the neural responses in body perception. *Neuroscience Letters*, *481*(1), 36–40. https://doi.org/10.1016/j.neulet.2010.06.047

Jiang, X., Rosen, E., Zeffiro, T., VanMeter, J., Blanz, V., & Riesenhuber, M. (2006). Evaluation of a Shape-Based Model of Human Face Discrimination Using fMRI and Behavioral Techniques. *Neuron*, *50*(1), 159–172. https://doi.org/10.1016/j.neuron.2006.03.012

Jokisch, D., Daum, I., & Troje, N. F. (2006). Self recognition versus recognition of others by biological motion: Viewpoint-dependent effects. *Perception*, *35*(7), 911–920. https://doi.org/10.1068/p5540

Kadipasaoglu, C. M., Conner, C. R., Whaley, M. L., Baboyan, V. G., & Tandon, N. (2016). Category-selectivity in human visual cortex follows cortical topology: A grouped icEEG study. *PLoS ONE*, *11*(6), 1–28. https://doi.org/10.1371/journal.pone.0157109

Kalfas, I., Kumar, S., & Vogels, R. (2017). Shape Selectivity of Middle Superior Temporal Sulcus Body Patch Neurons. *Eneuro*, *4*(3), ENEURO.0113-17.2017. https://doi.org/10.1523/ENEURO.0113-17.2017

Kaliukhovich, D. A., & Vogels, R. (2016). Divisive Normalization Predicts Adaptation-Induced Response Changes in Macaque Inferior Temporal Cortex. *The Journal of Neuroscience*, *36*(22), 6116–6128. https://doi.org/10.1523/JNEUROSCI.2011-15.2016

Kanwisher, N., McDermott, J., & Chun, M. M. (1997). The fusiform face area: A module in human extrastriate cortex specialized for face perception. *The Journal of Neuroscience : The Official Journal of the Society for Neuroscience*, *17*(11), 4302–4311. https://doi.org/10.1098/Rstb.2006.1934

Kay, K. N., & Yeatman, J. D. (2017). Bottom-up and top-down computations in word- and face-selective cortex. *ELife*, *6*, e22341. https://doi.org/10.7554/eLife.22341

Kayaert, G., Biederman, I., Op De Beeck, H. P., & Vogels, R. (2005). Tuning for shape dimensions in macaque inferior temporal cortex. *European Journal of Neuroscience*, *22*(1), 212–224. https://doi.org/10.1111/j.1460-9568.2005.04202.x

Kayaert, G., Biederman, I., & Vogels, R. (2003). Shape Tuning in Macaque Inferior Temporal Cortex. *The Journal of Neuroscience*, *23*(7), 3016–3027. https://doi.org/10.1523/JNEUROSCI.23-07-03016.2003

Kemper, V. G., De Martino, F., Emmerling, T. C., Yacoub, E., & Goebel, R. (2018). High resolution data analysis strategies for mesoscale human functional MRI at 7 and 9.4 T. *NeuroImage*, *164*(April 2017), 48–58. https://doi.org/10.1016/j.neuroimage.2017.03.058

Kessler, E., Walls, S. A., & Ghuman, A. S. (2013). Bodies adapt orientation-independent face representations. *Frontiers in Psychology*, *4*(JUL), 1–8. https://doi.org/10.3389/fpsyg.2013.00413

Kiani, R., Esteky, H., Mirpour, K., & Tanaka, K. (2007). Object Category Structure in Response Patterns of Neuronal Population in Monkey Inferior Temporal Cortex. *Journal of Neurophysiology*, *97*, 4296–4309. https://doi.org/10.1152/jn.00024.2007.

Kourtzi, Z., Erb, M., Grodd, W., & Bülthoff, H. H. (2003). Human Lateral Occipital Complex Representation of Perceived Object Shape by the Human Lateral Occipital Complex. *Cerebral Cortex*, *13*(9), 911–920. https://doi.org/10.1126/science.1061133

Kriegeskorte, N., Mur, M., Ruff, D. A., Kiani, R., Bodurka, J., Esteky, H., Tanaka, K., & Bandettini, P. A. (2008). Matching Categorical Object Representations in Inferior Temporal Cortex of Man and Monkey. *Neuron*, *60*(6), 1126–1141. https://doi.org/10.1016/j.neuron.2008.10.043

Kubiak, A., & Króliczak, G. (2016). Left extrastriate body area is sensitive to the meaning of symbolic gesture: Evidence from fMRI repetition suppression. *Scientific Reports*, *6*(1), 31064. https://doi.org/10.1038/srep31064

Kumar, S., Popivanov, I. D., & Vogels, R. (2017). Transformation of Visual Representations Across Ventral Stream Body-selective Patches. *Cerebral Cortex*, *November 2017*, 1–15. https://doi.org/10.1093/cercor/bhx320

Landis, T., Cummings, J. L., Christen, L., Bogen, J. E., & Imhof, H. G. (1986). Are Unilateral Right Posterior Cerebral Lesions Sufficient to Cause Prosopagnosia? Clinical and Radiological Findings in Six Additional Patients. *Cortex*, *22*(2), 243–252. https://doi.org/10.1016/S0010-9452(86)80048-X

Lawrence, S. J. D., Formisano, E., Muckli, L., & de Lange, F. P. (2019). Laminar fMRI: Applications for cognitive neuroscience. *NeuroImage*, *197*(May), 785–791. https://doi.org/10.1016/j.neuroimage.2017.07.004

Lawson, R. P., Clifford, C. W. G., & Calder, A. J. (2009). About Turn The Visual Representation of Human Body Orientation Revealed by Adaptation. *Psychological Science*, *20*(3), 363–371.

Le Grand, R., Cooper, P. A., Mondloch, C. J., Lewis, T. L., Sagiv, N., de Gelder, B., & Maurer, D. (2006). What aspects of face processing are impaired in developmental prosopagnosia? *Brain and Cognition*, *61*(2), 139–158. https://doi.org/10.1016/j.bandc.2005.11.005

Leaver, A. M., & Rauschecker, J. P. (2016). Functional Topography of Human Auditory Cortex. *Journal of Neuroscience*, *36*(4), 1416–1428. https://doi.org/10.1523/JNEUROSCI.0226-15.2016

Leopold, D. A., O'Toole, A. J., Vetter, T., & Blanz, V. (2001). Prototype-referenced shape encoding revealed by high-level aftereffects. *Nature Neuroscience*, *4*(1), 89–94. https://doi.org/10.1038/82947

Levine, D. N., & Calvanio, R. (1989). Prosopagnosia: A defect in visual configural processing. *Brain and Cognition*, *10*(2), 149–170. https://doi.org/10.1016/0278-2626(89)90051-1

Liu, H., Agam, Y., Madsen, J. R., & Kreiman, G. (2009). Timing, Timing, Timing: Fast Decoding of Object Information from Intracranial Field Potentials in Human Visual Cortex. *Neuron*, *62*(2), 281–290. https://doi.org/10.1016/j.neuron.2009.02.025

Liu, T. T. (2004). Efficiency, power, and entropy in event-related fMRI with multiple trial types. Part II: design of experiments. *NeuroImage*, *21*(1), 401–413. https://doi.org/10.1016/j.neuroimage.2003.09.030

Liu, X., & Engel, S. A. (2020). Higher-Level Meta-Adaptation Mitigates Visual Distortions Produced by Lower-Level Adaptation. *Psychological Science*, *31*(6), 654–662. https://doi.org/10.1177/0956797620907090

Loffler, G., Yourganov, G., Wilkinson, F., & Wilson, H. R. (2005). FMRI evidence for the neural representation of faces. *Nature Neuroscience*, *8*(10), 1386–1390. https://doi.org/10.1038/nn1538

Lohse, M., Garrido, L., Driver, J., Dolan, R. J., Duchaine, B. C., & Furl, N. (2016). Effective Connectivity from Early Visual Cortex to Posterior Occipitotemporal Face Areas Supports Face Selectivity and Predicts Developmental Prosopagnosia. *The Journal of Neuroscience*, *36*(13), 3821–3828. https://doi.org/10.1523/JNEUROSCI.3621-15.2016

Lu, H., Tjan, B. S., & Liu, Z. (2006). Shape recognition alters sensitivity in stereoscopic depth discrimination. *Journal of Vision*, *6*(1), 7. https://doi.org/10.1167/6.1.7

Maurer, D., Grand, R. L., & Mondloch, C. J. (2002). The many faces of configural processing. *Trends in Cognitive Sciences*, *6*(6), 255–260. https://doi.org/10.1016/S1364-6613(02)01903-4

McCarthy, G., Puce, A., Belger, A., & Allison, T. (1999). Electrophysiological Studies of Human Face Perception. II:Response Properties of Face-specific Potentials Generated in Occipitotemporal Cortex. *Cerebral Cortex*, *9*, 1047–3211.

McConachie, H. R. (1976). Developmental Prosopagnosia. A Single Case Report. *Cortex*, *12*(1), 76–82. https://doi.org/10.1016/S0010-9452(76)80033-0

Meadows, J. C. (1974). The Anatomical Basis of Anosognosia. *Journal of Neurology, Neurosurgery, and Psychiatry*, *37*, 489–501.

Meeren, H. K. M., de Gelder, B., Ahlfors, S. P., Hämäläinen, M. S., & Hadjikhani, N. (2013). Different Cortical Dynamics in Face and Body Perception: An MEG study. *PLoS ONE*, *8*(9). https://doi.org/10.1371/journal.pone.0071408

Merzenich, M. M., & Brugge, J. F. (1973). Representation of the cochlear partition on the superior temporal plane of the macaque monkey. *Brain Research*, *50*(2), 275–296. https://doi.org/10.1016/0006-8993(73)90731-2

Meyers, E. M., Borzello, M., Freiwald, W. A., & Tsao, D. (2015). Intelligent Information Loss: The Coding of Facial Identity, Head Pose, and Non-Face Information in the Macaque Face Patch System. *Journal of Neuroscience*, *35*(18), 7069–7081. https://doi.org/10.1523/JNEUROSCI.3086-14.2015

Minnebusch, D. A., Suchan, B., & Daum, I. (2009). Losing your head: Behavioral and electrophysiological effects of body inversion. *Journal of Cognitive Neuroscience*, *21*(5), 865–874. https://doi.org/10.1162/jocn.2009.21074

Moeller, Sebastin, Freiwald, W. A., & Tsao, D. Y. (2008). Patches with Links: A Unified Macaque Temporal Lobe. *Science*, *320*, 1355–1359.

Moeller, Steen, Pisharady, P. K., Ramanna, S., Lenglet, C., Wu, X., Dowdle, L., Yacoub, E., Uğurbil, K., & Akçakaya, M. (2020). *NOise Reduction with DIstribution Corrected (NORDIC) PCA in dMRI with complex-valued parameter-free locally low-rank processing* [Preprint]. Neuroscience. https://doi.org/10.1101/2020.08.25.267062

Mohamed, T. N., Neumann, M. F., & Schweinberger, S. R. (2011). Combined effects of attention and inversion on event-related potentials to human bodies and faces. *Cognitive Neuroscience*, *2*(3–4), 138–146. https://doi.org/10.1080/17588928.2011.597848

Moreau, Q., Pavone, E. F., Aglioti, S. M., & Candidi, M. (2018). Theta synchronization over occipito-temporal cortices during visual perception of body parts. *European Journal of Neuroscience*, *48*(8), 2826–2835. https://doi.org/10.1111/ejn.13782

Moro, V., Pernigo, S., Avesani, R., Bulgarelli, C., Urgesi, C., Candidi, M., & Aglioti, S. M. (2012). Visual body recognition in a prosopagnosic patient. *Neuropsychologia*, *50*(1), 104–117. https://doi.org/10.1016/j.neuropsychologia.2011.11.004

Moro, Valentina, Urgesi, C., Pernigo, S., Lanteri, P., Pazzaglia, M., & Aglioti, S. M. (2008). The Neural Basis of Body Form and Body Action Agnosia. *Neuron*, *60*(2), 235–246. https://doi.org/10.1016/j.neuron.2008.09.022

Mountcastle, V. B. (1957). MODALITY AND TOPOGRAPHIC PROPERTIES OF SINGLE NEURONS OF CAT'S SOMATIC SENSORY CORTEX. *Journal of Neurophysiology*, *20*(4), 408–434. https://doi.org/10.1152/jn.1957.20.4.408

Mugler, J. P., & Brookeman, J. R. (1990). Three-dimensional magnetization-prepared rapid gradient-echo imaging (3D MP RAGE). *Magnetic Resonance in Medicine*, *15*(1), 152–157. https://doi.org/10.1002/mrm.1910150117

Murray, S. O., Kersten, D., Olshausen, B. A., Schrater, P., & Woods, D. L. (2002). Shape perception reduces activity in human primary visual cortex. *Proceedings of the National Academy of Sciences*, *99*(23), 15164–15169. https://doi.org/10.1073/pnas.192579399

Op de Beeck, H. P., Brants, M., Baeck, A., & Wagemans, J. (2010). Distributed subordinate specificity for bodies, faces, and buildings in human ventral visual cortex. *NeuroImage*, *49*(4), 3414–3425. https://doi.org/10.1016/j.neuroimage.2009.11.022

Op De Beeck, H., Wagemans, J., & Vogels, R. (2001). Inferotemporal neurons represent low-dimensional configurations of parameterized shapes. *Nature Neuroscience*, *4*(12), 1244–1252. https://doi.org/10.1038/nn767

Orlov, T., Makin, T. R., & Zohary, E. (2010). Topographic Representation of the Human Body in the Occipitotemporal Cortex. *Neuron*, *68*(3), 586–600. https://doi.org/10.1016/j.neuron.2010.09.032

Palumbo, R., D'Ascenzo, S., & Tommasi, L. (2015). Cross-category adaptation: Exposure to faces produces gender aftereffects in body perception. *Psychological Research*, *79*(3), 380–388. https://doi.org/10.1007/s00426-014-0576-2

Palumbo, R., Laeng, B., & Tommasi, L. (2013). Gender-specific aftereffects following adaptation to silhouettes of human bodies. *Visual Cognition*, *21*(1), 1–12. https://doi.org/10.1080/13506285.2012.753970

Park, S., Nie, B. X., & Zhu, S.-C. (2018). Attribute And-Or Grammar for Joint Parsing of Human Pose, Parts and Attributes. *IEEE Transactions on Pattern Analysis and Machine Intelligence*, *40*(7), 1555–1569. https://doi.org/10.1109/TPAMI.2017.2731842

Peelen, M. V., & Downing, P. E. (2005). Selectivity for the human body in the fusiform gyrus. *Journal of Neurophysiology*, *93*(1), 603–608. https://doi.org/10.1152/jn.00513.2004

Pinsk, M. A., Arcaro, M., Weiner, K. S., Kalkus, J. F., Inati, S. J., Gross, C. G., & Kastner, S. (2009). Neural Representations of Faces and Body Parts in Macaque and Human Cortex: A Comparative fMRI Study. *Journal of Neurophysiology*, 2581–2600. https://doi.org/10.1152/jn.91198.2008.

Pinsk, M. A., DeSimone, K., Moore, T., Gross, C. G., & Kastner, S. (2005). Representations of faces and body parts in macaque temporal cortex: A functional MRI study. *Proceedings of the National Academy of Sciences*, *102*(19), 6996–7001. https://doi.org/10.1073/pnas.0502605102

Pitcher, D., Charles, L., Devlin, J. T., Walsh, V., & Duchaine, B. (2009). Triple Dissociation of Faces, Bodies, and Objects in Extrastriate Cortex. *Current Biology*, *19*(4), 319–324. https://doi.org/10.1016/j.cub.2009.01.007

Popivanov, I. D., Jastorff, J., Vanduffel, W., & Vogels, R. (2012). Stimulus representations in body-selective regions of the macaque cortex assessed with

event-related fMRI. *NeuroImage*, *63*(2), 723–741. https://doi.org/10.1016/j.neuroimage.2012.07.013

Popivanov, I. D., Jastorff, J., Vanduffel, W., & Vogels, R. (2014). Heterogeneous Single-Unit Selectivity in an fMRI-Defined Body-Selective Patch. *Journal of Neuroscience*, *34*(1), 95–111. https://doi.org/10.1523/JNEUROSCI.2748-13.2014

Popivanov, I. D., Jastorff, J., Vanduffel, W., & Vogels, R. (2015). Tolerance of Macaque Middle STS Body Patch Neurons to Shape-preserving Stimulus Transformations. *Journal of Cognitive Neuroscience*, *27*(5), 1001–1016. https://doi.org/10.1162/jocn

Popivanov, I. D., Schyns, P. G., & Vogels, R. (2016). Stimulus features coded by single neurons of a macaque body category selective patch. *Proceedings of the National Academy of Sciences*, *113*(17), E2450–E2459. https://doi.org/10.1073/pnas.1520371113

Pourtois, G., Peelen, M. V., Spinelli, L., Seeck, M., & Vuilleumier, P. (2007). Direct intracranial recording of body-selective responses in human extrastriate visual cortex. *Neuropsychologia*, *45*(11), 2621–2625. https://doi.org/10.1016/j.neuropsychologia.2007.04.005

Premereur, E., Taubert, J., Janssen, P., Vogels, R., & Vanduffel, W. (2016). Effective Connectivity Reveals Largely Independent Parallel Networks of Face and Body Patches. *Current Biology*, *26*(24), 3269–3279. https://doi.org/10.1016/j.cub.2016.09.059

Proklova, D., Kaiser, D., & Peelen, M. V. (2016). Disentangling Representations of Object Shape and Object Category in Human Visual Cortex: The Animate–Inanimate Distinction. *Journal of Cognitive Neuroscience*, *28*(5), 680–692. https://doi.org/10.1162/jocn

Proverbio, A. M., Gabaro, V., Orlandi, A., & Zani, A. (2015). Semantic brain areas are involved in gesture comprehension: An electrical neuroimaging study. *Brain and Language*, *147*, 30–40. https://doi.org/10.1016/j.bandl.2015.05.002

Puce, A., & Perrett, D. (2003). Electrophysiology and brain imaging of biological motion. *Social Neuroscience: Key Readings*, 115–130. https://doi.org/10.4324/9780203496190

Qiu, C., Burton, P. C., Kersten, D., & Olman, C. A. (2016). Responses in early visual areas to contour integration are context dependent. *Journal of Vision*, *16*(2016), 1–18. https://doi.org/10.1167/16.8.19.doi

Reed, C. L., Stone, V. E., Bozova, S., & Tanaka, J. (2003). THE BODY-INVERSION EFFECT. *Psychological Science*, *14*(4), 302–308.

Reed, C. L., Stone, V. E., Grubb, J. D., & McGoldrick, J. E. (2006). Turning configural processing upside down: Part and whole body postures. *Journal of Experimental Psychology: Human Perception and Performance*, *32*(1), 73–87. https://doi.org/10.1037/0096-1523.32.1.73

Righart, R., & de Gelder, B. (2007). Impaired face and body perception in developmental prosopagnosia. *Proceedings of the National Academy of Sciences*, *104*(43), 17234–17238. https://doi.org/10.1073/pnas.0707753104

Rizzolatti, G., & Matelli, M. (2003). Two different streams form the dorsal visual system: Anatomy and functions. *Experimental Brain Research*, *143*, 146–157. https://doi.org/10.1007/s00221-003-1588-0

Rovamo, J., & Virsu, V. (1979). An estimation and application of the human cortical magnification factor. *Experimental Brain Research*, *37*(3). https://doi.org/10.1007/BF00236819

Ryu, J. J., & Chaudhuri, A. (2006). Representations of familiar and unfamiliar faces as revealed by viewpoint-aftereffects. *Vision Research*, *46*(23), 4059–4063. https://doi.org/10.1007/s11422-007-9078-5

Sacchett, C., & Humphreys, G. W. (1992). Calling a squirrel a squirrel but a canoe a wigwam: A category-specific deficit for artefactual objects and body parts. *Cognitive Neuropsychology*, *9*(1), 73–86. https://doi.org/10.1080/02643299208252053

Saxe, R., Jamal, N., & Powell, L. (2006). My body or yours? The effect of visual perspective on cortical body representations. *Cerebral Cortex*, *16*(2), 178–182. https://doi.org/10.1093/cercor/bhi095

Schiltz, C., & Rossion, B. (2006). Faces are represented holistically in the human occipito-temporal cortex. *NeuroImage*, *32*, 1385–1394. https://doi.org/10.1016/j.neuroimage.2006.05.037

Schwarzlose, R. F., Baker, C. I., & Kanwisher, N. (2005). Separate Face and Body Selectivity on the Fusiform Gyrus. *The Journal of Neuroscience*, *25*(47), 11055–11059. https://doi.org/10.1523/JNEUROSCI.2621-05.2005

Sekunova, A., Black, M., Parkinson, L., & Barton, J. J. S. (2013). Viewpoint and pose in body-form adaptation. *Perception*, *42*(2), 176–186. https://doi.org/10.1068/p7265

Stigliani, A., Weiner, K. S., & Grill-spector, K. (2015). Temporal Processing Capacity in High-Level Visual Cortex Is Domain Specific. *Journal of Neuroscience*, *35*(36), 12412–12424. https://doi.org/10.1523/JNEUROSCI.4822-14.2015

Susilo, T., & Duchaine, B. (2013). Advances in developmental prosopagnosia research. *Current Opinion in Neurobiology*, *23*(3), 423–429. https://doi.org/10.1016/j.conb.2012.12.011

Susilo, T., Yang, H., Potter, Z., Robbins, R., & Duchaine, B. (2015). Normal Body Perception despite the Loss of Right Fusiform Gyrus. *Jorunal of Cognitive Neuroscience*, *27*(3), 614–622. https://doi.org/10.1162/jocn

Suzuki, K., Yamadori, A., & Fujii, T. (1997). Category-specific comprehension deficit restricted to body parts. *Neurocase*, *3*(3), 193–199. https://doi.org/10.1093/neucas/3.3.193

Swindale, N. V. (1996). The development of topography in the visual cortex: A review of models. *Network: Computation in Neural Systems*, *7*(2), 161–247. https://doi.org/10.1088/0954-898X_7_2_002

Takahashi, H., Shibuya, T., Kato, M., Sassa, T., Koeda, M., Yahata, N., Suhara, T., & Okubo, Y. (2008). Enhanced activation in the extrastriate body area by goal-directed actions. *Psychiatry and Clinical Neurosciences*, *62*(2), 214–219. https://doi.org/10.1111/j.1440-1819.2008.01757.x

Taylor, J. C., Roberts, M. V., Downing, P. E., & Thierry, G. (2010). Functional characterisation of the extrastriate body area based on the N1 ERP component. *Brain and Cognition*, *73*(3), 153–159. https://doi.org/10.1016/j.bandc.2010.04.001

Taylor, J. C., Wiggett, A. J., & Downing, P. E. (2007). Functional MRI analysis of body and body part representations in the extrastriate and fusiform body areas. *Journal of Neurophysiology*, *98*(3), 1626–1633. https://doi.org/10.1152/jn.00012.2007

Taylor, J. C., Wiggett, A. J., & Downing, P. E. (2010). FMRI-adaptation studies of viewpoint tuning in the extrastriate and fusiform body areas. *Journal of Neurophysiology*, *103*(December 2009), 1467–1477. https://doi.org/10.1152/jn.00637.2009

Thierry, G., Pegna, A. J., Dodds, C., Roberts, M., Basan, S., & Downing, P. (2006). An event-related potential component sensitive to images of the human body. *NeuroImage*, *32*(2), 871–879. https://doi.org/10.1016/j.neuroimage.2006.03.060

Thoma, V., & Henson, R. N. (2011). Object representations in ventral and dorsal visual streams: FMRI repetition effects depend on attention and part–whole configuration. *NeuroImage*, *57*(2), 513–525. https://doi.org/10.1016/j.neuroimage.2011.04.035

Thomas, C., Avidan, G., Humphreys, K., Jung, K. J., Gao, F., & Behrmann, M. (2009). Reduced structural connectivity in ventral visual cortex in congenital prosopagnosia. *Nature Neuroscience*, *12*(1), 29–31. https://doi.org/10.1038/nn.2224

Thorpe, S. J., Fize, D., & Marlot, C. (1996). Speed of processing in the human visual system. *Letters to Nature*, *381*(6), 520–522. https://doi.org/10.1038/381520a0

Tomasino, B., Weiss, P. H., & Fink, G. R. (2012). Imagined tool-use in near and far space modulates the extra-striate body area. *Neuropsychologia*, *50*(10), 2467–2476. https://doi.org/10.1016/j.neuropsychologia.2012.06.018

Tootell, R. B. H., Silverman, M. S., Hamilton, S. L., Switkes, E., & De Valois, R. L. (1988). Functional anatomy of macaque striate cortex. V. Spatial frequency. *J Neurosci*, *8*(5), 1610–1624.

Troje, N. F. (2003). Reference frames for orientation anisotropies in face recognition and biological-motion perception. *Perception*, *32*(2), 201–210. https://doi.org/10.1068/p3392

Troje, N. F., Sadr, J., Geyer, H., & Nakayama, K. (2006). Adaptation aftereffects in the perception of gender from biological motion. *Journal of Vision*, *6*(8), 7. https://doi.org/10.1167/6.8.7

Troje, N. F., & Westhoff, C. (2006). The Inversion Effect in Biological Motion Perception: Evidence for a "Life Detector"? *Current Biology*, *16*(8), 821–824. https://doi.org/10.1016/j.cub.2006.03.022

Tsao, D. Y., Moeller, S., & Freiwald, W. A. (2008). Comparing face patch systems in macaques and humans. *Proceedings of the National Academy of Sciences*, *105*(49), 19514–19519. https://doi.org/10.1073/pnas.0809662105

Tsao, Doris Y., Freiwald, W. A., Knutsen, T. A., Mandeville, J. B., & Tootell, R. B. H. (2003). Faces and objects in macaque cerebral cortex. *Nature Neuroscience*, *6*(9), 989–995. https://doi.org/10.1038/nn1111

Tsao, Doris Y., Freiwald, W. A., Tootell, R. B. H., & Livingstone, M. S. (2006). A Cortical Region Consisting Entirely of Face-Selective Cells. *Science*, *311*, 212–216.

Urgesi, C., Berlucchi, G., & Aglioti, S. M. (2004). Magnetic Stimulation of Extrastriate Body Area Impairs Visual Processing of Nonfacial Body Parts. *Current Biology*, *14*, 2130–2134. https://doi.org/10.1016/j

Urgesi, C., Candidi, M., Ionta, S., & Aglioti, S. M. (2007). Representation of body identity and body actions in extrastriate body area and ventral premotor cortex. *Nature Neuroscience*, *10*(1), 30–31. https://doi.org/10.1038/nn1815

Uttner, I., Bliem, H., & Danek, A. (2002). Prosopagnosia after unilateral right cerebral infarction. *Journal of Neurology*, *249*(7), 933–935. https://doi.org/10.1007/s00415-002-0710-8

Valentine, T. (1988). Upside-down faces: A review of the effect of inversion upon face. *British Journal of Psychology*, *79*(4), 471–491.

van Koningsbruggen, M. G., Peelen, M. V., & Downing, P. E. (2013). A Causal Role for the Extrastriate Body Area in Detecting People in Real-World Scenes. *Journal of Neuroscience*, *33*(16), 7003–7010. https://doi.org/10.1523/JNEUROSCI.2853-12.2013

Vanduffel, W., Zhu, Q., & Orban, G. A. (2014). Monkey Cortex through fMRI Glasses. *Neuron*, *83*(3), 533–550. https://doi.org/10.1016/j.neuron.2014.07.015

VanRullen, R., & Thorpe, S. J. (2001). Is it a bird? Is it a plane? Ultra-rapid visual categorisation of natural and artifactual objects. *Perception*, *30*(6), 655–668. https://doi.org/10.1068/p3029

Vogels, R., & Orban, G. A. (1996). Coding of stimulus invariances by inferior temporal neurons. *Progress in Brain Research*, *112*, 195–211.

Vuilleumier, P., Armony, J. L., Driver, J., & Dolan, R. J. (2001). Effects of Attention and Emotion on Face Processing in the Human Brain: An Event-Related fMRI Study. *Neuron*, *30*, 829–841.

Waehnert, M. D., Dinse, J., Weiss, M., Streicher, M. N., Waehnert, P., Geyer, S., Turner, R., & Bazin, P. L. (2014). Anatomically motivated modeling of cortical laminae. *NeuroImage*, *93*, 210–220. https://doi.org/10.1016/j.neuroimage.2013.03.078

Wallis, G., & Rolls, E. T. (1997). Invariant Face and Object Recognition in the Visual System. *Progress in Neurobiology*, *51*, 167–194.

Webster, M. A. (2015). Visual Adaptation. *Annual Review of Vision Science*, *1*(1), 547–567. https://doi.org/10.1146/annurev-vision-082114-035509

Webster, M. A., Kaping, D., Mizokami, Y., & Duhamel, P. (2004). Adaptation to natural facial categories. *Nature*, *428*, 557–561. https://doi.org/10.1038/nature02361.1.

Weigelt, S., Koldewyn, K., & Doehrmann, O. (2010). Cross-Category Adaptation Reveals Tight Coupling of Face and Body Perception. *Journal of Neurophysiology*, *104*(2), 581–583. https://doi.org/10.1152/jn.00288.2010

Weiner, K. S., & Grill-Spector, K. (2011). Not one extrastriate body area: Using anatomical landmarks, hMT+, and visual field maps to parcellate limb-selective activations in human lateral occipitotemporal cortex. *NeuroImage*, *56*(4), 2183–2199. https://doi.org/10.1016/j.neuroimage.2011.03.041

Weiner, K. S., & Grill-Spector, K. (2013). Neural representations of faces and limbs neighbor in human high-level visual cortex: Evidence for a new organization principle. *Psychological Research*, *77*(1), 74–97. https://doi.org/10.1007/s00426-011-0392-x

Willems, R. M., Peelen, M. V., & Hagoort, P. (2010). Cerebral Lateralization of Face-Selective and Body-Selective Visual Areas Depends on Handedness. *Cerebral Cortex*, *20*(7), 1719–1725. https://doi.org/10.1093/cercor/bhp234

Winkler, C., & Rhodes, G. (2005). Perceptual adaptation affects attractiveness of female bodies. *British Journal of Psychology*, *96*(2), 141–154. https://doi.org/10.1348/000712605X36343

Wojciulik, E., Kanwisher, N., & Driver, J. (1998). Covert Visual Attention Modulates Face-Specific Activity in the Human Fusiform Gyrus: FMRI Study. *Journal of Neurophysiology*, *79*(3), 1574–1578. https://doi.org/10.1152/jn.1998.79.3.1574

Xu, H., Dayan, P., Lipkin, R. M., & Qian, N. (2008). Adaptation across the Cortical Hierarchy: Low-Level Curve Adaptation Affects High-Level Facial-Expression Judgments. *Journal of Neuroscience*, *28*(13), 3374–3383. https://doi.org/10.1523/JNEUROSCI.0182-08.2008

Xu, J., Moeller, S., Auerbach, E. J., Strupp, J., Smith, S. M., Feinberg, D. A., Yacoub, E., & Kâmil, U. (2013). Evaluation of slice accelerations using multiband echo planar imaging at 3 T. *NeuroImage*, *83*, 991–1001. https://doi.org/10.1016/j.neuroimage.2013.07.055

Yacoub, E., Harel, N., & Ugurbil, K. (2008). High-field fMRI unveils orientation columns in humans. *Proceedings of the National Academy of Sciences of the United States of America*, *105*(30), 10607–10612. https://doi.org/10.1073/pnas.0804110105

Yacoub, E., Shmuel, A., Logothetis, N., & Uğurbil, K. (2007). Robust detection of ocular dominance columns in humans using Hahn Spin Echo BOLD functional MRI at 7 Tesla. *NeuroImage*, *37*(4), 1161–1177. https://doi.org/10.1016/j.neuroimage.2007.05.020

Yang, J., Huber, L., Yu, Y., Chai, Y., Khojandi, A., & Bandettini, P. A. (2019). *High-resolution fMRI maps of columnar organization in human primary somatosensory cortex*. 4.

Yin, R. K. (1969). Looking At Upside-Down Faces. *Journal of Experimental Psychology*, *81*(1), 141–145. https://doi.org/10.1037/h0027474

Yovel, G., & Kanwisher, N. (2004). Face perception: Domain specific, not process specific. *Neuron*, *44*(5), 889–898. https://doi.org/10.1016/j.neuron.2004.11.018

Yovel, G., & Kanwisher, N. (2005). The neural basis of the behavioral face-inversion effect. *Current Biology*, *15*(24), 2256–2262. https://doi.org/10.1016/j.cub.2005.10.072

Yovel, G., Pelc, T., & Lubetzky, I. (2010). It's all in your head: Why is the body inversion effect abolished for headless bodies? *Journal of Experimental Psychology: Human Perception and Performance*, *36*(3), 759–767. https://doi.org/10.1037/a0017451

Zimmermann, J., Goebel, R., Martino, F. D., Moortele, P. V. D., & Yacoub, E. (2011). Mapping the Organization of Axis of Motion Selective Features in Human Area MT Using High-Field fMRI. *PLoS ONE*, *6*(12), 1–10. https://doi.org/10.1371/journal.pone.0028716

Zimmermann, M., Mars, R. B., de Lange, F. P., Toni, I., & Verhagen, L. (2018). Is the extrastriate body area part of the dorsal visuomotor stream? *Brain Structure and Function*, *223*(1), 31–46. https://doi.org/10.1007/s00429-017-1469-0

Zimmermann, M., Verhagen, L., de Lange, F. P., & Toni, I. (2016). The Extrastriate Body Area Computes Desired Goal States during Action Planning. *Eneuro*, *3*(2), ENEURO.0020-16.2016. https://doi.org/10.1523/ENEURO.0020-16.2016

Appendix 1: Supplemental Information for Chapter 2

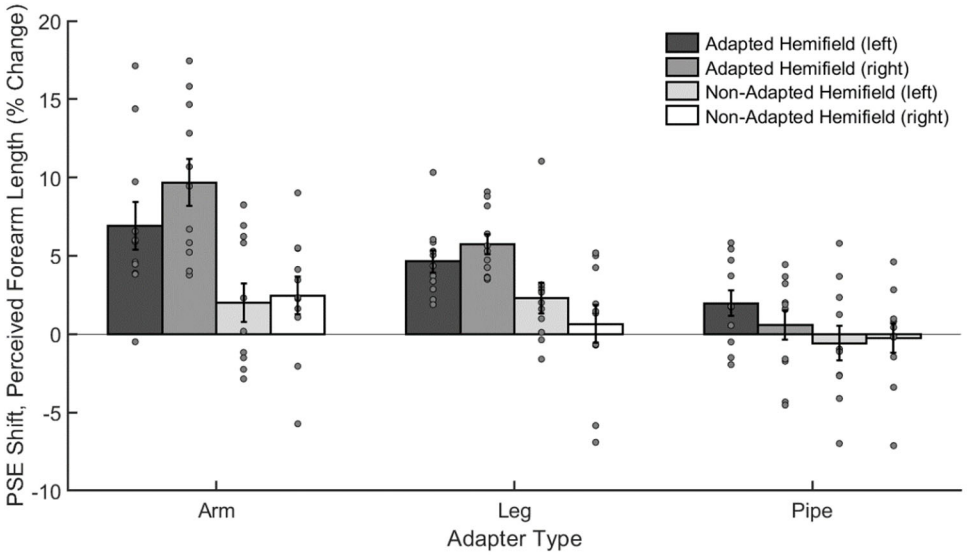

Figure A1.1. Results of Experiment 2 when divided by hemifield of adaptation (left vs right). The average PSE shift (PSE at Post-test minus PSE at Baseline) is shown for each adapter type, in the adapted and non-adapted hemifields, and as a function of hemifield in which each observer adapted (left vs right). Datapoints for individual observers are shown as gray dots. Error bars represent SEM.

Appendix 2: Supplemental Information for Chapter 4

Nordic Denoising: data quality assessment

In this study, we applied a version of the NORDIC denoising algorithm (Steen Moeller et al., 2020) designed for use with magnitude-only data. To ensure that a high degree of smoothing wasn't being introduced when applying this method (potentially biasing the results in favor of cluster and, particularly, columnar interpretations), we computed the smoothness of the fully preprocessed data, both before and after NORDIC, over the entire acquisition volume. Computations were performed using AFNI's (Cox, 1996) 3dFWHMx function. We found that the application of this denoising method only increased data smoothness by ~11%. This would suggest that that our interpretations are unlikely the result of bias resulting from smoothness introduced by denoising. Results for each subject can be found in Appendix Table A2.1.

Table A2.1. FWHM estimates for the fully preprocessed original and Nordic data

	Subject 1	Subject 2	Subject 3	Subject 4
Original	0.93 mm	0.97 mm	0.98 mm	0.94 mm
Nordic	1.01 mm	1.08 mm	1.12 mm	1.04 mm

Additionally, we examined the raw time series of our data within our ROIs. This was to assess the quality of the denoising performance and to ensure that nothing obviously artifactual was potentially being introduced. Time courses for a given run within the rEBA for each subject. All data shown were extracted from layer 4 of the cortex. Generally, we observed that obvious noisy variations at the peaks and troughs of the time series (corresponding to the middle of stimulus and rest blocks, respectively) appear more controlled in the denoised data. Furthermore, nothing obviously artifactual (i.e., major differences in the time series pre and post denoising) was noted in the denoised time series.

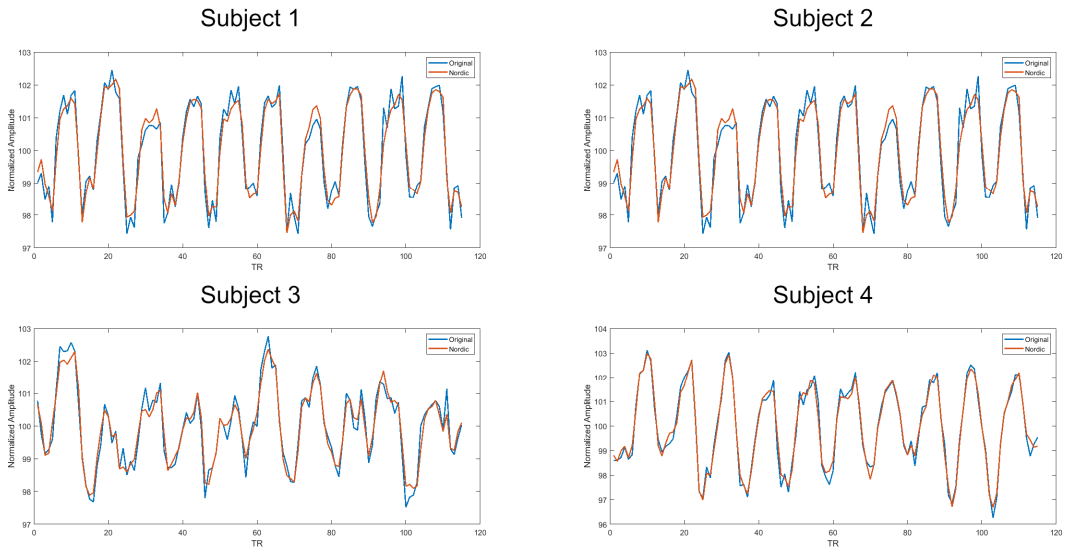

Figure A2.1. Comparison of the time series for a given layer and run before and after the application of denoising.

Supplemental Results

Below are supplemental results, including additional figures and the single subject ROI statistical outputs.

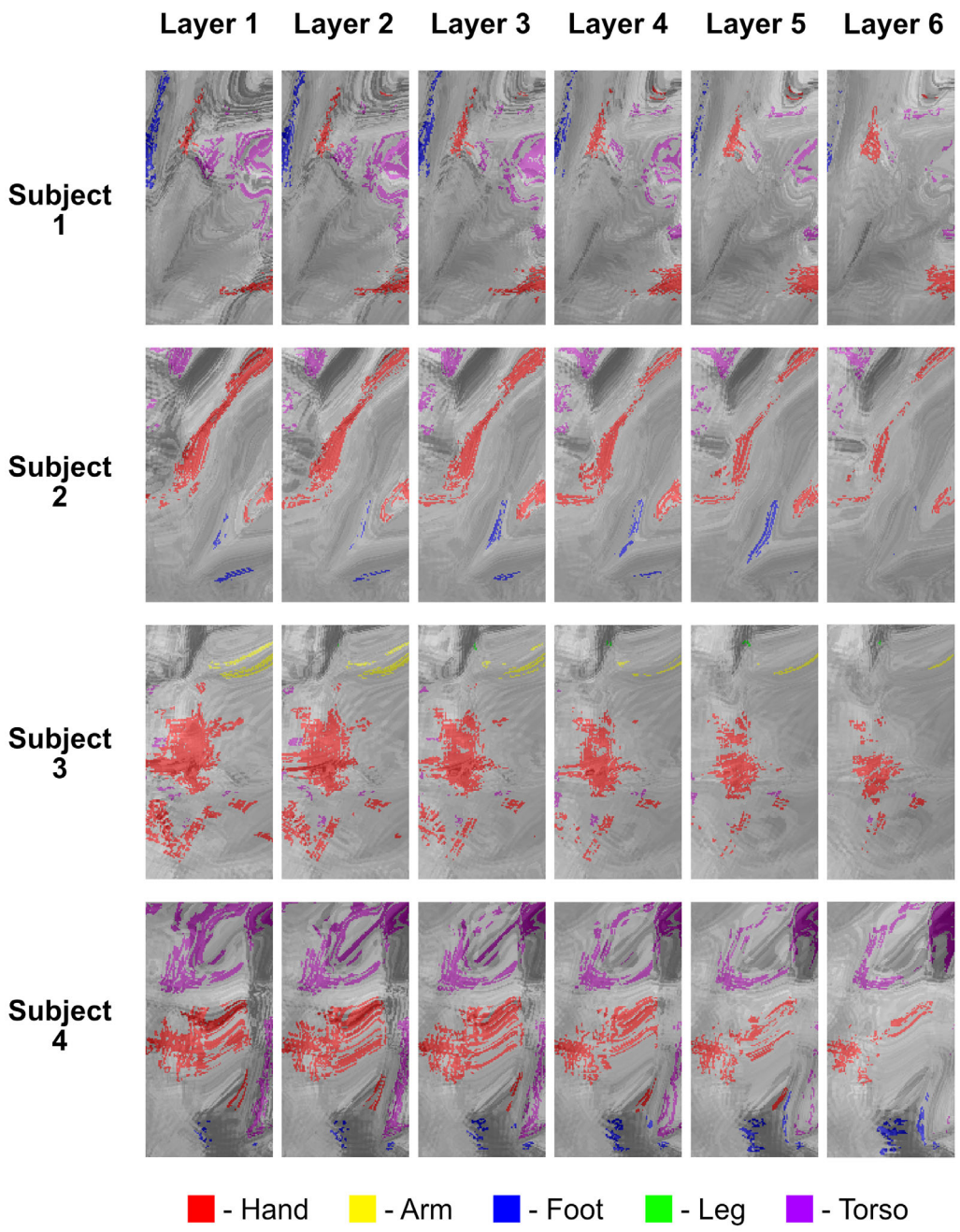

Figure A2.2. Body part preference maps for each subject, overlayed on the mean EPI image. Color legend at the bottom of the figure shows the colors corresponding to each body part category.

*Table A2.2. Results of the individual subject ANOVAs. Significance codes: '***' - p < 0.001 '**' - p < 0.01 '*' - p < 0.05 '.' - p < 0.1 ' ' - p > 1*

		Df	Sum Sq	Mean Sq	F value	Pr(>F)	Significance
Subject 1	layers	5	351.6511	70.33023	161.8241	7.1E-107	***
	conditions	4	67.22962	16.80741	38.67246	1.18E-28	***
	layers:conditions	20	7.304561	0.365228	0.84036	0.664355	
	Residuals	570	247.7272	0.434609	NA	NA	
Subject 2	layers	5	754.1007	150.8201	756.4633	7.2E-249	***
	conditions	4	38.14272	9.535681	47.82778	1.1E-34	***
	layers:conditions	20	7.912465	0.395623	1.984314	0.006732	**
	Residuals	570	113.644	0.199375	NA	NA	
Subject 3	layers	5	281.1133	56.22266	208.6759	3.1E-126	***
	conditions	4	116.4497	29.11242	108.0536	1.75E-68	***
	layers:conditions	20	15.40916	0.770458	2.85963	3.64E-05	***
	Residuals	570	153.5726	0.269426	NA	NA	
Subject 4	layers	5	862.3009	172.4602	637.7523	9.8E-231	***
	conditions	4	28.96284	7.240711	26.77592	2.24E-20	***
	layers:conditions	20	1.963587	0.098179	0.363064	0.995459	
	Residuals	570	154.1387	0.270419	NA	NA	

*Table A2.3. Results of the individual subject condition-based post hoc assessments. Significance codes: '***' - p < 0.001 '**' - p < 0.01 '*' - p < 0.05 '.' - p < 0.1 ' ' - p > 1*

		Value	Df	Sum of Sq	F	Pr(>F)	Significance
Subject 1	Arm-Foot	-0.20364	1	2.488107	5.72493	0.034097	*
	Arm-Hand	-0.54397	1	17.75434	40.85127	2.39E-09	***
	Arm-Leg	0.450871	1	12.19707	28.06445	1.01E-06	***
	Arm-Torso	-0.30223	1	5.4804	12.60995	0.001662	**
	Foot-Hand	-0.34033	1	6.949634	15.99054	0.00036	***
	Foot-Leg	0.654509	1	25.70291	59.14028	5.18E-13	***
	Foot-Torso	-0.09859	1	0.583164	1.341813	0.2472	
	Hand-Leg	0.994843	1	59.38274	136.6348	1.91E-27	***
	Hand-Torso	0.241747	1	3.506495	8.068157	0.013998	*
	Leg-Torso	-0.7531	1	34.02921	78.29841	1E-16	***
	Residuals	NA	570	247.7272	NA	NA	
Subject 2	Arm-Foot	-0.14554	1	1.270871	6.374262	0.023698	*
	Arm-Hand	-0.49258	1	14.55813	73.01869	9.42E-16	***
	Arm-Leg	0.250646	1	3.769419	18.90614	8.13E-05	***
	Arm-Torso	0.092702	1	0.515616	2.586158	0.108355	
	Foot-Hand	-0.34704	1	7.226324	36.24482	1.87E-08	***
	Foot-Leg	0.396184	1	9.417707	47.23606	1.16E-10	***
	Foot-Torso	0.238239	1	3.405477	17.08073	0.000165	***
	Hand-Leg	0.743227	1	33.14317	166.235	1.48E-32	***
	Hand-Torso	0.585282	1	20.55331	103.0885	2.02E-21	***
	Leg-Torso	-0.15794	1	1.496793	7.507412	0.019011	*
	Residuals	NA	570	113.644	NA	NA	
Subject 3	Arm-Foot	-0.22125	1	2.937218	10.90177	0.002124	**
	Arm-Hand	-1.04193	1	65.13654	241.7607	9.48E-45	***
	Arm-Leg	0.278912	1	4.6675	17.32389	0.000146	***
	Arm-Torso	-0.22818	1	3.123945	11.59483	0.002124	**
	Foot-Hand	-0.82067	1	40.41005	149.9859	7.11E-30	***
	Foot-Leg	0.500166	1	15.00998	55.71101	1.58E-12	***
	Foot-Torso	-0.00692	1	0.002877	0.010678	0.917734	
	Hand-Leg	1.320837	1	104.6767	388.5177	2.44E-65	***
	Hand-Torso	0.813746	1	39.73099	147.4655	1.7E-29	***
	Leg-Torso	-0.50709	1	15.42846	57.26426	9.23E-13	***
	Residuals	NA	570	153.5726	NA	NA	
Subject 4	Arm-Foot	-0.10388	1	0.647403	2.394077	0.222481	
	Arm-Hand	-0.48894	1	14.34369	53.04253	9.82E-12	***

Arm-Leg	0.107087	1	0.688053	2.544399	0.222481	
Arm-Torso	-0.34228	1	7.029525	25.99496	2.8E-06	***
Foot-Hand	-0.38506	1	8.896459	32.89883	1.1E-07	***
Foot-Leg	0.210962	1	2.670294	9.874662	0.007051	**
Foot-Torso	-0.23841	1	3.410343	12.61134	0.002076	**
Hand-Leg	0.596026	1	21.31481	78.8215	8.81E-17	***
Hand-Torso	0.146655	1	1.290455	4.772061	0.087995	.
Leg-Torso	-0.44937	1	12.11607	44.80485	4.17E-10	***
Residuals	NA	570	154.1387	NA	NA	

*Table A2.4. Results of the individual subject layer-based post hoc assessments. Significance codes: '***' - p < 0.001 '**' - p < 0.01 '*' - p < 0.05 '.' - p < 0.1 ' ' - p > 1*

		Value	Df	Sum of Sq	F	Pr(>F)	Significance
Subject 1	1	3.664193	1	1342.631	3089.284	1.6E-231	***
	2	3.292019	1	1083.739	2493.595	1.3E-209	***
	3	2.820705	1	795.6377	1830.697	1.6E-179	***
	4	2.310226	1	533.7143	1228.033	7.8E-144	***
	5	1.8248	1	332.9896	766.1816	3.1E-107	***
	6	1.515348	1	229.6279	528.355	3.12E-83	***
	Residuals	NA	570	247.7272	NA	NA	
Subject 2	1	4.3902	1	1927.386	9667.12	0	***
	2	2.966751	1	880.161	4414.592	7.1E-270	***
	3	2.659077	1	707.0691	3546.421	2.8E-246	***
	4	2.011924	1	404.7837	2030.26	1.6E-189	***
	5	1.565639	1	245.1227	1229.453	4.1E-144	***
	6	0.868444	1	75.41948	378.2788	5.25E-65	***
	Residuals	NA	570	113.644	NA	NA	
Subject 3	1	2.670461	1	713.1363	2646.876	1.4E-215	***
	2	2.069392	1	428.2384	1589.449	2.7E-166	***
	3	1.618195	1	261.8556	971.9027	1.1E-124	***
	4	1.2094	1	146.2649	542.8767	2.2E-84	***
	5	0.908179	1	82.47892	306.1286	6.99E-55	***
	6	0.680052	1	46.24705	171.6505	1.81E-34	***
	Residuals	NA	570	153.5726	NA	NA	
Subject 4	1	4.646326	1	2158.834	7983.301	0	***
	2	4.127371	1	1703.519	6299.559	0	***
	3	3.499586	1	1224.71	4528.941	8.8E-273	***
	4	2.324059	1	540.125	1997.365	6E-188	***
	5	1.754298	1	307.7561	1138.073	1.2E-137	***
	6	1.454139	1	211.4519	781.9426	5.5E-109	***
	Residuals	NA	570	154.1387	NA	NA	

*Table A2.5. Results of the individual subject layer x condition based post hoc assessments for the two subjects who showed significant interaction effects. Significance codes: '***' - p < 0.001 '**' - p < 0.01 '*' - p < 0.05 '.' - p < 0.1 ' ' - p > 1*

		Value	Df	Sum of Sq	F	Pr(>F)	Significance
Subject 3	Arm-Foot : 1	-0.32172	1	1.035054	5.191482	0.853478	
	Arm-Hand : 1	-0.82861	1	6.865931	34.43721	4.18E-07	***
	Arm-Leg : 1	0.464588	1	2.15842	10.82591	0.046741	*
	Arm-Torso : 1	0.21341	1	0.455437	2.284319	1	
	Foot-Hand : 1	-0.50689	1	2.569341	12.88695	0.016892	*
	Foot-Leg : 1	0.786311	1	6.182842	31.01107	2.18E-06	***
	Foot-Torso : 1	0.535132	1	2.863664	14.36318	0.008171	**
	Hand-Leg : 1	1.293197	1	16.72359	83.87992	5.63E-17	***
	Hand-Torso : 1	1.042019	1	10.85803	54.46025	3.33E-11	***
	Leg-Torso : 1	-0.25118	1	0.630906	3.164411	1	
	Arm-Foot : 2	-0.1991	1	0.396421	1.988317	1	
	Arm-Hand : 2	-0.62075	1	3.853294	19.32683	0.000683	***
	Arm-Leg : 2	0.310788	1	0.965893	4.844594	0.956524	
	Arm-Torso : 2	0.117631	1	0.138371	0.694024	1	
	Foot-Hand : 2	-0.42165	1	1.777851	8.917103	0.123752	
	Foot-Leg : 2	0.509891	1	2.599893	13.04019	0.015925	*
	Foot-Torso : 2	0.316735	1	1.003209	5.031758	0.884449	
	Hand-Leg : 2	0.931537	1	8.677615	43.52401	5.56E-09	***
	Hand-Torso : 2	0.73838	1	5.452055	27.34568	1.29E-05	***
	Leg-Torso : 2	-0.19316	1	0.373096	1.871322	1	
	Arm-Foot : 3	-0.18996	1	0.360831	1.809809	1	
	Arm-Hand : 3	-0.55908	1	3.125701	15.67747	0.004231	**
	Arm-Leg : 3	0.274648	1	0.754316	3.783395	1	
	Arm-Torso : 3	0.070599	1	0.049843	0.249994	1	
	Foot-Hand : 3	-0.36912	1	1.362526	6.833975	0.367218	
	Foot-Leg : 3	0.464604	1	2.158566	10.82664	0.046741	*
	Foot-Torso : 3	0.260555	1	0.678889	3.405078	1	
	Hand-Leg : 3	0.833728	1	6.95102	34.86399	3.46E-07	***
	Hand-Torso : 3	0.629679	1	3.964957	19.8869	0.000525	***
	Leg-Torso : 3	-0.20405	1	0.416359	2.088317	1	
	Arm-Foot : 4	-0.11307	1	0.12784	0.641204	1	
	Arm-Hand : 4	-0.42091	1	1.771644	8.885975	0.123752	
	Arm-Leg : 4	0.194186	1	0.377082	1.891317	1	
	Arm-Torso : 4	0.047179	1	0.022259	0.111641	1	
	Foot-Hand : 4	-0.30784	1	0.947671	4.753198	0.978523	
	Foot-Leg : 4	0.307252	1	0.944041	4.734993	0.978523	
	Foot-Torso : 4	0.160245	1	0.256786	1.287952	1	
	Hand-Leg : 4	0.615095	1	3.78342	18.97636	0.000801	***

	Hand-Torso : 4	0.468088	1	2.191064	10.98964	0.044824	*
	Leg-Torso : 4	-0.14701	1	0.216111	1.083939	1	
	Arm-Foot : 5	-0.06289	1	0.039548	0.198359	1	
	Arm-Hand : 5	-0.32329	1	1.045161	5.242175	0.851592	
	Arm-Leg : 5	0.143892	1	0.207048	1.038483	1	
	Arm-Torso : 5	0.042325	1	0.017914	0.089851	1	
	Foot-Hand : 5	-0.2604	1	0.678094	3.401092	1	
	Foot-Leg : 5	0.206779	1	0.427574	2.144569	1	
	Foot-Torso : 5	0.105212	1	0.110696	0.555214	1	
	Hand-Leg : 5	0.467181	1	2.182581	10.9471	0.044849	*
	Hand-Torso : 5	0.365615	1	1.33674	6.704639	0.384614	
	Leg-Torso : 5	-0.10157	1	0.103158	0.517404	1	
	Arm-Foot : 6	0.01351	1	0.001825	0.009154	1	
	Arm-Hand : 6	-0.20285	1	0.411465	2.063769	1	
	Arm-Leg : 6	0.115777	1	0.134043	0.672315	1	
	Arm-Torso : 6	0.065066	1	0.042336	0.212341	1	
	Foot-Hand : 6	-0.21636	1	0.468097	2.34782	1	
	Foot-Leg : 6	0.102267	1	0.104586	0.524568	1	
	Foot-Torso : 6	0.051556	1	0.02658	0.133318	1	
	Hand-Leg : 6	0.318623	1	1.015206	5.091931	0.878954	
	Hand-Torso : 6	0.267912	1	0.717767	3.600079	1	
	Leg-Torso : 6	-0.05071	1	0.025716	0.128984	1	
	Residuals	NA	570	113.644	NA	NA	
	Arm-Foot : 1	-0.31234	1	0.975579	3.620957	1	
	Arm-Hand : 1	-1.62426	1	26.38227	97.92039	1.2E-19	***
	Arm-Leg : 1	0.433483	1	1.879074	6.974368	0.271849	
	Arm-Torso : 1	-0.30723	1	0.943885	3.503321	1	
	Foot-Hand : 1	-1.31192	1	17.21133	63.88153	3.98E-13	***
	Foot-Leg : 1	0.745825	1	5.562556	20.64597	0.000304	***
	Foot-Torso : 1	0.005116	1	0.000262	0.000971	1	
	Hand-Leg : 1	2.057745	1	42.34314	157.1607	3.1E-30	***
	Hand-Torso : 1	1.317035	1	17.34581	64.38068	3.23E-13	***
Subject 4	Leg-Torso : 1	-0.74071	1	5.486512	20.36373	0.000342	***
	Arm-Foot : 2	-0.28294	1	0.800571	2.971398	1	
	Arm-Hand : 2	-1.36805	1	18.71573	69.46528	3.27E-14	***
	Arm-Leg : 2	0.389527	1	1.517316	5.631668	0.503146	
	Arm-Torso : 2	-0.25642	1	0.657535	2.440507	1	
	Foot-Hand : 2	-1.08511	1	11.77466	43.7028	4.4E-09	***
	Foot-Leg : 2	0.672471	1	4.522173	16.78449	0.00187	**
	Foot-Torso : 2	0.026519	1	0.007033	0.026102	1	
	Hand-Leg : 2	1.757582	1	30.89094	114.6548	9.86E-23	***
	Hand-Torso : 2	1.11163	1	12.35721	45.86501	1.64E-09	***

Leg-Torso : 2	-0.64595	1	4.172539	15.48679	0.003547	**
Arm-Foot : 3	-0.23183	1	0.53743	1.994726	1	
Arm-Hand : 3	-1.11088	1	12.34058	45.80329	1.66E-09	***
Arm-Leg : 3	0.313583	1	0.983341	3.649766	1	
Arm-Torso : 3	-0.21458	1	0.460437	1.708958	1	
Foot-Hand : 3	-0.87906	1	7.7274	28.68101	5.83E-06	***
Foot-Leg : 3	0.545408	1	2.9747	11.04089	0.034141	*
Foot-Torso : 3	0.017247	1	0.002975	0.011041	1	
Hand-Leg : 3	1.424464	1	20.29099	75.31201	2.4E-15	***
Hand-Torso : 3	0.896304	1	8.033605	29.81752	3.48E-06	***
Leg-Torso : 3	-0.52816	1	2.789537	10.35364	0.046429	*
Arm-Foot : 4	-0.19281	1	0.371759	1.379819	1	
Arm-Hand : 4	-0.88584	1	7.847156	29.12549	4.78E-06	***
Arm-Leg : 4	0.232775	1	0.541841	2.011096	1	
Arm-Torso : 4	-0.19532	1	0.3815	1.415976	1	
Foot-Hand : 4	-0.69303	1	4.802924	17.82653	0.001155	**
Foot-Leg : 4	0.425585	1	1.811228	6.72255	0.292935	
Foot-Torso : 4	-0.00251	1	6.3E-05	0.000234	1	
Hand-Leg : 4	1.118617	1	12.51303	46.44334	1.27E-09	***
Hand-Torso : 4	0.690521	1	4.768198	17.69764	0.001203	**
Leg-Torso : 4	-0.4281	1	1.832654	6.802077	0.28966	
Arm-Foot : 5	-0.17345	1	0.300832	1.116569	1	
Arm-Hand : 5	-0.70389	1	4.95464	18.38964	0.000909	***
Arm-Leg : 5	0.166686	1	0.277842	1.031237	1	
Arm-Torso : 5	-0.20161	1	0.406465	1.508637	1	
Foot-Hand : 5	-0.53045	1	2.813738	10.44347	0.045565	*
Foot-Leg : 5	0.340131	1	1.156891	4.293916	0.967451	
Foot-Torso : 5	-0.02816	1	0.007932	0.029442	1	
Hand-Leg : 5	0.870578	1	7.579059	28.13042	7.48E-06	***
Hand-Torso : 5	0.502282	1	2.522874	9.363894	0.076464	.
Leg-Torso : 5	-0.3683	1	1.356417	5.034476	0.681229	
Arm-Foot : 6	-0.13416	1	0.179991	0.668055	1	
Arm-Hand : 6	-0.55862	1	3.120581	11.58234	0.026365	*
Arm-Leg : 6	0.137416	1	0.188831	0.700866	1	
Arm-Torso : 6	-0.19392	1	0.376032	1.39568	1	
Foot-Hand : 6	-0.42446	1	1.80167	6.687077	0.292935	
Foot-Leg : 6	0.271577	1	0.737539	2.737449	1	
Foot-Torso : 6	-0.05975	1	0.035706	0.132527	1	
Hand-Leg : 6	0.696038	1	4.844683	17.98152	0.001093	**
Hand-Torso : 6	0.364706	1	1.330106	4.936819	0.693738	
Leg-Torso : 6	-0.33133	1	1.097805	4.074611	1	
Residuals	NA	570	153.5726	NA	NA	